INFORMATION TO USERS

This manuscript has been reproduced from the microfilm master. UMI films the text directly from the original or copy submitted. Thus, some thesis and dissertation copies are in typewriter face, while others may be from any type of computer printer.

The quality of this reproduction is dependent upon the quality of the copy submitted. Broken or indistinct print, colored or poor quality illustrations and photographs, print bleedthrough, substandard margins, and improper alignment can adversely affect reproduction.

In the unlikely event that the author did not send UMI a complete manuscript and there are missing pages, these will be noted. Also, if unauthorized copyright material had to be removed, a note will indicate the deletion.

Oversize materials (e.g., maps, drawings, charts) are reproduced by sectioning the original, beginning at the upper left-hand corner and continuing from left to right in equal sections with small overlaps. Each original is also photographed in one exposure and is included in reduced form at the back of the book.

Photographs included in the original manuscript have been reproduced xerographically in this copy. Higher quality 6" x 9" black and white photographic prints are available for any photographs or illustrations appearing in this copy for an additional charge. Contact UMI directly to order.

UMI®

Bell & Howell Information and Learning
300 North Zeeb Road, Ann Arbor, MI 48106-1346 USA
800-521-0600

Reproduced with permission of the copyright owner. Further reproduction prohibited without permission.

Reproduced with permission of the copyright owner. Further reproduction prohibited without permission.

RESONANT TUNNELING THROUGH A DIODE ACCUMULATION LAYER

by

Daniel P. Morris

A dissertation submitted to the Graduate Faculty in Physics in partial fulfilment of the requirements for the degree of Doctor of Philosophy, The City University of New York

1999

Reproduced with permission of the copyright owner. Further reproduction prohibited without permission.

UMI Number: 9946202

Copyright 1999 by
Morris, Daniel Peter

All rights reserved.

UMI Microform 9946202
Copyright 1999, by UMI Company. All rights reserved.

This microform edition is protected against unauthorized
copying under Title 17, United States Code.

UMI
300 North Zeeb Road
Ann Arbor, MI 48103

Reproduced with permission of the copyright owner. Further reproduction prohibited without permission.

© 1999

DANIEL P. MORRIS

All Rights Reserved

Reproduced with permission of the copyright owner. Further reproduction prohibited without permission.

This manuscript has been read and accepted for the Graduate Faculty in Physics in satisfaction of the dissertation requirement for the degree of Doctor of Philosophy.

9/3/99 — Date

Chair of Examining Committee

9/3/99 — Date

Executive Officer

Peter J. Price

Joseph Birman

Godfrey Gumbs

Cai Wei

Supervisory Committee

THE CITY UNIVERSITY OF NEW YORK

Reproduced with permission of the copyright owner. Further reproduction prohibited without permission.

ABSTRACT

RESONANT TUNNELING THROUGH A
DIODE ACCUMULATION LAYER
by
Daniel P. Morris

Advisor: Professor Melvin Lax

The phenomenon equivalent to resonant tunneling, in a double-barrier diode with a spacer layer and consequent accumulation layer on the cathode (source) side, is elucidated. The accumulation layer and the inter-barrier well is a double barrier reflecting structure in which each support an electron quasi-level (or several) which may be expected to combine coherently into a doublet of states that are filled by in-scattering of the source electrons and emptied by tunneling to the "anode" side. A rectangular model potential is computationally investigated to elucidate the properties of the double barrier reflecting structure, including the Gamow-like tunneling out of the double-well system. These properties are shown to be accurately represented by a two level model The resulting current depends on the distribution of electron density (norm) between these two component orbitals, with a peak (as a function of bias) at the "level crossing" point where the norms are each 1/2. The in-scattering rate due to acoustic-mode phonons in particular is calculated. Corresponding diode current characteristics are obtained.

Reproduced with permission of the copyright owner. Further reproduction prohibited without permission.

Dedicated to my wife, Lucille, and my children, Lauren and Mitchell, who endured my absence while I pursued this work, and in particular to my wife who also endured my absence while I obtained a Juris Doctor degree.

Reproduced with permission of the copyright owner. Further reproduction prohibited without permission.

ACKNOWLEDGMENT

I am grateful to Prof. Melvin Lax, my thesis advisor, who supported my re-entry into the doctoral program in physics of the City University after a long leave of absence. I am grateful to other faculty members of the Physics Department of the City College, in particular, Prof. Timothy Boyer, the graduate student advisor at the time of my re-entry, who encouraged me seeking re-entry into the doctoral program. I am grateful to Peter Price who supervised this work at the Thomas J. Watson Research Center while he held a position as an Emeritus scientist. Since I engaged in this research while holding a full time job, he patiently endured long delays always encouraging me to persist through to completion. For this, I shall always have the greatest respect and admiration for him as a scientist and a person of outstanding character.

Reproduced with permission of the copyright owner. Further reproduction prohibited without permission.

TABLE OF CONTENTS

Reproduced with permission of the copyright owner. Further reproduction prohibited without permission.

Reproduced with permission of the copyright owner. Further reproduction prohibited without permission.

LIST OF FIGURES

Reproduced with permission of the copyright owner. Further reproduction prohibited without permission.

Reproduced with permission of the copyright owner. Further reproduction prohibited without permission.

Reproduced with permission of the copyright owner. Further reproduction prohibited without permission.

Reproduced with permission of the copyright owner. Further reproduction prohibited without permission.

Reproduced with permission of the copyright owner. Further reproduction prohibited without permission.

TABLE OF SYMBOLS

$\Lambda(E)$ is the Lorentzian function.

d_w^l is the width of the left well.

d_w^r is the width of the right well.

d_b^l is the width of the left barrier.

d_b^r is the width of the right barrier.

$\Delta x_w = d_w^l - d_w^r$.

$\Delta x_b = d_b^l - d_b^r$.

$\ell_w^l(E)$ is the norm in the left well at real energy E.

$\ell_w^r(E)$ is the norm in the right well at real energy E.

$\ell^T(E)$ is the total norm in regions 1 to 5 of the potental of Figure 1.7.

E_{0+} is the real energy corresponding to the peak of $\ell^T(E)$ for the higher energy state of the doublet.

E_{0-} is the real energy corresponding to the peak of $\ell^T(E)$ for the lower energy state of the doublet.

E_{0-} is the real energy corresponding to the peak of file higher energy of the doublet corresponding to a re

E_l is the energy eigenvalue for an isolated left well.

E_r is the energy eigenvalue for an isolated right well.

$E_m = (E_l + E_r)/2$.

$n_{+,w}^l$ is the fraction of the norm in the left well at real energy E_{0+}.

$n_{-,w}^l$ is the fraction of the norm in the left well at real energy E_{0-}.

$n_{+,w}^r$ is the fraction of the norm in the right well at real energy E_{0+}.

Reproduced with permission of the copyright owner. Further reproduction prohibited without permission.

$n^{L}_{,w}$ is the fraction of the norm in the right well at real energy E_{0} –.

$\tau_{\bar{a}}^{+}$ is the decay time of the higher energy quasi-evel of a doublet.

$\tau_{\bar{a}}^{-}$ is the decay time of the lower energy quasi-level of a doublet.

$1/\tau_{l}$ is the scattering rate into a quasi-level from a state in the cathode continuum.

$1/\tau_{r}$ is the scattering rate out of a quasi-level to an anode state.

$S(E)$ is the S-Matrix.

$E_{r} + iE_{i}$ is the complex energy at a pole of $S(E)$.

$\theta(E)$ is the phase of the one component S-Matrix.

τ_{a}^{+} is the lifetime for a transition from a cathode continuum state to a quasi-level of higher energy of a doublet.

τ_{a}^{-} is the lifetime for a transition from a cathode continuum state to a quasi-level of lower energy of a doublet.

$g_{0}(E)$ is the logarithmic derivative of the wave function at the outer boundary of a potential.

Reproduced with permission of the copyright owner. Further reproduction prohibited without permission.

CHAPTER 1

INTRODUCTION

The concept of tunneling through a potential barrier manifests the fundamental principle of the quantum theory of matter - the wave-like property of matter. The concept of tunneling was incorporated into solid state physics in 1928 by Fowler and Nordheim, [1] and by Oppenheimer [2] to describe field emission from metals and later by Zener [3] in 1934 to describe internal field emission in semiconductors. Tunneling between the valence and conduction bands of a semiconductor p-n diode was reported by Leo Esaki in 1958 [4]. Such devices are referred to as Esaki or tunnel diodes. Since the first observation of resonant tunneling. by Tsu, Esaki and Chang [4, 5] in the early 1970's, double-barrier resonant tunneling structures (DBRTS) have attracted much interest due to their potential applications [7-9] and the opportunities they offer for the theoretical and experimental study of quantum effects and tunneling processes [10, 11]. The first theoretical treatment of resonant tunneling appears to be by Bohm [12] in 1951 using the WKB approximation. The early work on tunneling in solids has been thoroughly reviewed by Duke [13]. A recent review of tunneling in semiconductors has been done by Price [17]. There are a number of recent books on various aspects of the theory of resonant tunnelling and its practical applications [14, 15, 16].

Reproduced with permission of the copyright owner. Further reproduction prohibited without permission.

The observations of Tsu, Esaki and Chang appeared shortly after molecular beam epitaxy (MBE) was introduced into compound semiconductor crystal growth techniques. Electron tunneling was predicted for an AlGaAs/GaAs/AlGaAs double barrier heterostructure based on electron wave resonance [5]. In the particle picture each electron is constrained inside the GaAs quantum well for a certain dwell time before escaping into the anode region. The bias dependence of the tunneling current through the DBRTS shows negative differential resistance as a result of the resonant tunneling. Resonant tunneling can be described by the transmission and reflection process of resonant electron waves through the DBRTS [16 at pp. 1-6].

1.1 Overview of Physics of Resonant Tunneling

Double barrier resonant tunneling structures are made from planar layers of material having conduction or valence band edges at different energies. Typically a layer of one material is sandwiched between two layers of the other material to result in a potential profile shown in Figure 1.1. This figure shows a schematic diagram of a DBRTS formed from two barrier regions of GaAlAs (of width W_1 and W_3 and barrier height Δ E) and a well region of n-doped GaAs (dopant N_{D2} and of width W_2) The cathode and anode regions are heavily n-doped GaAs (cathode dopant N_{D1} and the anode dopant N_{D3}). E_f is the Fermi energy in the cathode and anode regions. The shaded regions are the occupied continuum states in the cathode and anode regions. E_1 is a resonant level in the well region.

Reproduced with permission of the copyright owner. Further reproduction prohibited without permission.

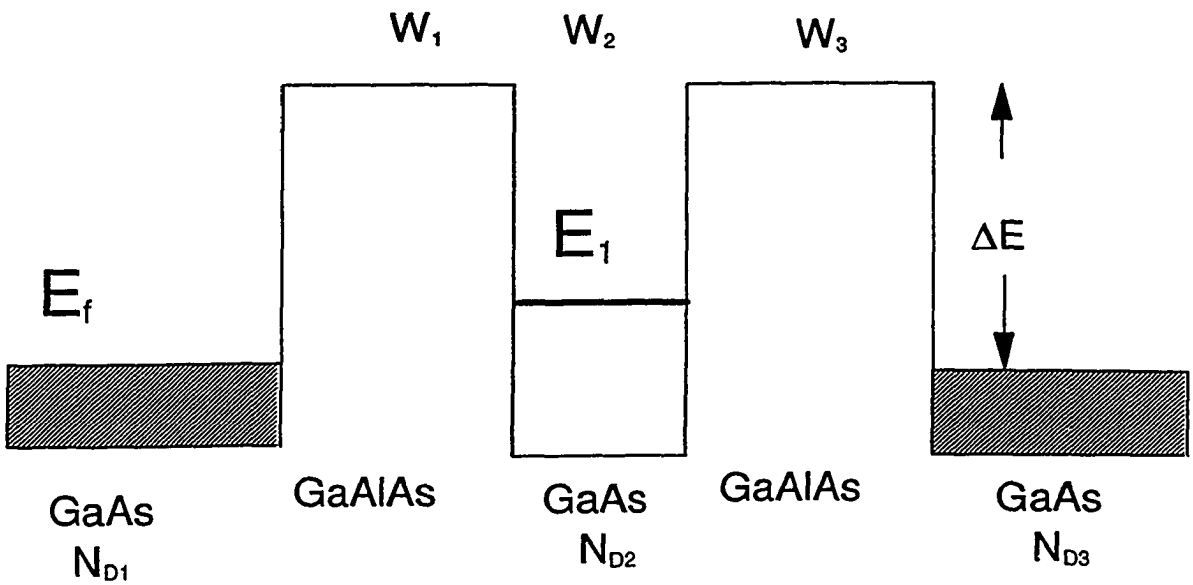

Fig. 1.1

Schematic diagram of a DBRTS formed from two barrier regions of GaAlAs (of width W_1 and W_3 and barrier height ΔE) and a well region of n-doped GaAs (dopant N_{D2} and of width W_2). The cathode and anode regions are heavily n-doped GaAs (cathode dopant N_{D1} and anode dopant N_{D3}). E_f is the Fermi energy in the cathode and anode regions. The shaded areas are the occupied continuum states in the cathode and anode regions. E_1 is a resonant level in the well region.

Reproduced with permission of the copyright owner. Further reproduction prohibited without permission.

Since there is no variation in the electrostatic potential parallel to the interfaces at x_i between the layers of different material, only a one dimensional Schrödinger equation need be considered for the envelope wave function ψ:

$$-\frac{d^2}{dx^2}\psi(x) + k(E,x)^2\psi = 0 \tag{1.1}$$

A particle of energy E in a one dimensional potential, $V(E)$, has wave vector $k(E,x)$ which is in general complex and given by $k(x) = \sqrt{(2m^*/\hbar^2)[V(x) - E]}$ where m^* is the effective mass which is constant in each layer. $\psi(x)$ may be assumed to satisfy the following conditions at an interface at locations x_i where + and - correspond to the right and left side of x_i

$$\psi(x_i^-) = \psi(x_i^+) \tag{1.2}$$

$$\frac{1}{m_-^*}\frac{d\psi(x)}{dx}\bigg|_{x_i^-} = \frac{1}{m_+^*}\frac{d\psi(x)}{dx}\bigg|_{x_i^+} \tag{1.3}$$

Eq. (1.3) is the typically used effective mass approximation to satisfy continuity of current through an interface at which there is a discontinuity in the band-edge energy and m^* [18].

The current per unit area, $\vec{J}$, for the DBRTS of Figure 1.1, is given by:

$$\vec{J} = 2e\sum_k n(k)\vec{v}(k) \rightarrow 2e\int (2\pi)^{-3}\,\vec{v}(k)f(k)\,d^3k \tag{1.4}$$

Reproduced with permission of the copyright owner. Further reproduction prohibited without permission.

where the 2 is for two spin states, $n(k)$ is the number of electrons per unit volume having wave vector k, $\vec{v}(k)$ is the group velocity given by

$$\vec{v}(k) = \frac{1}{\hbar} \nabla_k E \tag{1.5}$$

$n(k) = (2\pi)^{-3} f(k)$ where $(2\pi)^{-3}$ is the density of states and $f(k)$ is the probability that a state is occupied which is given by the Fermi distribution function. (Two-dimensional vectors parallel to the interface planes of the diode structure are represented by capitals K and the components normal to the planes by k, z, J.)

If the current is incident on a potential barrier, each electron has probability $T(E)$ of going through the barrier. The total energy $E = E_{||} + E_{\perp}$ where $E_{||} = (\hbar \mathbf{K})^2/(2m)$ is the energy parallel to the surface of the potential and $E_{\perp} = (\hbar k)^2/(2m)$ is the energy perpendicular to the surface of constant potential. Therefore, from Eqns. (1.4) and (1.5) the current J perpendicular to the potential surfaces is given by

$$J = \frac{e}{\hbar 4\pi^3} \int f(E) T(E) \frac{\partial E}{\partial k} \, dk \, d\mathbf{K} \tag{1.6}$$

When no bias is applied across the potential barrier, as shown in Figure 1.1, the current through the barrier is equal to zero since the current from left to right equals the current from right to left.

Reproduced with permission of the copyright owner. Further reproduction prohibited without permission.

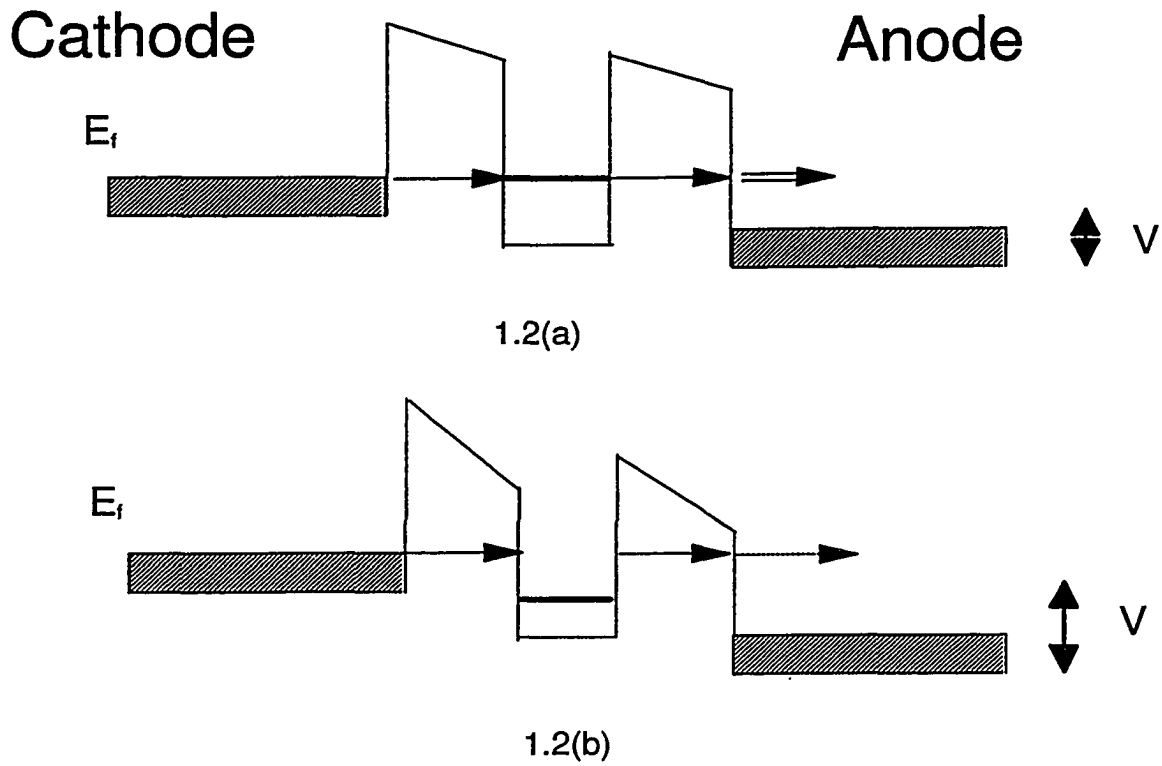

Fig. 1.2

Schematic diagram of the DBRTS of Fig. 1.1 with a voltage applied between the cathode and anode. In Fig. 1.2(a) the resonant level E_1 of Fig. 1.1 is aligned with the cathode continuum states permitting resonant tunneling (double lined arrow) to an unoccupied anode continuum state. In Fig. 1.2(b) the applied voltage is large enough to place the well resonant level below the cathode continuum. Electrons in the cathode continuum reach unoccupied levels in the anode continuum by nonresonant tunneling (dotted arrow).

Reproduced with permission of the copyright owner. Further reproduction prohibited without permission.

If an external bias, V, is applied to the barrier as shown in Figure 1.2, the net current flow through the barrier is [19]

$$J = \frac{e}{\hbar 4\pi^3} \int [f(E) - f(E + eV)] T(E_\perp) \frac{\partial E}{\partial k} dk\, d\mathbf{K} \qquad (1.7)$$

The transmission probability through a potential barrier, T, can be determined by solving the Schrödinger equation. For a DBRTS shown in Figures 1.1-1.2 in the off resonance condition $T \simeq T_L T_R$ and in the resonance range the peak value of T is $T = 4T_L T_R/(T_L + T_R)^2$ which is a function of the ratio of T_L and T_R where T_L and T_R are the transmission probabilities for the left and right barriers, respectively [20].

Figure 1.3 shows a schematic plot of the I/V characteristics of the DBRTS of Figure 1.2 [21]. When the energy of the resonant state of the barrier well is lower than the occupied (hatched region in Figures 1.2) states of the cathode or above the Fermi energy of the cathode, the current is due to electrons reaching anode states through non-resonant states of the barrier well. The current reaches a maximum when the applied voltage equals $2E_1/e$ which corresponds to the energy of a resonant state in the barrier well being aligned with the states of the cathode continuum as shown in Figure 1.2(a). The current then decreases showing a negative resistance when the resonant state of the barrier falls below the states of the cathode continuum as shown in Figure 1.2(b). The current increases again as another resonance is approached.

Reproduced with permission of the copyright owner. Further reproduction prohibited without permission.

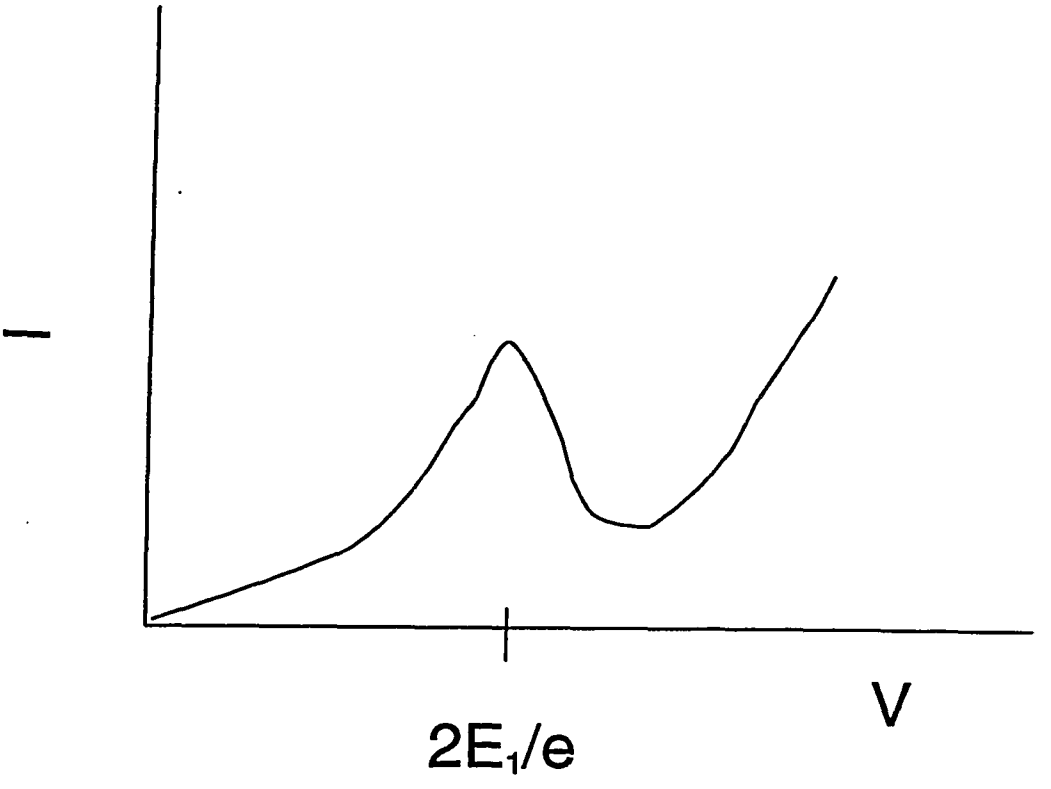

Fig. 1.3

Current/voltage characterized of the DBRTS of Figs. 1.1 and 1.2 showing a peak at a voltage equal to $2E_1/e$ after which there is a negative resistance region.

Reproduced with permission of the copyright owner. Further reproduction prohibited without permission.

In many cases of interest, such as a DBRTS, the Schrödinger equation cannot be solved analytically and approximation methods are not applicable. In such a situation numerical solutions of the Schrödinger equation must be obtained to determine $T(E)$ and the current.

1.2 Problem Investigated In This Thesis

In the DBRTS schematically shown in Figure 1.1 the cathode and anode regions are sufficiently highly doped so that none of the voltage applied between the cathode and anode contacts is dropped across the anode and cathode regions which are the regions to the right and left of the barriers in Figure 1.1. This is shown in Figure 1.2 by the bands in the anode and cathode regions remaining flat when a voltage is applied.

If the regions just outside the two barrier regions in Figure 1.1 are undoped or lightly doped, part of the voltage between the cathode and anode contacts will be dropped in the cathode and anode regions resulting in bending of the energy bands [22]. Figure 1.4 schematically shows a DBRTS structure, which has lightly doped anode and cathode regions (N GaAs regions) and thin undoped GaAs spacer layers, of the type measured by Wu et al. [24].

Figure 1.5 is a schematic diagram of the energy band of the structure of Figure 1.4 with a voltage applied between the cathode and anode contacts. The top and bottom electrodes of

Reproduced with permission of the copyright owner. Further reproduction prohibited without permission.

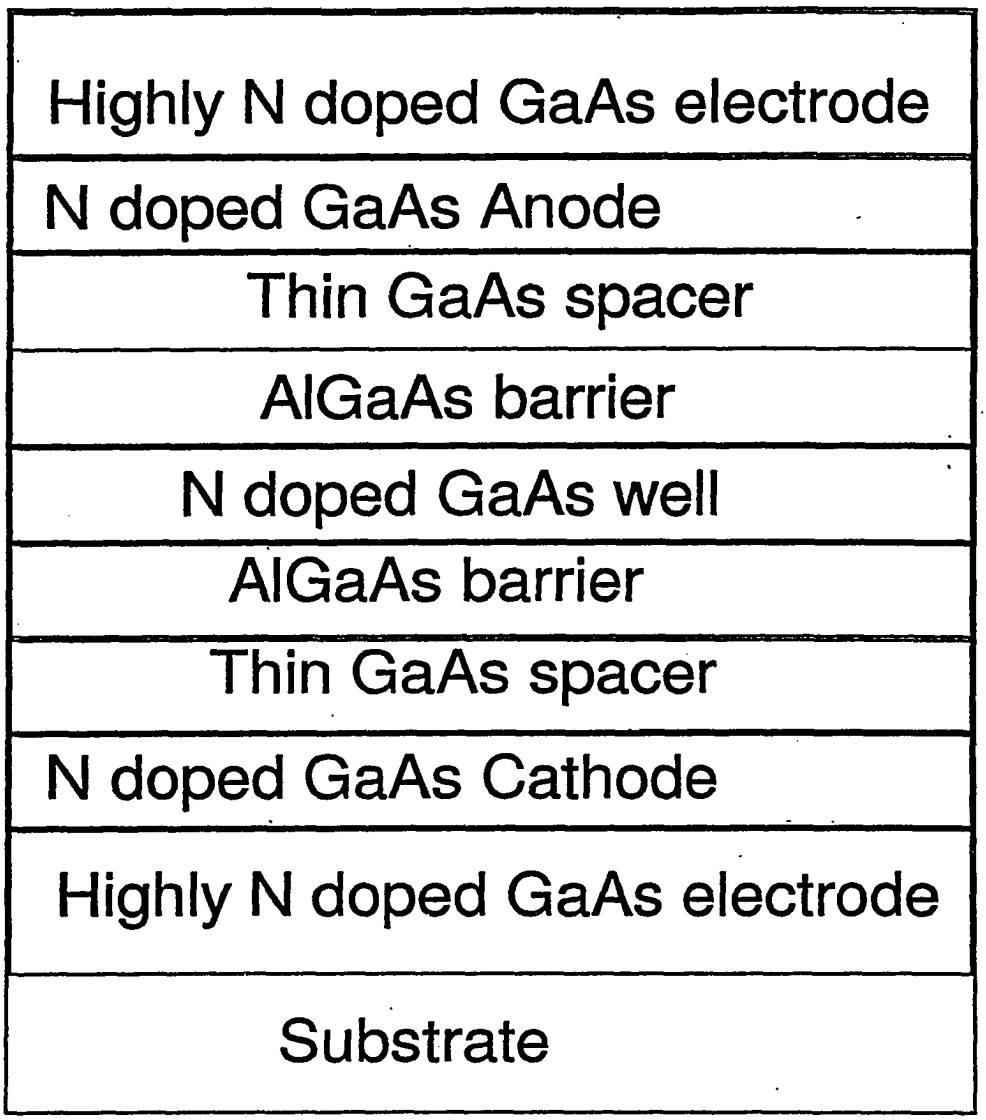

Fig. 1.4
Schematic cross section of a DBRTS with lightly doped anode and cathode regions.

Reproduced with permission of the copyright owner. Further reproduction prohibited without permission.

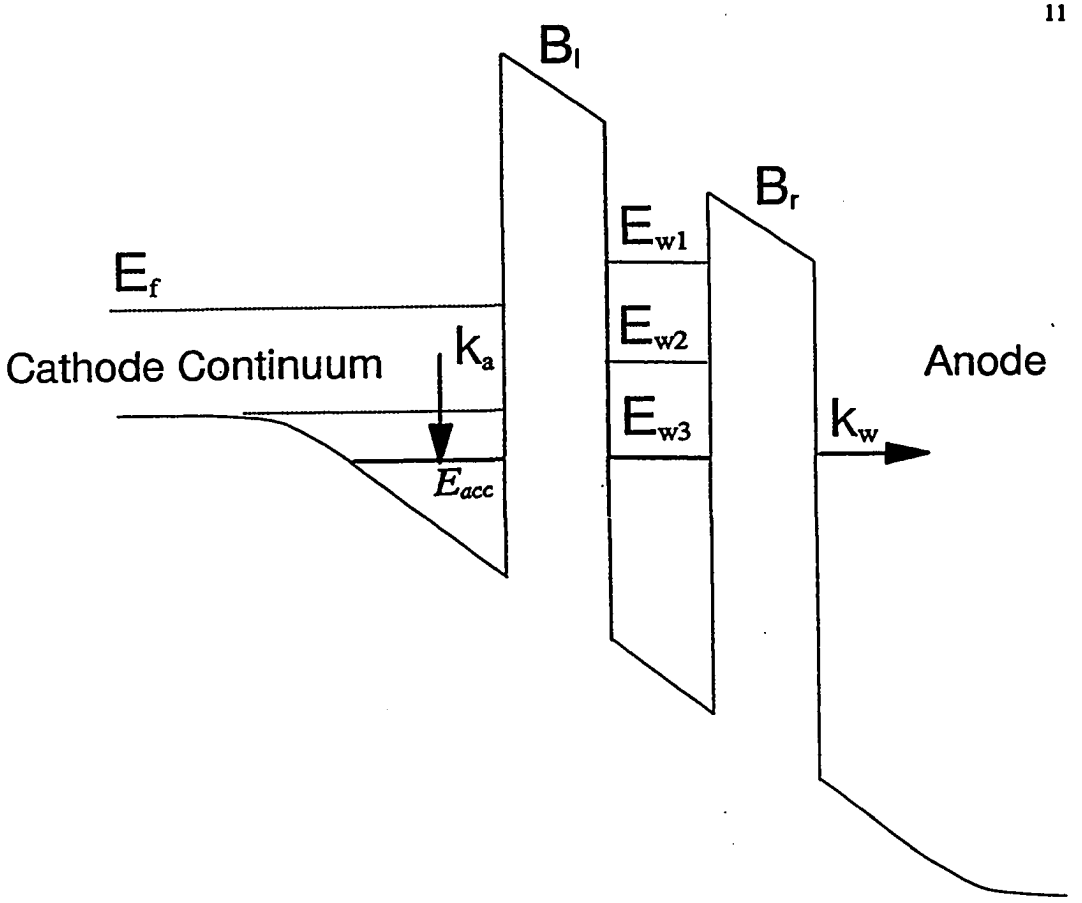

Fig. 1.5

Schematic diagram of the potential profile for a DBRTS of Fig. 1.4. E_{acc} is a quantized level in the accumulation layer. E_{W1}, E_{W2} and E_{W3} are quantized levels in the well. E_f is the Fermi energy. k_a is the transition rate from a cathode continuum state to E_{acc}. k_W is the transition rate from resonant level E_{W3} to an unoccupied anode continuum state.

Reproduced with permission of the copyright owner. Further reproduction prohibited without permission.

Figure 1.4 correspond to the left and right, respectively, of Figure 1.5. When the top electrode is biased negatively with respect to the bottom electrode, the top electrode is the cathode and the bottom electrode is the anode. The potential shows band bending caused by a voltage drop in the lightly doped spacer layers. The band bending originates from the accumulation of electrons in the lightly doped region adjacent the cathode side barrier and from the buildup of space charges in the lightly doped region adjacent the anode side barrier. The N doped GaAs layer and the thin undoped GaAs layer on the cathode and anode sides of the structure of Figure 1.4 result in the bending of the conduction band edge in the regions to the left and right of the two potential barriers in Figure 1.5.

In Figure 1.5, E_f is the Fermi energy in the cathode region. There are a continuum of cathode states between the Fermi energy and the conduction band edge energy which is shown as a dashed line in the accumulation layer region, but the lower energy range is quantized. Figure 1.5 illustrates that one can expect to have levels associated with the quantization of the accumulation layer by itself as well as levels associated with the double barrier resonant structure, but as they approach coincidence these will interact through the interconnecting barrier between the well and the accumulation layer. For energies less than the conduction band edge in the cathode region, the structure of Figure 1.5 is a reflecting double barrier structure, that is, a wave function incident from the anode side of the DBRTS is completely reflected with a change in phase by the DBRTS.

Reproduced with permission of the copyright owner. Further reproduction prohibited without permission.

In Figure 1.5 as the applied voltage is varied the effective width of the accumulation layer changes. The DBRTS of Figure 1.5 has a well with three resonance levels E_{w1}, E_{w2} and E_{w3}. Since resonance level E_{w1} is not in the occupied energy range of the cathode continuum, the probability of an electron tunneling through the DBRTS through these levels is zero except by some inelastic scattering process. On the other hand, resonance level E_{w2} is within the range of the cathode continuum and the probability of an electron tunneling through the DBRTS will be high [27, 28, 30]. Well resonance level E_{w3} is shown aligned with the accumulation layer resonance level E_{acc}. Therefore, electrons can "tunnel" from level E_{acc} to level E_{w3}. Accumulation layer quasi-level E_{acc} can be filled with electrons scattered from the cathode continuum with a rate constant, schematically shown as k_a in Figure 1.5. Because of the lateral two-dimensional wave-vector component for electron states in a three dimensional parallel-plane structure, it is possible for elastic disorder-induced scattering as well as elastic-phonon induced scattering to contribute to these processes. The transition from the resonance level E_{w3} to the anode side will be given by a rate constant, schematically shown as k_w in Figure 1.5 which depends on the time to escape from the resonance level E_{acc} which is the lifetime, τ_g (Gamow decay time), of the electron in the accumulation layer resonance energy level. These resonance levels will be referred to a as quasi-levels since an electron is not trapped in this level but can leak out into the anode region.

Reproduced with permission of the copyright owner. Further reproduction prohibited without permission.

The quantized levels in the accumulation layer are in fact not distinct levels from the quantized levels in the barrier. The accumulation layer and barrier layer levels are resonance-associated quasi-levels forming a single "hybrid" quantum state. The "hybrid" quantum state is characterized by an escape time for an electron scattered into the "hybrid" state to reach an anode state.

The escape time for these resonance-associated quasi-levels will be of the same order of magnitude as the isolated ("stand alone") resonant structure's response time, $\sim \hbar/\Delta E$, where ΔE is the resonance half width. Where an appreciable fraction F of the norm for these electron states belongs to the accumulation layer part of the structure, scattering rates should be comparable to those for the usual "two-dimensional electron-gas" sub-bands of a completely confining accumulation layer plus conventional barrier.

Eq. (1.7) for the current applies to electrons tunneling through the double barrier from a cathode state in a semi-infinite space (cathode region) to an anode state in a semi-infinite space (anode region), such as when well level E_{w2} is aligned with the cathode continuum states as shown in Figure 1.5. Eq. (1.7) does not apply to electrons reaching such an anode state from a quantized level in the accumulation layer, such as E_{acc} which is filled with an electron by transitions from occupied cathode continuum states. Therefore, a different approach is needed to calculate the I/V characteristics when there is an accumulation layer with quantized states. Such an approach is described in this thesis.

Reproduced with permission of the copyright owner. Further reproduction prohibited without permission.

Eq. (1.7) is not sufficient since it applies to an electron wave function which is incident from infinity on a potential barrier which transmits a part of the wave function to infinity in the opposite direction. The portion of the wave function which is not transmitted through the barrier is reflected back to the infinity from which it originated. Thus the wave function is a reflected but not a bound state. An electron in an accumulation layer state reflects back and forth between the potential side walls of the accumulation layer. A portion of the wave function is transmitted through the potential barrier into the anode region each time the electron is incident on the barrier. The entire wave function eventually escapes to the anode region. Thus an electron in an accumulation layer state is characterized by an escape time from the accumulation layer state which is not taken into account by Eq. (1.7).

Figure 1.6 which is a schematic plot of data reported by Wu et al. [24.] shows I/V and the G/V (G=dI/dV) characteristics of a DBRTS structure schematically shown in Figure 1.4. Wu et al. reports data with the lightly doped N-GaAs layers having $N_d = 2 \times 10^{18}$, 2×10^{17}, 2×10^{16} and 2×10^{15} atoms/cm^2. The presence of the "kink" increases as dopant decreases. The black diamond in Figure 1.6 marks a "kink" in the I vs.V and G vs. V characteristics which Wu et al. attribute to alignment of a well resonant state, such as E_{W3}, and an accumulation layer state, such as E_{acc}, shown in Figure 1.5.

Reproduced with permission of the copyright owner. Further reproduction prohibited without permission.

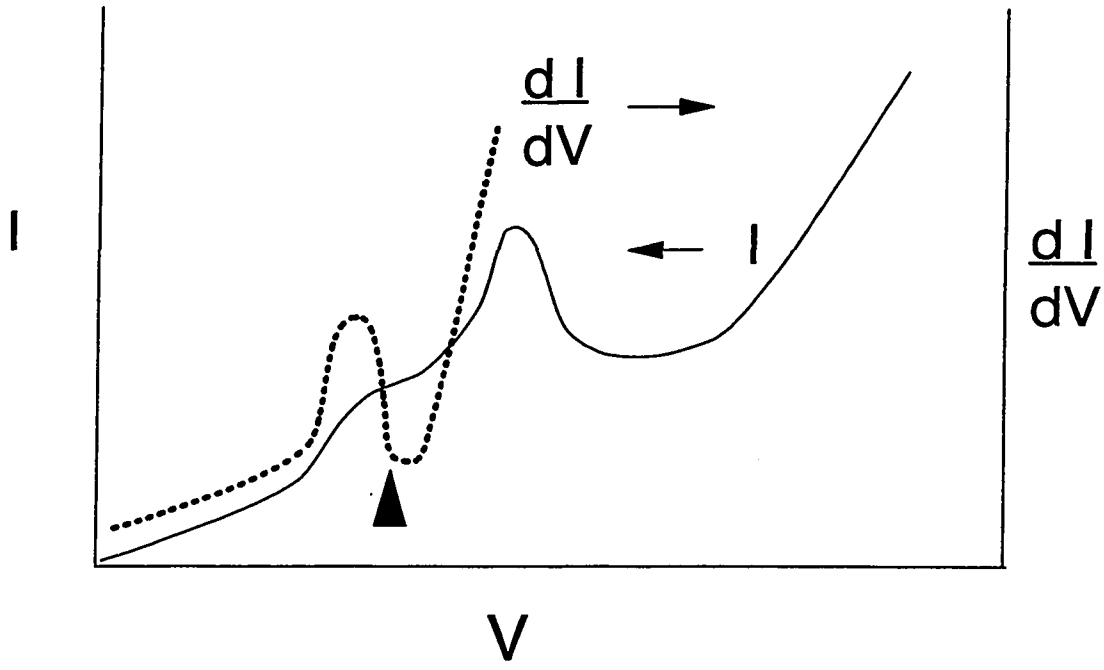

Fig. 1.6
Schematic plot of I vs. V and dI/dV vs. V characteristics of a DBRTS structure of Fig. 1.4 for a lightly doped spacer layer.

Reproduced with permission of the copyright owner. Further reproduction prohibited without permission.

Resonant tunneling of electrons has also been observed from the accumulation layer adjoining a DBRTS formed from undoped regions (0.3 μm thickness) [23]. This effect has also been observed in a DBRTS with a spacer layer [24]. Others have also reported that tunneling of electrons from the first excited quantum level in the accumulation layer has been found to produce kinks in the current voltage characteristics [25]. It has been recently reported that the photoluminescent intensity from the quantum well as a function of bias sharply peaks at the voltage corresponding to the kink. The experimental evidence has been interpreted as evidence of the interaction of the first excited quantum state in the accumulation layer and the resonant state in the quantum well [26].

A general analytic treatment of resonant tunneling via an accumulation layer in a DBRTS has been presented by Price [31]. A more complete computational analytical treatment to understand the origin of the "kinks" shown in Fig. 1.6 is presented in this thesis. In this thesis the double well structure is treated as a coherent quantum system. It is shown that the resonance levels are in doublets of quasi-levels where the "level crossing phenomena" as the bias is varied is the critical property of the system. As described in Chapter 2 a model potential is initially investigated to understand the properties of a reflecting double barrier quantum system. The model potential is a surrogate system which replaces the potential of Figure 1.5 with a rectangular potential which can be represented by algebraic expressions and numerically computed. From this investigation of the model

Reproduced with permission of the copyright owner. Further reproduction prohibited without permission.

potential an understanding of the "level crossing phenomena" of the potential of Figure 1.5 is obtained. This understanding is applied in Chapter 3 to derive an expression for the current which results from the "level crossing phenomena" which results in an expression for the current which has Lorentzian form. The electrons in the cathode continuum reach the quasi-levels of the accumulation layer by inelastic collisions where acoustic phonon scattering is the dominant scattering mechanism. If $z > 0$ is the direction of current flow, then in a transition from a cathode continuum state to an accumulation layer state, the z component, k_z, of the wave vector changes from an initial value to a final value. Since the collision is inelastic, the initial and final total energy differ by the phonon energy. In Chapter 3 it is shown that the phonon energy can be neglected in comparison with the initial and final state energies. Parabolic energy bands will be assumed therefore

$$E = \frac{\hbar^2}{2m^*}(k_x^2 + k_y^2 + k_z^2) \tag{1.8}$$

The surface of constant energy in k space is a sphere. Therefore, for fixed k_z there is a circle on the sphere of constant energy which are the initial states and there is another circle on the sphere of constant energy which are the final states. The final states for a given initial state will incorporate a change in lateral 2D wave-vector,K, so as to give the same final as initial state energy for inelastic scattering processes for which the the phonon energy can be neglected. A factor in the rate (incident velocity times probability) is the density of the final states at this energy.

Reproduced with permission of the copyright owner. Further reproduction prohibited without permission.

With the final states being the "outward waves" ones of the type calculated in Chapter 2. The occupation probability of the final state is $(1-f)$ and of the initial state is f where f is the Fermi distribution function which is a factor in the rate. All transitions from each initial state to each final state are possible and have to be summed. Fermi's golden rule is used to calculate the transition rate from each initial to each final state. It is assumed that the energy of the initial state E_i satisfies $0 < E_i < E_f$ where E_f is the Fermi energy. Thus $f = 1$ for $0 < E_i < E_f$ and $f = 0$ for $E_i > E_f$.

1.3 Initial Investigation of a Model Potential

Reflecting Multibarrier Resonant Quantum System

Initially a model potential of a DBRTS with an accumulation layer has been investigated. The system initially investigated is the idealized model potential shown in Figure 1.7, in which each segment of the potential has zero field (constant potential). It has been found that the model potential is an interesting quantum system for separate investigation aside from being a model of the potential of Figure 1.5. There have been a number of recent theoretical studies of multibarrier transmission resonant tunneling structures [32-41]. There appears to have been no thorough investigation of reflecting multibarrier resonant tunneling structures. My investigation of the model potential has elucidated properties of reflecting multibarrier quantum systems which appear not to have been investigated before. My investigation elucidates the properties of a quantum system

Reproduced with permission of the copyright owner. Further reproduction prohibited without permission.

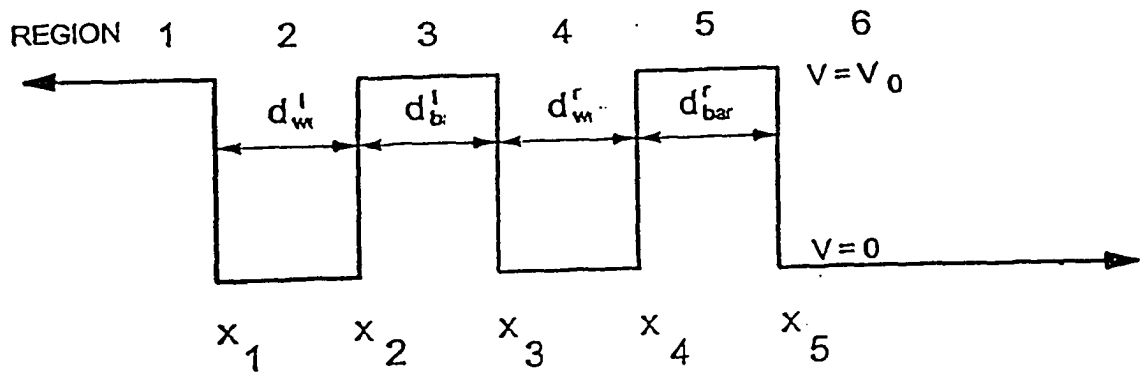

Fig. 1.7

Model potential for a DBRTS with an accumulation layer.

Reproduced with permission of the copyright owner. Further reproduction prohibited without permission.

which is not a bound state but a quasi-level of a reflecting double barrier system which leaks out of the double barrier system with a finite lifetime. It has been surprisingly found that pairs of quasi-levels have significant changes in some properties when the right barrier (Region 5) is made thinner than the left barrier (Region 3). There is a change in lifetime of the quasi-level and distribution of the quasi-level within the DBRTS structure which is most significant when the right barrier is made much thinner than the left barrier. Even when the right barrier is so thin as to be almost completely transparent, the system maintains properties of a double barrier system.

Parameters of the model potential are easily varied to gain an understanding of the properties of a reflecting double barrier structure to more easily understand the properties of the potential of Figure 1.5. This initial work is reported in Chapter 2. The application of this understanding to the potential of Figure 1.5 is described in Chapter 3.

The model potential, while expected to have the same qualitative properties as for the potential of Figure 1.5, can be analyzed and hence numerically computed in terms of elementary functions using the transfer matrix formalism. Its properties have been investigated by varying the thicknesses of the two barriers and the two "potential wells."

In the potential of Figure 1.5 (which is a representation of the the actual potential profile of a DBRTS with an accumulation

Reproduced with permission of the copyright owner. Further reproduction prohibited without permission.

layer) the left is higher in energy than the right since a bias is applied to the left (cathode) electode which is negative with respect to the right (anode) electrode. Since the regions to the left and the right of the two barriers are lightly doped or undoped, there is a field in these regions. In the left region (the accumulation layer) a well is formed which has approximately triangular shape. At a particular value of the field, F_0 and at an energy E' above the bottom of the triangular well the triangular well has a width, W'. As the magnitude of the field is increased to greater than $|F_0|$, W' decreases. As the magnitude of the field is decreased to less than $|F_0|$, W' increases. At energy E' the width of the left and right barriers and of the well between the left and right barriers remains constant as the field is varied. Thus, for the model potential of Figure 1.7, this effect is simulated by varying the the width of the left well, d_w^l. As the field is varied about F_0, the top of the right barrier is lowered with respect to E'. Thus for the right barrier $|V_0 - E'|$ decreases as the magnitude of the field is made greater than $|F_0|$ which results in the transmission probability through the right barrier decreasing. Also, for the right barrier $|V_0 - E'|$ increases as the magnitude of the field is made less than $|F_0|$ which results in the transmission probability through the right barrier increasing. This effect can be simulated by varying the thickness of the right barrier for the model potential of Figure 1.7.

Therefore, the effects of applying a potential across the DBRTS are simulated by varying the width of the left well and the width of the barrier on the anode side (right side) of the DBRTS.

Reproduced with permission of the copyright owner. Further reproduction prohibited without permission.

These widths are varied separately to understand the effect each has on the properties of the DBRTS.

The calculated resonances of the DBRTS are pairs of closely spaced quasi-levels (having a higher and lower energy quasi-level) derived from one level generated by each of the wells.

1.4 Numerical Solutions of Schrödinger's Equation

When $V(x)$ is constant, the one dimensional Schrödinger equation has a solution of the form

$$\psi(x) = A\exp(ikx) + B\exp(-ikx) \tag{1.9}$$

For $E > V$, k is real and for $E < V$, k is imaginary. At interfaces between regions of constant potential using Eqns. (1.2) and (1.3) setting the wave function and its derivative divided by the effective mass equal on both sides of the boundary results in a 2×2 transfer matrix, M, relating the coefficients A and B from one region of constant potential to the adjacent region of constant potential. When there are n regions the coefficients A_1 and B_1 are related to the coefficients A_n and B_n by the following equation:

$$\begin{bmatrix} A_1 \\ B_1 \end{bmatrix} = [M_1 M_2 \ldots M_{n-1}] \begin{bmatrix} A_n \\ B_n \end{bmatrix} \tag{1.10}$$

Eq. (1.10) can be used to solve the Schrödinger equation for the potential profile of Figure 1.5 by approximating the potential in

Reproduced with permission of the copyright owner. Further reproduction prohibited without permission.

regions where the potential is not constant by a number of regions of constant potential of different magnitude as shown in Figure 1.7.

1.5 Conclusion

In this thesis I investigate resonant tunneling from a quantized source layer (i.e. an accumulation layer). Understanding of this investigation is facilitated by the investigation of a reflecting multibarrier resonant quantum system described in Chapter 2. The results of Chapter 2 are applied in Chapter 3 to derive an expression for the current in a diode having a DBRTS with an accumulation layer.

Reproduced with permission of the copyright owner. Further reproduction prohibited without permission.

CHAPTER 2

RESONANCE IN A ONE-SIDED NON-SYMETRICAL DOUBLE BARRIER STRUCTURE

2.1 Introduction

Since the first observation of resonant tunneling [5, 6], double-barrier resonant tunneling structures (DBRTS) have attracted much interest due to their potential applications [7, 8, 9]. Moreover, they offer opportunities for the theoretical and experimental study of quantum effects and tunneling processes [10, 11].

The quantum system that is investigated in this chapter is chosen to serve as a model for a special case of resonant tunneling diode discussed in Chapter 3, and it is also found to have quantum-mechanical properties that are of interest in themselves. As described in Chapter 1 the semiconductor diodes in question have a spacer layer separating the n-doped (source) region from the nearer of the two barrier layers, resulting in an accumulation layer containing one or more distinct quantum levels of the electrons. Consequently these levels, rather than the usual one-dimensional continuum of states, serve as a "cathode" source for tunneling current.

Reproduced with permission of the copyright owner. Further reproduction prohibited without permission.

Recently in the literature there has been a number of studies of multiple barrier resonant structures [32-41]. These structures provide new opportunities for electronic applications and show new aspects of resonant tunneling not present in double barrier structures.

In this chapter a multiple barrier structure is studied theoretically. The structure comprises a double barrier structure adjoining a reflecting structure. This structure is investigated as a simple model of actual diodes in which there is a double barrier combined with an accumulation layer, which display a variety of resonant tunneling characteristics.

Figure 1.5 shows the conventional potential diagram to represent this situation. The accumulation layer and the standard inter-barrier layer, when each is considered apart from the rest of the system, support quasi-levels as shown. The former can be filled from the source continuum by elastic or inelastic scattering processes (remembering the two-dimensional lateral wave vectors, not shown), while the latter empty by electron tunneling into the anode continuum. These two steps are connected by a "tunneling interaction" in the barrier on the left (cathode) side; and accordingly it is the resulting combined quantum state that fills from the source region and empties (decays) by tunneling to the right (anode side). The current through the diode, considered in this way, will depend on the fraction of the norm, for the state given by the combined levels, that belongs to the accumulation layer, and hence must depend on a kind of dwell time.

Reproduced with permission of the copyright owner. Further reproduction prohibited without permission.

As the two "combining levels" cross (which should occur with increasing bias voltage) one expects -- and, in this chapter, finds -- an "anti-crossing effect" in which the pair of combined levels approach only to a minimum energy separation; that will be the "resonance" phenomenon in this system.

The tunneling decay for such a combination level must give an energy broadening effect on the level properties, proportional to the rate (inverse of lifetime). This decay rate should increase with forward bias as the anode-side barrier is effectively lowered. Then it is of interest to examine what happens to the properties of these electron states when the broadening exceeds the anti-crossing level splitting.

The system that is actually investigated here is the idealized model depicted in Figure 1.7, in which each segment of the potential has zero field (constant potential). This model, while expected to have the same qualitative properties as for Figure 1.5, can be analyzed and hence numerically computed in terms of elementary functions. Its properties will be varied by varying the thicknesses of the two barriers and the two "potential wells."

In Chapter 3 a more complete investigation, involving scattering from the cathode continuum into the quasi-levels of the accumulation layer, is presented of current/voltage characteristics of a DBRTS with an accumulation layer having the potential of Figure 1.5. For such a potential, if a quasi-level of the accumulation layer is aligned with a quasi-level of the barrier well,

Reproduced with permission of the copyright owner. Further reproduction prohibited without permission.

coherent tunneling is expected from the accumulation layer quasi-level through the barrier well quasi-level to an unoccupied state on the anode side of the DBRTS. Consequently, the electrons of the cathode continuum may, via scattering processes at the site of the accumulation layer [31] reach a resonant level, and hence the anode states.

In the typical model of a DBRTS at zero bias, the resonance levels of the quantum well lie above the energy range of the continuum of occupied electron states (electron sea) of the cathode (emitter). The resonance level of the well can be displaced to within the energy range of the electron sea by an anode to cathode potential bias. The current through the diode is then at a relative maxima because of the possibility of direct coherent tunneling through the resonance level to an unoccupied level at the anode side of the DBRTS [28, 42-45].

Diode configurations having an undoped cathode or undoped spacer layer between a heavily doped cathode and the barrier layer will have an accumulation layer on the cathode side of the DBRTS [46]. Consequently, due to quantum confinement in both the accumulation layer and the barrier well between the two barriers of the DBRTS there are quasi-levels [47]. A potential well bounded on both sides by a potential barrier of infinite width or height has discrete energy levels in which an electron can be trapped. Where a potential well is instead bounded on at least one side by a potential of finite height and width, the discrete levels are broadened into quasi-levels since an electron

Reproduced with permission of the copyright owner. Further reproduction prohibited without permission.

in such a level can escape with a lifetime related to the energy width of the quasi-level.

In order to properly account analytically for the contribution to the current through the accumulation layer via the energy levels of the accumulation layer and the energy levels of the quantum well, the associated wave functions in the accumulation layer and quantum well and the interaction between the energy levels of the accumulation layer and the quantum well must be understood as a function of the variation of the accumulation layer width with bias and as a function of the difference between the energy of the quasi-level and the top of the anode side barrier.

Figure 1.5 shows schematically a DBRTS with an accumulation layer formed by the application of bias between the anode and cathode regions which is assumed to result in a constant electric field. As the electric field is varied the effective width of the accumulation layer changes. The DBRTS of Figure 1.5 has a well with three resonance levels E_{w1}, E_{w2} and E_{w3}. Since quasi-level E_{w1} is not in the occupied energy range of the cathode continuum, the probability of an electron tunneling through the DBRTS through this energy level is zero except if an electron reaches this level by some scattering process. On the other hand, quasi-level E_{w2} is within the range of the cathode continuum and the probability of an electron tunneling through the DBRTS will be high [27-29].

Reproduced with permission of the copyright owner. Further reproduction prohibited without permission.

Well quasi-level E_{w3} is shown aligned with the accumulation layer quasi-level E_{acc}. Then electrons can "tunnel" from level E_{acc} to level E_{w3}. Accumulation layer quasi-level E_{acc} can be filled with electrons scattered from the cathode continuum with a rate constant, schematically shown as k_a in Figure 1.5. The transition from the quasi-level E_{w3} to the anode side will be given by a rate constant, schematically shown as k_w in Figure 1.5 which depends on the time to escape from the quasi-level E_{acc} which is the life-time, τ, of the electron in the accumulation layer quasi-level.

To investigate these properties numerically for a DBRTS with an accumulation layer, it is desirable to consider first a somewhat simpler potential system as in Figure 1.7 where the cathode-side barrier is of infinite width. In this chapter the idealized system consisting of the rectangular model potential, shown in Figure 1.7, of a DBRTS with an associated accumulation layer is investigated analytically. In this case, the quantities of interest may be expressed algebraically, and then evaluated numerically by computer. The model potential is non-symmetric. It is a one sided resonance structure which is closed on the cathode side and open on the anode side for which the source is the accumulation layer. The accumulation layer, Region 2 (left well), and the well between the barriers, Region 4 (right well), are represented here by a rectangular well. An electron in a quasi-level within the accumulation layer can escape to the right to the anode continuum, Region 6. There is no electric field applied to the potential of Figure 1.7. The effect of an electric field on the effective width of the accumulation is simu-

Reproduced with permission of the copyright owner. Further reproduction prohibited without permission.

lated by varying the width of the left well of Figure 1.7. The quasi-levels within the left well and the right well are studied as a function of the difference:

$$\Delta x_w = d_w^l - d_w^r \tag{2.1}$$

(where d_w^l, the width of the left well, is variable and d_w^r, the width of the right well, is held fixed) with the width of the left barrier, d_b^l, equal to the width of the right barrier, d_b^r and as a function of the difference:

$$\Delta x_b = d_b^l - d_b^r \tag{2.2}$$

with $d_w^l = d_w^r$ (where d_b^r is variable and d_b^l is held fixed).

The electron system investigated here differs from the usual double-barrier system of resonant tunneling diodes in two respects: (a) the electron states of interest are not transmitted between semi-infinite spaces, instead they are reflected from a "potential well" on the cathode side; (b) the two spaces between the barriers each support quasi-levels - what would be the isolated quantum states if there were no tunneling through the barriers - and the resonances effect involves the degree of alignment of those levels in the two well spaces. The combination of the wells results in a kind of quasi-level, an "almost stationary" state of the electron escaping slowly from this structure into the anode continuum.

Reproduced with permission of the copyright owner. Further reproduction prohibited without permission.

To help elucidate the properties of the electron states that are involved, we first discuss a simpler case. Instead of the two tunneling barriers of Figure 1.7, let there be a single barrier and hence a single "well" region. The stationary states of an electron (real energy) represent reflection from this structure. That is, if the wave function in the anode continuum space is given by:

$$\psi(x) = A(E)e^{ikx} + B(E)e^{-ikx} \tag{2.3}$$

then (for E real) $|A(E)| = |B(E)|$. In general the right side of Eq. (2.3) is multiplied by $v(E)^{-1/2}$ where

$$v(E) = \hbar^{-1} dE/dk \tag{2.4}$$

is the group velocity in the anode continuum. The form of the wave function in Eq. (2.3) depends on the form of the model potential of Figure 1.7. The velocity factor has to do with the wave functions in the leads which contact the anode and cathode regions. It is necessary in general, in the definition of the S-matrix, $S(E)$, for the wave functions in the anode and cathode regions to contain the velocity factor. In a multichannel system, the coefficients A and B are replaced by "outward" and "inward" arrays $\{A_n\}$ and $\{B_n\}$, linearly related by $A_n = \sum_m S_{n\,m} B_m$ where $S(E)$ is the S-matrix.[49.] In view of the velocity factor $v_n^{-1/2}$ in the definitions of the wave amplitudes, current conservation for the steady state (E real) implies $\sum |A_n|^2 = \sum |B_n|^2$ and hence that this S-matrix is unitary. If the velocity is the same in both regions, the velocity factors cancel out and can be eliminated in the definition of wave functions. The case being investigated here is a reflection structure and therefore has only one lead on the anode

Reproduced with permission of the copyright owner. Further reproduction prohibited without permission.

side, so the velocity factors drop out of the calculation formulas. The properties are contained in a "one-component S-matrix", the complex quantity $S(E) = A(E)/B(E)$ as a function of E. For a stationary state, E is real and the phase $\theta(E)$ in

$$S(E) = \exp i\theta(E) \tag{2.5}$$

describes the reflection process.

We are interested in the norm $\mathcal{I}(E) = \int |\psi|^2 dx$ integrated over the "well" structure, for which the coefficient $\ell(E)$ in $\mathcal{I}(E) = \ell(E)|B(E)|^2$ is related to the usual "dwell time" by:

$$\ell(E) = v(E)\tau_{dwell} \tag{2.6}$$

with $v(E)$ given by Eq. (2.4). $\ell(E)$ is the norm corresponding to an incident wave function having unit amplitude (which is reflected as a wave function having unit amplitude delayed in phase by the reflection process).Eq. (2.6) is the mathematical definition of the dwell time. The heuristic depiction is that the electron enters the system (for which the dwell time is defined) hangs around for that long and then exits.

As in conventional scattering phenomena, the continuation of $S(E)$ to complex energy, $E = E_r + iE_i$, such that $B(E) = 0$ for nonzero $A(E)$, and so a pole of $S(E)$ (zero of $S(E)^{-1}$) gives the quasi-level state for which the localized wave function then decays by

$$|\Psi(x,t)|^2 = e^{-t/\tau_{decay}} |\psi(x)|^2 \tag{2.7}$$

Reproduced with permission of the copyright owner. Further reproduction prohibited without permission.

where

$$\tau_d = -\hbar/(2E_i) \tag{2.8}$$

with $E_i < 0$.

If we have a simple isolated quasi-level, then the E dependence of $S(E)$ is $S \sim (E - E_r + iE_i)/(E - E_r - iE_i)$ in its energy neighborhood. Applying this to real E (the stationary reflection states) we obtain $\tau_{phase}(E) = \tau_{dwell}(E) = \tau_d \Lambda(E)$ (This expression follows from Eqs. (2.8), (2.31) (first term) and (2.37)) where $\Lambda(E) = 1/[1 + \{(E - E_r)/E_i\}^2]$ is the usual Lorentzian form [50].

With the double barrier case of interest here, we are still concerned with the same properties but of more complicated localized states. The total norm is

$$\ell^T(E) = \sum_{i=1}^{5} \ell^i(E) \tag{2.9}$$

where $\ell^i(E)$ is the norm in the ith region of Figure 1.7 at real energy E. The major contribution to $\ell^T(E)$ comes from $\ell^l_w(E) = \ell^1(E)$, the norm in the left well (accumulation layer) and $\ell^r_w(E) = \ell^4(E)$, the norm in the right well (between the barriers). It is therefore, convenient to define a total norm by:

$$\ell(E)^t_w = \ell^l_w(E) + \ell^r_w(E) \tag{2.10}$$

Reproduced with permission of the copyright owner. Further reproduction prohibited without permission.

To calculate the current we need the decay times of associated quasi-levels. If the quasi-levels are far apart in energy, we expect $\ell^{T}(E)$ to be mainly in the right or left wells. As these quasi-levels cross each other (for example, as an applied potential is varied) we expect a "level crossing" effect [51] in which a pair of quasi-levels approach to a minimum energy distance then separate again; and the resulting properties will depend on the comparison of this minimum distance with the Lorentzian widths, as in recent studies of tunneling transmission in triple-well systems [52-55]. In the reflection structure investigated here the conventional transmission resonance behavior is replaced by this crossing phenomenon.

The numerical procedure is described in sections 2.2 and 2.5. There are two special features: (a) care is need in selecting the appropriate real and imaginary components of the wave vector for complex energies, and (b) a numerical procedure is required to locate the poles of $S(E)$ in the complex E plane.

In the analysis reported here, for the potential profile of Figure 1.7, the heights of the left and right barriers are chosen to be both equal to V_0. A typical value of 0.3 eV is used for V_0. The widths, d_b^l, and d_b^r are nominally 50 Å. The widths, d_w^l and d_w^r are nominally 100Å. The widths d_w^l and d_b^r in Eqs. (2.1) and (2.2), respectively, are variable.

Reproduced with permission of the copyright owner. Further reproduction prohibited without permission.

2.2 Solution by Transfer Matrix Formalism

The one dimensional Schrödinger equation is:

$$\frac{d^2}{dx^2}\psi(x) + k(E,x)^2\psi = 0 \tag{2.11}$$

and

$$k(E,x)^2 = \frac{2m^*}{\hbar^2}[E - V(x)] \tag{2.12}$$

For real energy,E, Eq (2.11) gives for $E > V(x)$, $\psi(x) = A(E)\exp(ikx) + B(E)\exp(-ikx)$, $k = [(2m^*/\hbar^2)(E - V)]^{1/2}$ and for $E < V(x)$, $\psi(x) = A(E)\exp(\kappa x) + B(E)\exp(-\kappa x)$, $\kappa = [(2m^*/\hbar^2)(V - E)]^{1/2}$ and k and κ are real.

In the complex energy ($E = E_r + iE_I$) domain, $k(E,x)^2$ is complex. In a region of constant potential, V, the wave function $\psi(x)$ has the form

$$\psi(x) = A_i(E)e^{ik_i(E)x} + B_i(E)e^{-ik_i(E)x} \tag{2.13}$$

with $k_i(E)$ the complex root of $k_i(E)^2$ given by Eq. (2.12) for x corresponding Regions $i = 1$ to 6 of Figure 1.7. $k(E,x)$ given by Eq. (2.12) in general has four values; two corresponding to $E_I > 0$ and two corresponding to $E_I < 0$. Only two of the four values for $k(E,x)$ correspond to the physical situation under ex-

Reproduced with permission of the copyright owner. Further reproduction prohibited without permission.

amination. These are determined from the time dependent wave function which has the form

$$\Psi(x,t) = e^{-iEt/\hbar}\psi(x) \tag{2.14}$$

Therefore, the squared wave function has form of Eq. (2.7) with the decay time of Eq. (2.8). For $E_I > 0$ the argument of the exponential is negative and corresponds to the squared wave function decreasing in time which is the solution of interest since this corresponds to a wave function leaking out of the DBRTS.

The complex wave vector $k(E,x) = k_R(E,x) + ik_I(E,x)$ is determined by writing Eq. (2.12) as $[k_R(E,x) + ik_I(E,x)]^2 = u + i\chi$ where $u = 2m[E_R - V(x)]/\hbar$ and $\chi = 2mE_I/\hbar$ which when solved gives $k_R(E,x) = \pm\sqrt{\left(u + \sigma\sqrt{u^2+\chi^2}\right)/2}$ and $k_I = \chi/2k_R(E,x)$ where $\sigma = +1$ when $u > 0$ and $\sigma = -1$ when $u < 0$.

In Regions 1 to 6 of the potential profile of Figure 1.7, the wave function has the form given by Eq. (2.13) with complex coefficients $A_i(E)$ and $B_i(E)$ for i = 1 to 6.

Using the transfer matrix formalism [35., 36.] at the locations, x_i, of the steps in the potential, matrices M_i, for i = 1 to 5, can be defined which relate the $A_i(E)$ and $B_i(E)$ coefficients on the left side of the ith step to the coefficients $A_{i+1}(E)$ and $B_{i+1}(E)$ on the right side through equations $(A_{i+1}(E), B_{i+1}(E)) = M_i \times (A_i(E), B_i(E))$. Uniform m^* is assumed. These matrices are de-

Reproduced with permission of the copyright owner. Further reproduction prohibited without permission.

termined by setting the wave function and its derivative equal on both sides of each potential step. Then

$$M_i = \tag{2.15}$$

$$\frac{1}{2k_{i+1}} \begin{bmatrix} [k_{i+1} + k_i]e^{i(k_i x_i - k_{i+1} x_i)} & [k_{i+1} - k_i]e^{i(-k_i x_i - k_{i+1} x_i)} \\ [k_{i+1} - k_i]e^{i(k_i x_i - k_{i+1} x_i)} & [k_{i+1} + k_i]e^{i(-k_i x_i - k_{i+1} x_i)} \end{bmatrix}$$

For real$E$ the matrices M_i guarantee continuity of current across the potential boundaries at x_i. The coefficients $A_1(E)$, $B_1(E)$, $A_6(E)$ and $B_6(E)$ are then related by the matrix equation:

$$\begin{pmatrix} A_6(E) \\ B_6(E) \end{pmatrix} = \prod_{i=1}^{5} M_i \times (A_1(E), B_1(E)) \tag{2.16}$$

The norm, $\ell(x', x'', E)$, between x' and x'' for a wave function of unit amplitude $|B_6(E)| = 1$ in the anode region ($x > x_5$) is real and is defined for real energies E by:

$$\ell(x', x'', E) = \int_{x'}^{x''} |\psi(E, x)|^2 dx \tag{2.17}$$

Since $|\psi(E, x)|^2$ is normalized in unit length for $x > x_5$, the norm has the units of length which is to be expressed in Å for the simulations reported here. The norm is expected to have sharp maxima versus E at resonance values [25].

Reproduced with permission of the copyright owner. Further reproduction prohibited without permission.

Provided that the sharp maxima do not overlap, they should have a Lorentzian form

$$\ell(E) = \ell(E_0)\Lambda(E) \tag{2.18}$$

where

$$\Lambda(E) = \left[1 + \left(\frac{E - E_0}{\Delta E}\right)^2\right]^{-1} \tag{2.19}$$

and E_0 is the real energy corresponding to the maximum of $\ell(E)$ and ΔE is a measure of the width of the Lorentzian peak. The decay time, τ_d, for an electron in a quasi-level which has the Lorentzian form of Eq. (2.19) is given by Eq. (2.8) with $E_i = \Delta E$ [27].

Peaks in the norm $\ell^l_w(E) = \ell(x_1, x_2, E)$ in Region 2 (left well) of the potential of Figure 1.7 correspond to quasi-levels in an accumulation layer of a DBRTS. Peaks in the norm $\ell^r_w(E) = \ell(x_3, x_4, E)$ in region 4 (right well) correspond to quasi-levels in the well between the two barriers of the DBRTS. The total norm in the two wells for an incident wave function of unit normal amplitude in the the anode region (Region 6) is given by Eq. (2.10).

For the potential of Figure 1.7

$$\ell^j_w(E) = [\,|A_j(E)|^2 + |B_j(E)|^2\,][x_j - x_{j-1}]$$

Reproduced with permission of the copyright owner. Further reproduction prohibited without permission.

$$+ 2\mathrm{Re}\left\{ \frac{A_j(E)B_j^*(E)}{ik_j(E)} \left[e^{i2k_j(E)x_j} - e^{i2k_j(E)x_{j-1}} \right] \right\} \quad (2.20)$$

where j=2 for the left well and j=4 for the right well.

It has been shown [59.] for a $Ga_{0.47}In_{0.53}As$-$Al_{0.48}In_{0.52}As$ based DRTS that the resonant energy values obtained using a position dependent effective mass and a non-parabolicity of the energy band differ from those obtained using a homogeneous effective mass and without including the non-parabolicity by less than 2 Mev. Therefore, a uniform effective mass, m^*, of $0.067m_0$, where m_0 is the free electron mass, is assumed here. This is equal to the gallium arsenide electron effective mass.

Since a solution of the Schrödinger equation is known up to an arbitrary complex constant, $A_1(E)$ is arbitrarily chosen to be $\exp(i\pi/4)/M$ where M is an adjustable real parameter initially chosen to be 1. In Region 1, $B_1(E)$ is 0 since if it were not the wave function would be unbounded as x goes to negative infinity. The coefficients of the wave function $\psi_6(x)$ in Region 6, $A_6(E)$ and $B_6(E)$, are calculated using Eq. (2.16). Since the DBRTS is a reflection structure $|A_6(E)| = |B_6(E)| \equiv M'$. With the initial choice of M=1, $\psi_6(x)$ does not contain an incident component of unit amplitude for all E, that is $M' \neq 1$. For each value of E, the value of M' for $\psi_6(x)$ is determined. The coefficient $A_1(E)$ is replaced by $\exp(i\pi/4)/M'$ and $A_6(E)$ and $B_6(E)$ are recalculated to result in a $\psi_6(x)$ containing an incident compo-

Reproduced with permission of the copyright owner. Further reproduction prohibited without permission.

nent of unit amplitude for $x > x_5$. It is sufficient for M to be chosen to be real since it scales the magnitude of $A_1(E)$ so that $|B_6(E)| = 1$.

The norm $\ell^T(E)$ is calculated for E varying from 0 to V_0 in steps chosen small enough to identify the sharp maxima in $\ell^T(E)$. The computational routine to determine $\ell^T(E)$ is designed to automatically locate the real energy, E_0, corresponding to the maximum of $\ell^T(E)$. This is done by determining the energy corresponding to the maximum in $\ell^T(E)$ for the initial value of the energy step, δE_s, chosen and subdividing the energy range $2\delta E_s$ about this energy to determine a new value for the energy corresponding to the maximum in $\ell^T(E)$. This process is repeated until the maximum value of $\ell^T(E)$ changes by less than 0.5% between successive iterations.

2.3 Norms In the Left and Right Wells

The norms $\ell^L_w(E)$, in the left well, and $\ell^L_w(E)$, in the right well, for $0 < E < 0.3$ eV are plotted in Figure 2.1 and Figure 2.2, respectively, showing the quasi-levels in the potential wells of Region 2 and Region 4 of Figure 1.7 with $d^l_w = d^r_w = 100$Å, $d^l_b = d^r_b = 50$Å, $V_0 = 0.3eV$ and $m^* = 0.067m_0$. The vertical scales of Figures 2.1 and 2.2 are appreciably different. Both $\ell^L_w(E)$ and $\ell^L_w(E)$ have three pairs of closely spaced peaks. The higher energy peak of a pair is at real energy E_{0+} and the lower at real energy E_{0-}. Isolated wells would each have three single peaks. Since

Reproduced with permission of the copyright owner. Further reproduction prohibited without permission.

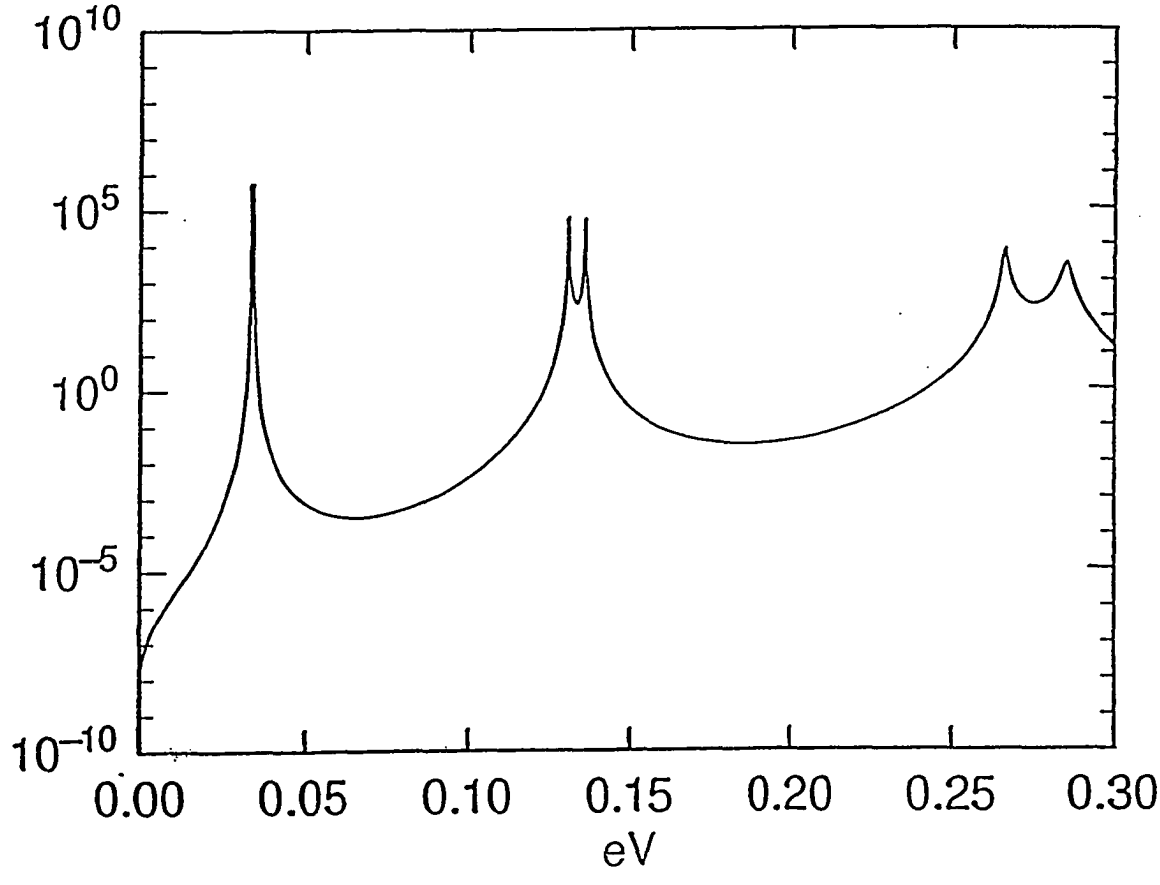

Fig. 2.1

$\ell^l_w(E)$ vs. Energy for $d^l_w = d^r_w = 100\text{Å}$, $d_b = d_b = 50\text{Å}$ and $V_0 = 0.3eV$.

Reproduced with permission of the copyright owner. Further reproduction prohibited without permission.

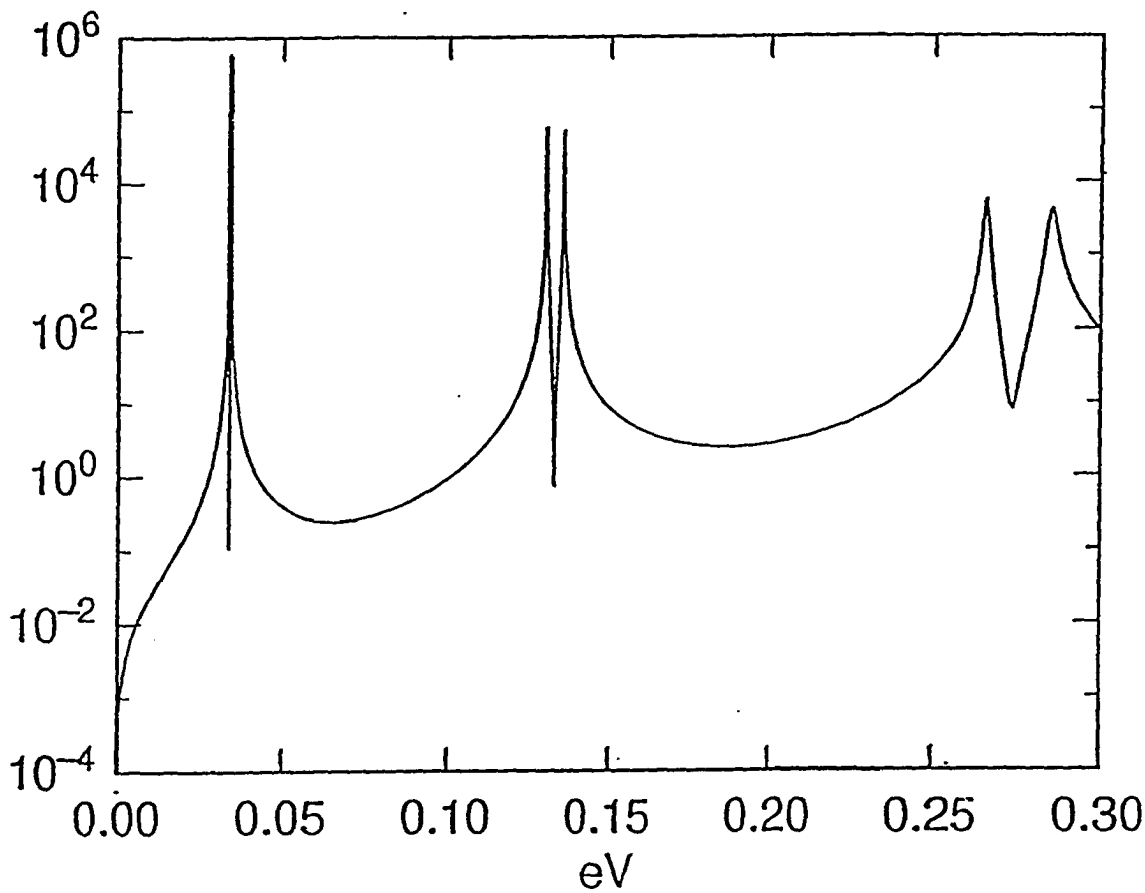

Fig. 2.2

$\ell^r_w(E)$ vs. Energy for $d^l_w = d^r_w = 100\text{Å}$, $d^l_b = d^r_b = 50\text{Å}$ and $V_0 = 0.3eV$.

Reproduced with permission of the copyright owner. Further reproduction prohibited without permission.

the two wells interact through the middle barrier (Region 3), each single peak becomes a double peak. (A heuristic expectation that turns out to be right.) The peaks of the norms in the right and left wells are at the same energy.

As seen in Figures 2.1 and 2.2, the energy spacing between each peak of a pair increases as the energy of the pair increases. This is also expected since at a lower energy there is greater quantum confinement. The magnitude of the wave function $\psi_3(x)$ in Region 3, the barrier between the wells, where $E < V(x)$ is less for lower energies and consequently the interaction between the left and right wells is less and therefore, the coupling between the energy levels contributed by the right and left wells is less and thus the energy separation of the quasi-levels is less.

For both Figures 2.1 and 2.2 the peaks in the norm decrease and the width becomes wider as the energy of the peaks, E_{0+} and E_{0-}, increase. This is not an unexpected result since as the energy of a wave function increases, it more easily leaks out into the anode, Region 6. The broadened peak corresponds to a shorter lifetime which corresponds to a less strongly bound wave function. The peak of the norm corresponds to the buildup of the wave function caused by reflecting off the regions of the potential where $E < V(x)$. As $V_0 - E$ decreases the wave function is less efficiently reflected by the barriers and is more efficiently transmitted through the barriers. Consequently, it is expected that $\ell^l_w(E_{0-}) > \ell^l_w(E_{0+})$ and $\ell^r_w(E_{0-}) > \ell^r_w(E_{0+})$ for each of the three pairs of peaks of Figures 2.1 and 2.2.

Reproduced with permission of the copyright owner. Further reproduction prohibited without permission.

2.4 Characteristics of a Single Pair of Quasi-levels

Figure 2.3 shows on an enlarged scale the energy range corresponding to the middle pair of peaks of Figures 2.1 and 2.2, within which there are two quasi-levels spaced apart by about 6 meV The solid line in Figure 2.3 is the norm $\ell^l_w(E)$ and the dashed line is the norm $\ell^r_w(E)$. The energy of the lower peak, E_{0-}, and the energy of the higher peak, E_{0+}, are the same for both $\ell^l_w(E)$ and $\ell^r_w(E)$. However, the shapes of $\ell^l_w(E)$ and $\ell^r_w(E)$ are not the same. $\ell^r_w(E)$ has a sharp minimum, in the off resonance condition between E_{0-} and E_{0+} which is absent in $\ell^l_w(E)$. For $E_{0-} < E < E_{0+}$ we have $\ell^r_w(E) \ll \ell^l_w(E)$. Therefore, the wave function is predominantly in the left well. In fact, for a real energy, E_m, midway between E_{0-} and E_{0+}, $\ell^l_w(E_m)$ is about three orders of magnitude greater than $\ell^r_w(E_m)$ and thus, the wave function is almost completely in the left well. On the other hand, in the off resonance condition for energies between pairs of peaks $\ell^l_w(E)$ is about three orders of magnitude lower than $\ell^r_w(E)$. Therefore, for these energies the wave function is predominantly in the right well. Therefore, it appears that for energies between the twin peaks an incident electron passes through the right and left barriers and is trapped in the left well. Whereas for energies between pairs of quasi-levels (between doublets), a wave function passes through the right barrier and is reflected from the left barrier resonating more in the right well.

In Figure 2.3 the higher and lower energy peaks for $\ell^l_w(E)$ remain approximately symmetric and Lorentzian as Δx_w is varied and

Reproduced with permission of the copyright owner. Further reproduction prohibited without permission.

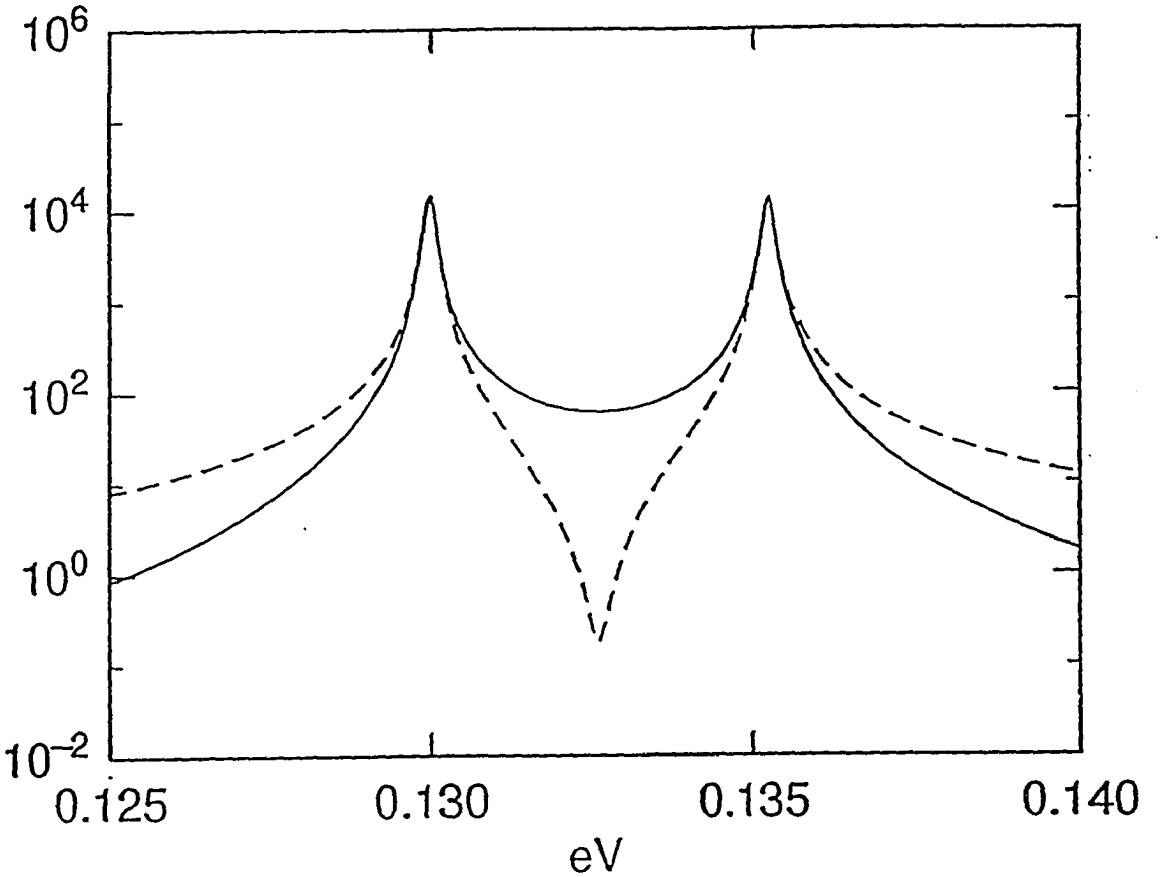

Fig. 2.3

$\ell^l_w(E)$ (solid line) and $\ell^r_w(E)$ (dashed line) vs. energy for $d^l_w = d^r_w = 100\text{Å}$, $d^l_b = d^r_b = 50\text{Å}$ and $V_0 = 0.3eV$.

Reproduced with permission of the copyright owner. Further reproduction prohibited without permission.

one of the higher and lower energy peaks for $\ell'_w(E)$ become asymmetric as Δx_w is varied. The asymmetry results from the sharp minima between the two peaks of $\ell'_w(E)$.

Sharp minima in nuclear scattering cross sections have been measured and shown to be caused by interference between the hard sphere scattering component and the resonant scattering component of the cross section [60, 61]. Sharp minima, referred to as Fano resonances, have been observed in auto-ionization line profiles [62] which have been shown to result from a configuration interaction between an energy level of a discrete energy configuration with a continuum energy configuration containing an energy equal to the discrete energy which results in a broadening of the discrete level [63]. A connection between the nuclear scattering asymmetric cross section and the asymmetric Fano resonance has been indicated [63]. The existence of Fano resonances in quasi-one-dimensional wave guides [64] and in resonance line shapes in quasi-one-dimensional scattering [65] have been theoretically shown. Here it is believed the sharp minima results when there is an interaction between the adjacent resonances of the pair of quasi-levels. This is further discussed later in this chapter.

Figure 2.4 shows a plot of E_{0-} (dashed curve) and E_{0+} (solid curve) vs. Δx_w (defined in Eq. (2.1)) which is varied to observe the crossing behavior of the quasi-levels. This plot shows a classic anticrossing behavior observed in atomic systems [51]. The plot of Figure 2.4 is the same for both right and left wells

Reproduced with permission of the copyright owner. Further reproduction prohibited without permission.

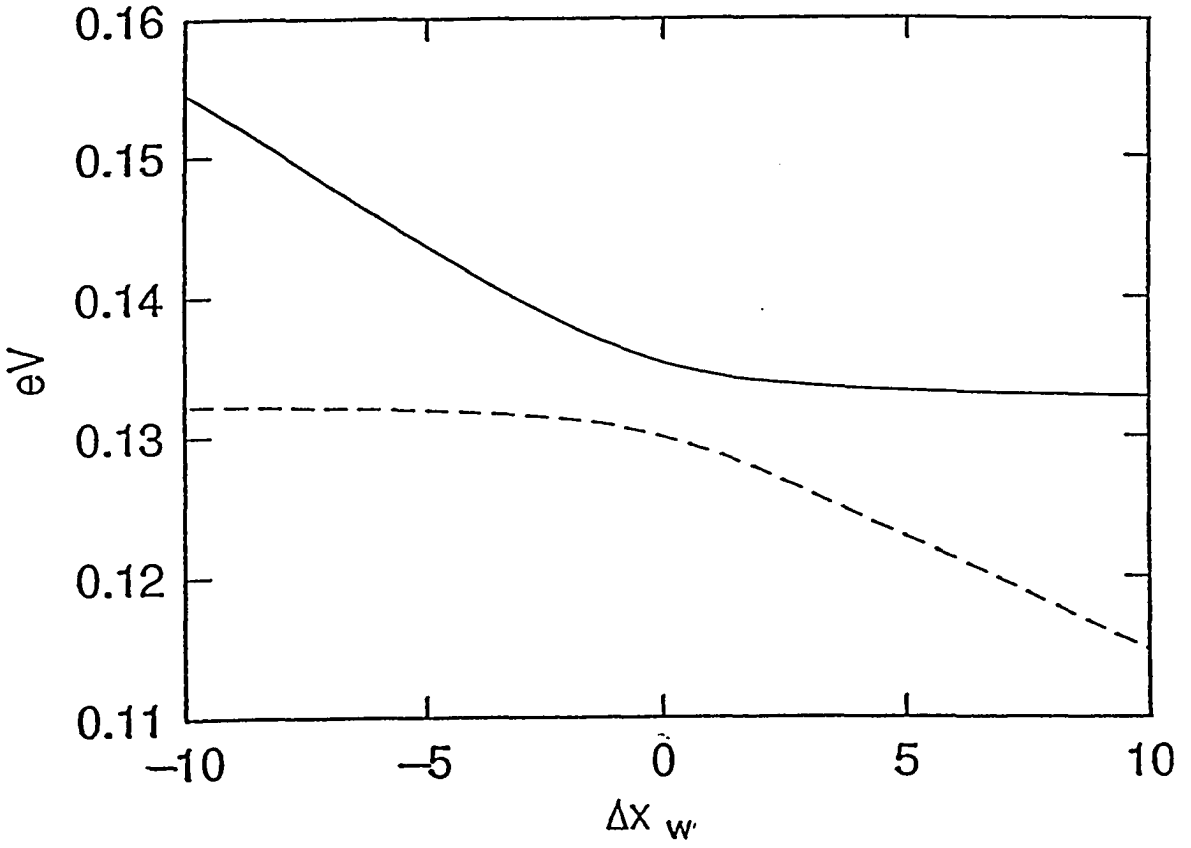

Fig. 2.4

Energy of the higher energy, E_{0+}, (solid line) and lower energy, E_{0-}, (dashed line) peaks of $\ell_w^T(E)$ vs. Δx_w.

Reproduced with permission of the copyright owner. Further reproduction prohibited without permission.

as it is expected to be since the energy levels are a characteristic of the entire potential profile of Figure 1.7. $|E_{0+} - E_{0-}|$ has a minimum for $\Delta x_w = 0$ and increases as $|\Delta x_{well}|$ increases. For larger Δx_w, $E_{0+} - E_{0-}$ varies approximately linearly with Δx_w, as expected.

For $\Delta x_w = 0$, each well contributes a level of the same energy which splits into the two quasi-levels E_{0+} and E_{0-} for the interacting wells. An isolated well having potential profile $V(x) = 0$ for $-d/2 < x < d/2$ and $V(x) = V_0$ for $|x| \geq d/2$ has a set of discrete energy levels, E_n, which decrease in energy as d increases. [66.] L_l, the level in the left well corresponds to E_{acc} in Figure 1.5 and L_r, the level in the right well corresponds to E_{W3} in Figure 1.5. To a first approximation the left and right wells of Figure 1.7 are a combination of two such wells which interact through the middle barrier, Region 3. It is therefore, expected that the quasi-levels in the left and right wells will have a dependence on the width of the wells in a manner similar to the individual non-interacting wells. When $\Delta x_w < 0$, the left well width is narrower than the right well width and for two isolated wells the energy level E_n in the left moves up in energy and remains unchanged in the right well. From Figure 2.4 it is evident that for $\Delta x_w < 0$ only the higher energy quasi-level, E_{0+}, moves up in energy. The lower energy quasi-level remains approximately fixed moving up to asymptotically approach $E_m = (E_{0+} + E_{0-})/2$. For the coupled system it is expected that the energies of both the higher and lower quasi-levels will have a functional relationship on Δx_w. The higher energy in the right well (which is

Reproduced with permission of the copyright owner. Further reproduction prohibited without permission.

fixed at $d_w^l = 100\text{Å}$) is pulled up by the movement of the higher energy level in the left well. Therefore, for $\Delta x_w < 0$ the higher energy level in the left well is strongly coupled to the higher energy level in the right well. The situation is reversed for $\Delta x_w > 0$, i. e. when the left well is wider than the right well, for which for two isolated wells, the energy level E_n in the isolated left well moves down in energy and remains unchanged in the isolated right well. For interacting wells, for $\Delta x_w > 0$, the lower energy level, E_{0-}, moves down in energy while the higher energy level, E_{0+}, remains approximately fixed moving down to asymptotically approach E_m. The lower energy level in the right well is pulled down by the movement of the lower energy level in the left well. Therefore, for $\Delta x_w > 0$, the lower energy level in the left well is strongly coupled to the lower energy level in the right well. The asymptotic energy E_m is a barrier across which the quasi-levels do not move.

In Figure 1.7, if $V_0 \rightarrow \infty$ in Regions 1 and 5, the potential becomes closed on both left and right and, therefore, has discrete energy levels. Analytical expressions which can be graphically solved for the discrete energy levels for this potential [67.] are given by:

$$\tan(kd) = -\frac{k}{\kappa}\tanh(\kappa' \frac{d_b^l}{2}) \qquad (2.21)$$

$$\tan(kd) = -\frac{k}{\kappa}\coth(\kappa' \frac{d_b^l}{2}) \qquad (2.22)$$

Reproduced with permission of the copyright owner. Further reproduction prohibited without permission.

where $k = [(2m^*/\hbar^2)E]^{1/2}$, $\kappa = [(2m^*/\hbar^2)(V_0 - E)]^{1/2}$, $\kappa' = \kappa[1 - \ln(z)/4dk]$ and

$$z = \frac{1 + \tan(\eta k \Delta x_w)[1 + \frac{k}{\kappa}\tan(kd)]/[\tan(kd) - \frac{k}{\kappa}]}{1 + \tan(\eta k \Delta x_w)[1 - \frac{k}{\kappa}\tan(kd)]/[\tan(kd) + \frac{k}{\kappa}]} \tag{2.23}$$

where $\eta = 1$ when $d = d_w^l$ and $\eta = -1$ when $d = d_w^r$. When $V_0 \to \infty$ in Region 3 these equations reduce to:

$$\tan(kd_w^{l,r}) = 0 \tag{2.24}$$

which have solutions

$$E_n^{l,r} = \frac{1}{2m^*}\left[\frac{\hbar n\pi}{d_w^{l,r}}\right]^2 \quad n = 1, 2, 3 \quad \ldots \tag{2.25}$$

which are the equations for the eigenvalues for isolated left (E_n^l) and right wells (E_n^r). When $d_w^l = d_w^r$, $E_n^l = E_n^r$ for which the graphical solution shows that the two energy levels of the same energy, one each from the right and left wells, are split into higher, E_h and a lower, E_l discrete energy levels by the interaction between the right and left wells through the barrier between them. A graphical solution of Eqs. (2.21) and (2.22) would show the anti-crossing behavior shown in Figure 2.4.

The electric-field-dependent intrinsic lifetime of resonances in biased multiple quantum wells have been studied using a complex energy analysis based on an Airy-function transfer matrix description of tunneling using a two level model approximation

Reproduced with permission of the copyright owner. Further reproduction prohibited without permission.

to the quantum resonances [69, 70]. The trend in the movement of the quasi-levels of Figure 2.4 is shown by a simple two level model [71]. A pair of quasi-levels can be considered to a first approximation as a two level system in isolation from the other pairs or quasi-levels. The total Hamiltonian of the system, $\mathscr{H}$, has orthonormal eigenfunctions $|\varphi_l>$ and $|\varphi_r>$, corresponding to eigenvalues E_l and E_r, respectively. $\mathscr{H}$ can be represented by the hermitian matrix:

$$\begin{bmatrix} E_l & E_s \\ E_s & E_r \end{bmatrix} \tag{2.26}$$

where $E_s = <\varphi_l|\mathscr{H}|\varphi_r> = <\varphi_r|\mathscr{H}|\varphi_l>$, $E_l = <\varphi_l|\mathscr{H}|\varphi_l>$ and $E_r = <\varphi_r|\mathscr{H}|\varphi_r>$. The eigenvalues of this matrix are:

$$E_{0\pm} = \frac{1}{2}(E_l + E_r) \pm \frac{1}{2}\sqrt{(E_l - E_r)^2 + 4E_s^2} \tag{2.27}$$

where E_l and E_r correspond to the energy levels of isolated left and right wells, respectively. If $E_l = E_r = E_m$, i.e. $\Delta x_w = 0$, $E_\pm = E_m \pm E_s$. Thus, the two levels from the isolated left and right wells are split with an energy separation of $2E_s$. If $\Delta x_w \neq 0$, $E_l = E_m + \varepsilon$ and $E_r = E_m$ with eigenvalues: $E_{0\pm} = E_m + (\varepsilon/2) \pm \sqrt{(\varepsilon/2)^2 + E_s^2}$ where $\varepsilon = \Delta x_w \alpha(E)$, the change in the energy of a quasi-level as the left well width is varied and $\alpha(E)$ is the rate of change of the energy of a quasi-level with respect to d_w^l which results in eigenvalues:

Reproduced with permission of the copyright owner. Further reproduction prohibited without permission.

$$E_{0\pm} = E_m - \Delta x_w \frac{\alpha(E)}{2} \pm \sqrt{\left(\Delta x_w \frac{\alpha(E)}{2}\right)^2 + E_s^2} \qquad (2.28)$$

which is an equation of a hyperbola with asymptotes $E = E_m$ and $E = E_0 - (\alpha(E)/2)\Delta x_w$ which generally agree with the plots in Figure 2.4 for $E_m = 0.1325eV$ and $\alpha(E) = 0.0035eV/\text{Å}$. Thus, for $\Delta x_w > 0$ both E_{0+} and E_{0-} decrease and for $\Delta x_w < 0$ both E_{0+} and E_{0-} increase as shown in Figure 2.4. One of these levels, depending on whether Δx_w is greater or less than 0 has an approximate linear dependance on Δx_w while the other asymptotically approaches E_m. This can be understood by considering the behavior of the logarithmic derivative of $\psi(x)$ (at $x = x_S$) given by Eq. (2.13) which can be written as: [72.]

$$\frac{d\psi(x)/dx}{\psi(x)} = -k(E)\tan\left[k(E)x + \frac{\theta(E,x)}{2}\right] \qquad (2.29)$$

which is 0 at an energy $E_{0\pm}$ corresponding to a resonance (i.e. $kx + \theta/2 = n\pi$ for n even integers) and goes to $\pm\infty$ between E_{0-} and E_{0+} (i.e. $kx + \theta/2 = n\pi/2$ for n odd integers) which are the boundaries across which the energy level does not cross as Δx_w is varied from 0. Eq. (2.29) follows from Eq. (2.13) if $A(E)/B(E)$ is replaced by $\exp[i\theta(E, x)]$ where $\theta(E, x)$ is the phase between the in going and out going waves. Eq. (2.29) is evaluated at $x = x_S$, i.e. just outside of the reflecting potential. The agreement between the values for $E_0 \pm$ from Eq. (2.27) with the plot of Figure 2.4 is improved by either using higher order terms of Δx_w in the equation for ε or by fitting a function of another form for ε. The following functional form $\varepsilon = \varepsilon' = -\Delta x_w E_m$

Reproduced with permission of the copyright owner. Further reproduction prohibited without permission.

$(0.016 + 0.001\ \exp(\Delta x_w/2))$ gives a close fit between the two level model prediction and the algebraic model calculation. Thus the two level model accurately predicts the $E_{0\pm}(\Delta x_w)$ computed by the algebraic model.

Figure 2.5 shows $\ell^l_w(E)$ (solid curve) and $\ell^r_w(E)$ (dashed curve) for the middle pair of peaks of Figures 2.1 and 2.2 for $\Delta x_w = 10$Å ($d^l_w > d^r_w$). The sharp minima of $\ell^r_w(E)$ shifts towards the lower energy peak of $\ell^r_w(E)$ which becomes more asymmetric than it is at $\Delta x_w = 0$. The higher energy peak of $\ell^r_w(E)$ becomes more symmetric. The integrated norm within a quasi-level, given by the integral of $\ell^r_w(E)$ over an energy range about E_0 increases for the higher energy peak of $\ell^r_w(E)$ and decreases for the lower energy peak of $\ell^r_w(E)$. Therefore, norm shifts from the lower energy peak to the higher energy peak of $\ell^r_w(E)$ as Δx_w increases from $\Delta x_w = 0$. As described above for $\Delta x_w > 0$, the lower energy level in the left well behaves more like the energy level of an isolated well and pulls the lower energy level in the right well down from its value at $\Delta x_w = 0$ while the upper energy level (in the right and left wells) remains approximately unchanged. Since the right well width remains unchanged it corresponds to an isolated right well for which the energy is fixed at a value midway between E_{0+} and E_{0-}. Therefore, in the right well the norm shifts into the upper energy level from the lower energy level as Δx_w increases from $\Delta x_w = 0$ and the upper energy level moves down to its value when there is no coupling to the left well.

Reproduced with permission of the copyright owner. Further reproduction prohibited without permission.

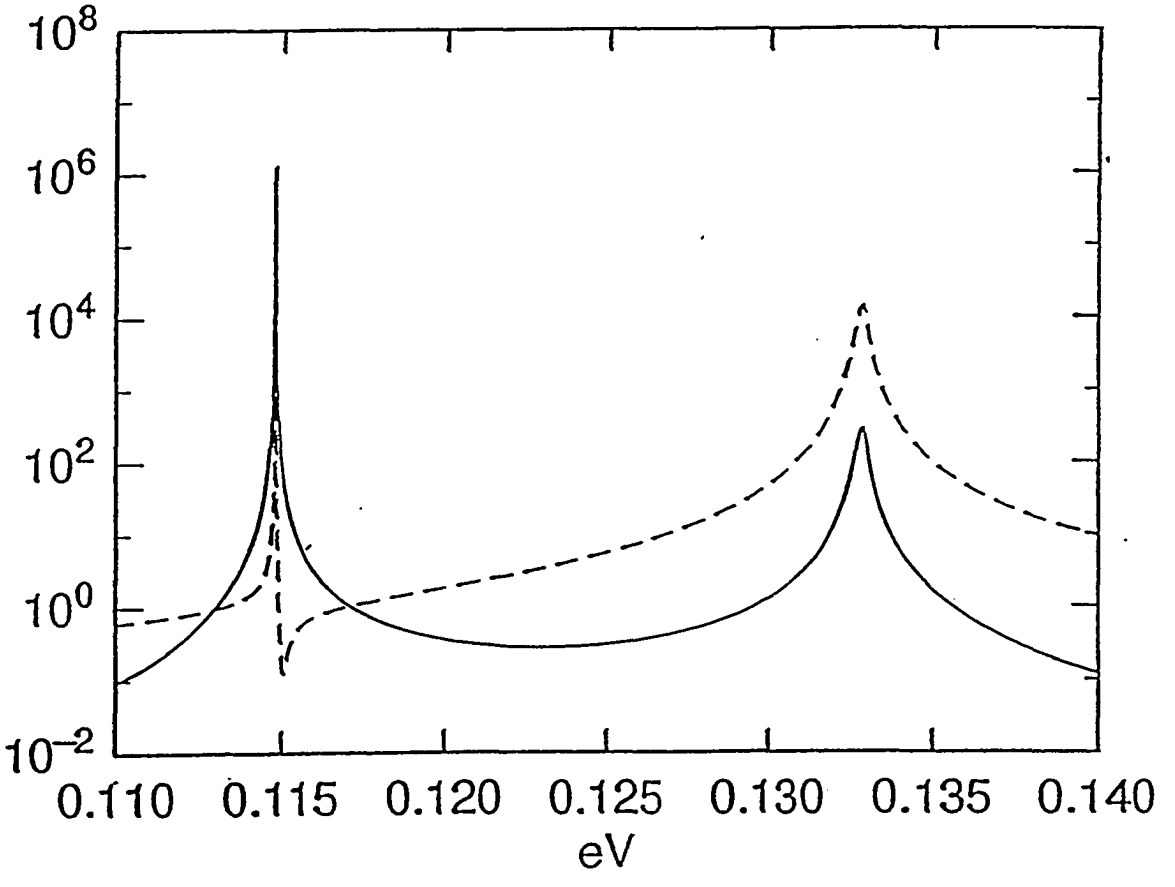

Fig. 2.5

$\ell^l_w(E)$ (solid line) and $\ell^r_w(E)$ (dashed line) vs. energy for $d^l_w = 110\text{Å}$, $d^r_w = 100\text{Å}$, $d^l_b = d^r_b = 50\text{Å}$, and $V_0 = 0.3eV$.

Reproduced with permission of the copyright owner. Further reproduction prohibited without permission.

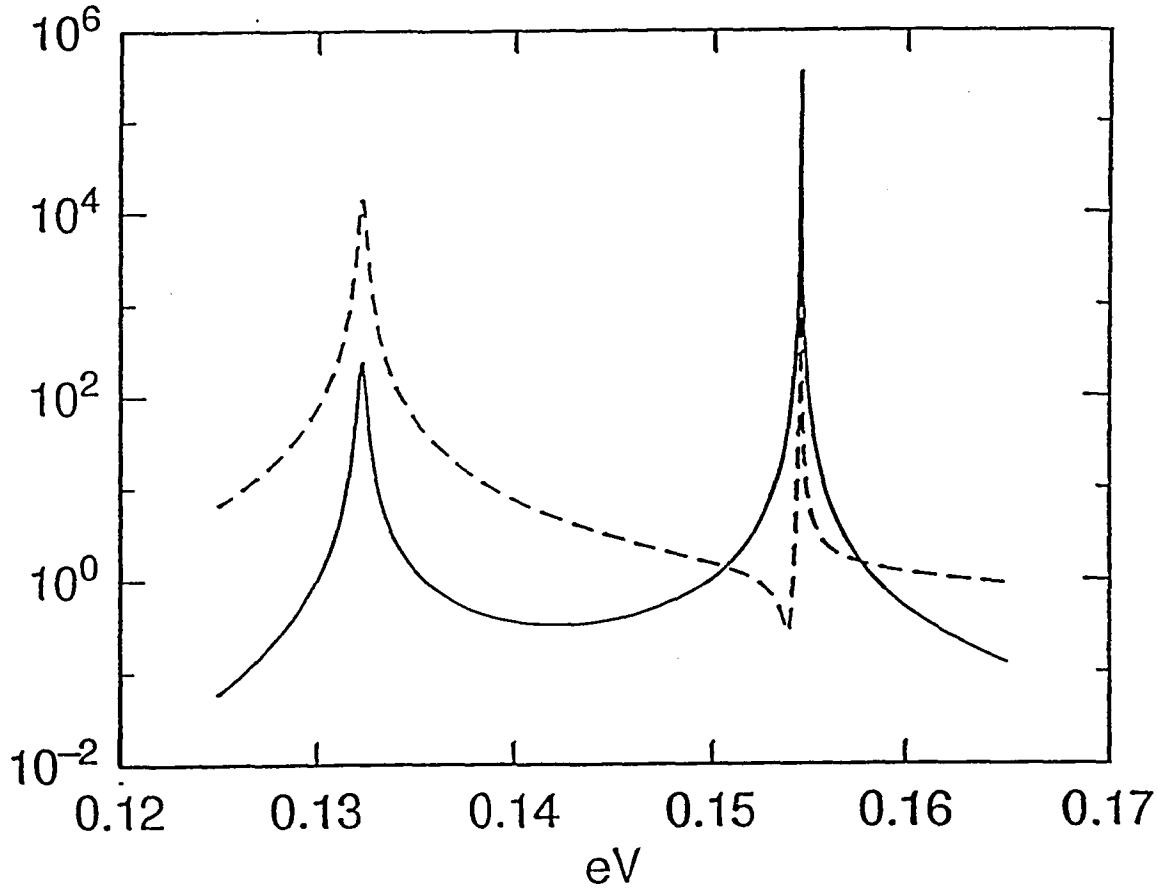

Fig. 2.6

$\ell^l_w(E)$ (solid line) and $\ell^r_w(E)$ (dashed line) vs. Energy for $d^l_w = 90\text{Å}$, $d^r_w = 100\text{Å}$, $d^l_b = d^r_b = 50\text{Å}$, and $V_0 = 0.3eV$.

Reproduced with permission of the copyright owner. Further reproduction prohibited without permission.

Figure 2.6 shows $\ell^{l}_{w}(E)$ (solid curve) and $\ell^{r}_{w}(E)$ (dashed curve) for the middle pair of peaks of Figures 2.1 and 2.2 for $\Delta x_w = -10$Å. This is essentially the condition opposite to that of Figure 2.5 and the shifting of the norm is opposite to that of Figure 2.5. The sharp minima of $\ell^{r}_{w}(E)$ shifts towards the higher energy peak. The higher energy peak of $\ell^{r}_{w}(E)$ becomes more asymmetric than it is at $\Delta x_w = 0$ and the lower energy peak of $\ell^{r}_{w}(E)$ becomes more symmetric. The integrated norm within a quasi-level, given by the integral of $\ell^{r}_{w}(E)$ over an energy range about E_0 increases for the lower energy peak of $\ell^{r}_{w}(E)$ and decreases for the higher energy peak of $\ell^{r}_{w}(E)$. Therefore, norm shifts from the higher energy peak to the lower energy peak of $\ell^{r}_{w}(E)$ as Δx_w decreases from $\Delta x_w = 0$. As described above for $\Delta x_w < 0$, the higher energy level in the left well behaves more like the energy level of an isolated well and pulls the higher energy level in the right well up from its value at $\Delta x_w = 0$ while the lower energy level remains approximately unchanged. Since the right well width remains unchanged, for an isolated right well, the energy would be fixed at a value midway between E_{0+} and E_{0-}. This corresponds to the lower energy level in the right well. Therefore, in the right well the norm shifts into the lower energy level from the higher energy level as Δx_w decreases from $\Delta x_w = 0$ and the lower energy level moves up to its value when there is no coupling to the left well.

From Figures 2.5 and 2.6 it is apparent that the sharp dip in $\ell^{r}_{w}(E)$ moves, as Δx_w varies from 0, towards the quasi-level which has a significant change in energy as $|\Delta x_w|$ increases, i.e. E_{0+}

Reproduced with permission of the copyright owner. Further reproduction prohibited without permission.

when $\Delta x_w < 0$ and E_{0-} when $\Delta x_w > 0$. These are the levels which the left well is strongly coupled to and which are not the levels which the right well would be in as a isolated well.

Figure 2.7 shows for the left well, a plot of the peak of the norm $\ell^l_w(E_{0-})$ for the lower energy level (dashed curve) and a plot of the peak of the norm $\ell^l_w(E_{0+})$ (solid curve) for the higher energy level vs. Δx_w. For $\Delta x_w = 0$, $\ell^l_w(E_{0-})$ is approximately equal to but slightly less than $\ell^l_w(E_{0+})$. For $\Delta x_w < 0$, $\ell^l_w(E_{0+})$ becomes much greater than $\ell^l_w(E_{0-})$ and for $\Delta x > 0$ $\ell^l_w(E_{0+})$, becomes much less than $\ell^l_w(E_{0-})$.

Comparing Figures 2.4 and 2.7, it is seen that for $\Delta x_w < 0$, E_{0+} increases and $\ell^l_w(E_{0+})$ increases, but E_{0-} remains about the same and $\ell^l_w(E_{0-})$ decreases. For $\Delta x_w = -10\text{Å}$, $\ell^l_w(E_{0+})$ is between 1 and 2 orders of magnitude greater than its value when $\Delta x_w = 0$ and $\ell^l_w(E_{0-})$ is between 1 and 2 orders of magnitude less than its value at $\Delta x_w = 0$. Therefore, as Δx_w becomes more negative, the norm in the left well shifts from the peak at lower energy to the peak at higher energy. Since for $\Delta x_w < 0$ the upper energy level behaves more like an energy level in an isolated well, it is not unexpected that the norm shifts into this level from the lower level.

Again comparing Figures 2.4 and 2.7, it is seen that for $\Delta x_w > 0$, E_{0-} decreases and $\ell^l_w(E_{0-})$ increases, but E_{0+} remains about the same and $\ell^l_w(E_{0+})$ decreases. For $\Delta x_w = 10\text{Å}$, $\ell^l_w(E_{0-})$

Reproduced with permission of the copyright owner. Further reproduction prohibited without permission.

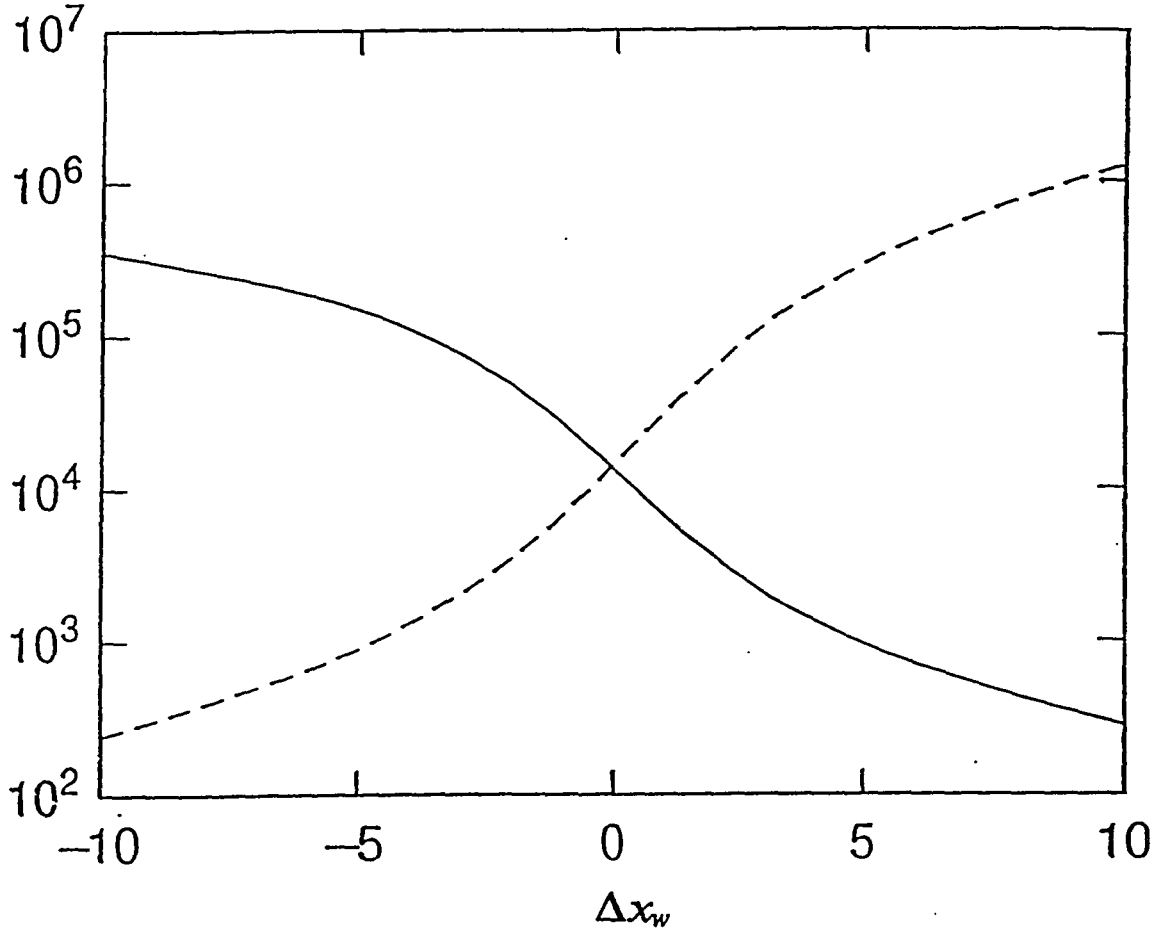

Fig. 2.7

$\ell^l_w(E_{0+})$ (solid line) and $\ell^l_w(E_{0-})$ (dashed line) vs. Δx_w for $d^r_w = 100\text{Å}$, $d^l_b = d^r_b = 50\text{Å}$, and $V_0 = 0.3eV$.

Reproduced with permission of the copyright owner. Further reproduction prohibited without permission.

is about 2 orders of magnitude greater than its value when $\Delta x_w = 0$ and $\ell^l_w(E_{0+})$ is between 1 and 2 orders of magnitude less than its value at $\Delta x_w = 0$. Therefore, as Δx_w becomes more positive, norm shifts from the peak at higher energy to the peak at lower energy. Since for $\Delta x_w > 0$ the lower energy level behaves more like an energy level in an isolated well, it is not unexpected that the norm shifts into this level from the higher level. Consequently, the crossing of the peaks of the norms in the left well as Δx_w varies is expected.

Figure 2.8 shows, for the right well, a plot of the peak of the norm at the lower energy level, $\ell^r_w(E_{0-})$ (dashed curve) and a plot of the peak of the norm at the higher energy level, $\ell^r_w(E_{0+})$ (solid curve). For $-10\text{Å} < \Delta x_w < 10\text{Å}$, $\ell^r(E_{0-}) > \ell^r(E_{0+})$. Unlike $\ell^l(E_{0+})$ and $\ell^l(E_{0-})$ which cross at $\Delta x_w = 0$, $\ell^r(E_{0+})$ and $\ell^r(E_{0-})$ anticross in a generally similar way to E_{0+} and E_{0-} as shown in Figure 2.4. The variation in the peak of the norm in the left well is substantially greater than the variation of the norm in the right well. (It is to be noted that the vertical axis in Figure 2.7 is a log scale and in Figure 2.8 is a linear scale.) Comparing Figures 2.4 and 2.8 it is seen that for $\Delta x_w < 0$, E_{0+} increases and $\ell^r_w(E_{0+})$ decreases, but E_{0-} remains about the same and $\ell^r_w(E_{0-})$ remains about the same. For $\Delta x_w = -10\text{Å}$, $\ell^r_w(E_{0-})$ decreases by about 40% from its value when $\Delta x_w = 0$. For $\Delta x_w > 0$, E_{0-} decreases and $\ell^r_w(E_{0-})$ remains about the same, E_{0+} remains about the same and $\ell^r_w(E_{0+})$ increases by about 40 % from its value when $\Delta x_w = 0$. It is expected that when $\Delta x_w < 0$ the norm in the right well will shift into the lower energy quasi-level which is the level

Reproduced with permission of the copyright owner. Further reproduction prohibited without permission.

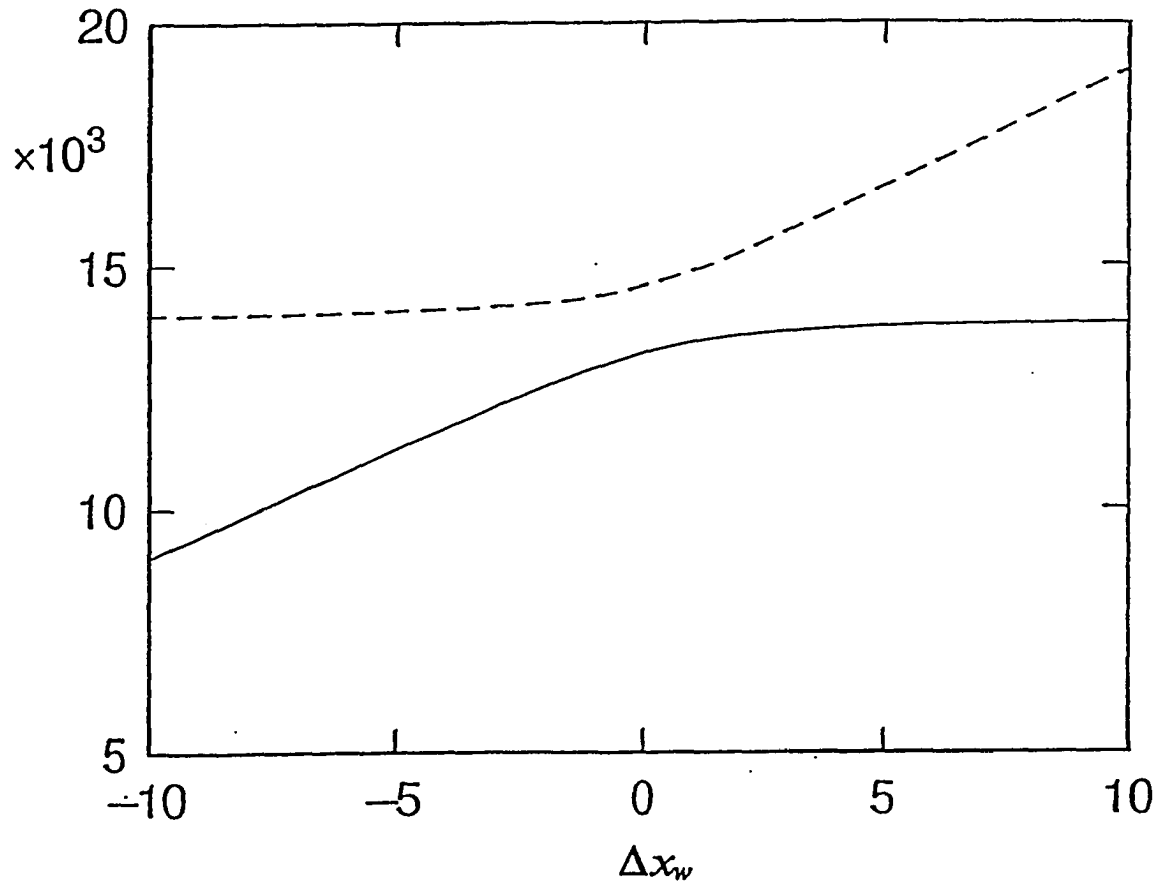

Fig. 2.8

$\ell^r_w(E_{0+})$ (solid line) and $\ell^r_w(E_{0-})$ (dashed line) vs. Δx_w for $d^r_w = 100\text{Å}$, $d^l_b = d^r_b = 50\text{Å}$, and $V_0 = 0.3eV$.

Reproduced with permission of the copyright owner. Further reproduction prohibited without permission.

corresponding to the isolated right well and that when $\Delta x_w > 0$ the norm in the right well will shift into the higher energy quasi-level which is the level corresponding to the isolated right well. Consequently, the anticrossing of the peaks of the norm in the right well is an expected result as is the crossing of the peaks of the norm in the left well.

2.5 Calculation of the Lifetime of the Quasi-levels

The peaks in $\ell^l_w(E)$ and $\ell^r_w(E)$ are in general not symmetric. This is not unexpected since the potential of Figure 1.7 is not symmetric. A wave function in the potential leaks out to the right but not to the left. Eq. (2.16) relates the coefficients of the wave function in Region 6 to Region 1 through the transfer matrix formalism. Eq. (2.16) can be rewritten in the scattering matrix formalism which relates the coefficients of the outwardly moving waves to the inwardly moving waves through the (one dimensional) scattering matrix $S(E)$. For complex energy, E, there are poles of $S(E)$ at which there is no incident wave but only a wave leaking out from within the structure. In the one dimensional reflection situation under investigation here, there is one wave moving to the left and one wave reflected moving to the right. Consequently, for real E the matrix equation reduces to the scalar equation $A_6(E) = S(E)B_6(E)$ where $S(E)$ is given by Eq. (2.5). Therefore, reflection from the potential of Figure 1.7 results in a phase change between the incident and reflected waves.

Reproduced with permission of the copyright owner. Further reproduction prohibited without permission.

When $\ell(E)$ is Lorentzian, ΔE in Eq. (2.19) is equal to E_i, the imaginary part of the complex energy at which there is a pole of $S(E)$. The real part of this complex energy is ideally equal to E_0, the real energy corresponding to the maximum in $\ell^T(E)$. As $\ell^T(E)$ becomes more asymmetric, the real part of the complex energy corresponding to a pole differs from E_0.

The poles of $S(E)$ can be found by locating the zeros $(E_r + iE_i)$ of $S(E)^{-1} = B_6(E)/A_6(E)$ by a Newton iteration in the complex energy domain. This was found to take many iterations. The zeros are more efficiently found by numerically locating the minima of $1/|S(E)|$. This has been done using a routine which automatically finds the minima by alternately varying the real and imaginary part of the complex energy starting from an initial complex energy, E_I. Initially, the imaginary part of the complex energy is moved (in the negative direction) until a minima in $1/|S(E)|$ is found in that direction. From that minima the real part of the complex energy is varied until a minima in $1/|S(E)|$ is found in the new direction. The procedure is repeated until $1/|S(E)|$ is less than a predetermined value which is chosen to be 1×10^{-10}. To minimize the number of computations it is desirable to choose E_I as close to the actual value of the zero of $S(E)^{-1}$ as possible. The E_I chosen is $E_0 + i\Delta E_{ave}$. The real part of E_I is the real energy, E_0, corresponding to a sharp maxima in $\ell^T(E)$. ΔE_{ave} is an average of ΔE determined from the computed values of $\ell(E)$ using $\Delta E = \sqrt{(E - E_0)^2 \ell(E)/\ell(E_0)}$. ΔE is calculated for a number of points to the right and to the left of E_0. It has been found that the calculated values of ΔE vary slightly

Reproduced with permission of the copyright owner. Further reproduction prohibited without permission.

as the value of E moves to the right and left away from E_0 . The average of the values to the left is ΔE_{ave-} and the average of the values to the right is ΔE_{ave+} . Since $\Delta E_{ave-} \neq \Delta E_{ave+}$, $\ell^T(E)$ has a non-symmetrical Lorentzian shape. The degree of asymmetry depends on the value of Δx_w and whether the higher or lower energy peak is under examination. The lifetime is determined from Eq. (2.8) using the imaginary part of the complex energy, E_i, at which $S(E)$ has a pole, i.e. $S(E)^{-1}$ has a zero. Except when ΔE_{ave} is large $E_i \simeq \Delta E_{ave}$.

Figure 2.9 shows a plot of τ_d vs.Δx_w for the quasi-levels of Figure 2.4. $\tau_d^{\ddagger}$ (solid line) is the lifetime of the higher energy level, E_{0+}, and $\tau_{\bar{d}}$ (dashed line) is the lifetime of the lower energy level, E_{0-}. At $\Delta x_w = 0$, $\tau_{\bar{d}}$ is slightly greater than $\tau_d^{\ddagger}$. This is not unexpected since the lower energy peak is more tightly bound in the potential. For $\Delta x_w < 0$, $\tau_d^{\ddagger}$ increases and $\tau_{\bar{d}}$ decreases from their value at $\Delta x_w = 0$. This is expected since for $\Delta x_w < 0$, $d_w^l < d_w^r$ and E_{0+} moves up in energy and $\ell_w^T(E_{0+})$ shifts into the left well causing $\tau_d^{\ddagger}$ to increase and $\ell_w^T(E_{0-})$ shifts into the right well causing $\tau_{\bar{d}}$ to decrease. This is not unexpected since E_{0+} increases while E_{0-} remains about the same. However, $\tau_d^{\ddagger}$ increases at a substantially faster rate than $\tau_{\bar{d}}$ decreases. For $\Delta x_w > 0$, $\tau_{\bar{d}}$ increases and $\tau_d^{\ddagger}$ decreases from their value at $\Delta x_w = 0$. This is expected since for $\Delta x_w > 0$, $d_w^l > d_w^r$ and E_{0-} moves down in energy and $\ell_w^T(E_{0-})$ shifts into the left well causing $\tau_{\bar{d}}$ to increase and $\ell_w^T(E_{0+})$ shifts into the right well causing $\tau_d^{\ddagger}$ to decrease. However, $\tau_{\bar{d}}$ increases at substantially faster rate than $\tau_d^{\ddagger}$ decreases. This is not unexpected since E_{0-} decreases while

Reproduced with permission of the copyright owner. Further reproduction prohibited without permission.

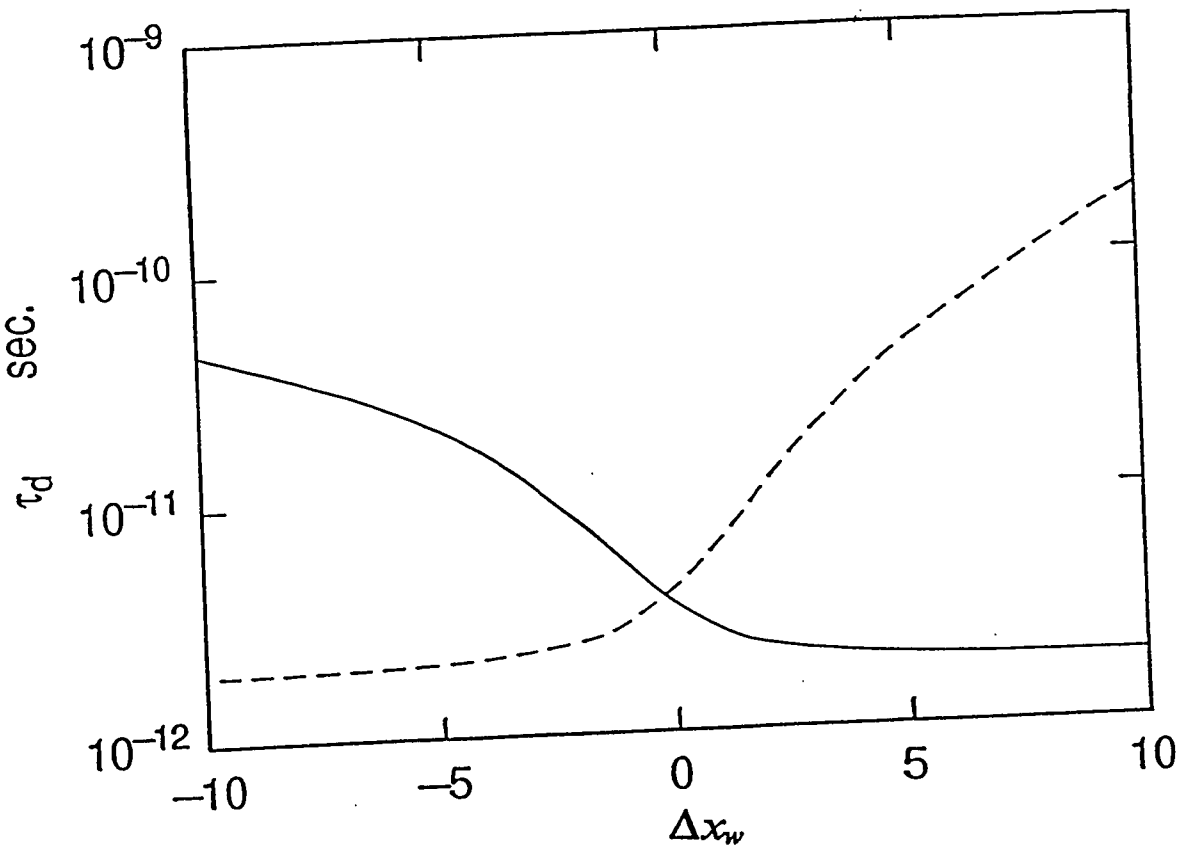

Fig. 2.9

τ_d^+ (solid line) and τ_d^- (dashed line) vs. Δx_w for $d_w^r = 100\text{Å}$, $d_b^l = d_b^r = 50\text{Å}$, and $V_0 = 0.3eV$.

Reproduced with permission of the copyright owner. Further reproduction prohibited without permission.

E_{0+} remains about the same. The lifetimes for the quasilevels using Eq. (2.8) correspond to an energy of a few milivolts whereas the splitting is a minimum of 5 meV from Figure 2.4

Figure 2.10 shows for the higher and lower quasi-levels of Figure 2.4 a plot of $\tau_d^{\ddagger}$ (solid curve) and $\tau_{\bar{d}}$ (dashed curve) vs. the corresponding real part of the complex energy at which $S(E)^{-1} = 0$. Since τ_d is inversely proportional to the imaginary part of the complex energy at which $S(E)^{-1} = 0$, the plot of Figure 2.10 corresponds to the curves in the complex E plane. From Figure 2.9 it is apparent that $\tau_d^{\ddagger}(\Delta x = 10\text{Å}) \approx \tau_{\bar{d}}(\Delta x = -10\text{Å})$. From Figure 2.4 it is apparent that E_{0+} $(\Delta x = 10\text{Å}) \approx E_{0-}$ $(\Delta x = -10\text{Å}) \approx 0.1325eV$. From Figure 2.10 it is seen that $\tau_d^{\ddagger} \approx \tau_{\bar{d}}$ for $E_r \approx 0.1325eV$ which is in agreement with Figures 2.4 and 2.9. From Figure 2.9 it is apparent that $\tau_d^{\ddagger}(\Delta x = -10\text{Å}) < \tau_{\bar{d}}(\Delta x = 10\text{Å})$. From Figure 2.4 it is apparent that $E_{0+}(\Delta x = -10\text{Å}) \approx$ 0.155 eV $> E_{0-}(\Delta x = 10\text{Å}) \approx 0.115eV$. From Figure 2.10 it is seen that the $\tau_d^{\ddagger}(E_r \approx 0.155eV) < \tau_{\bar{d}}(E_r \approx 0.115eV)$ which is in agreement with Figures 2.4 and 2.9. Therefore, as the real part of the complex energy of the higher and lower quasi-levels approach $E_m \approx 0.1325$ eV, the midpoint between E_{0-} and E_{0+}, the lifetime of each quasi-level approaches the same value which is at a minimum value. As the real part of the complex energy of the higher and lower quasi-levels diverge from E_m, the lifetime of each quasi-level increases. The plot in Figure 2.10 is not symmetrical about $E = E_m$, i.e., $\tau_{\bar{d}}(E_m - \delta E) > \tau_d^{\ddagger}(E_m + \delta E)$. This is not unexpected since a quasi-level of lower energy is more tightly bound.

Reproduced with permission of the copyright owner. Further reproduction prohibited without permission.

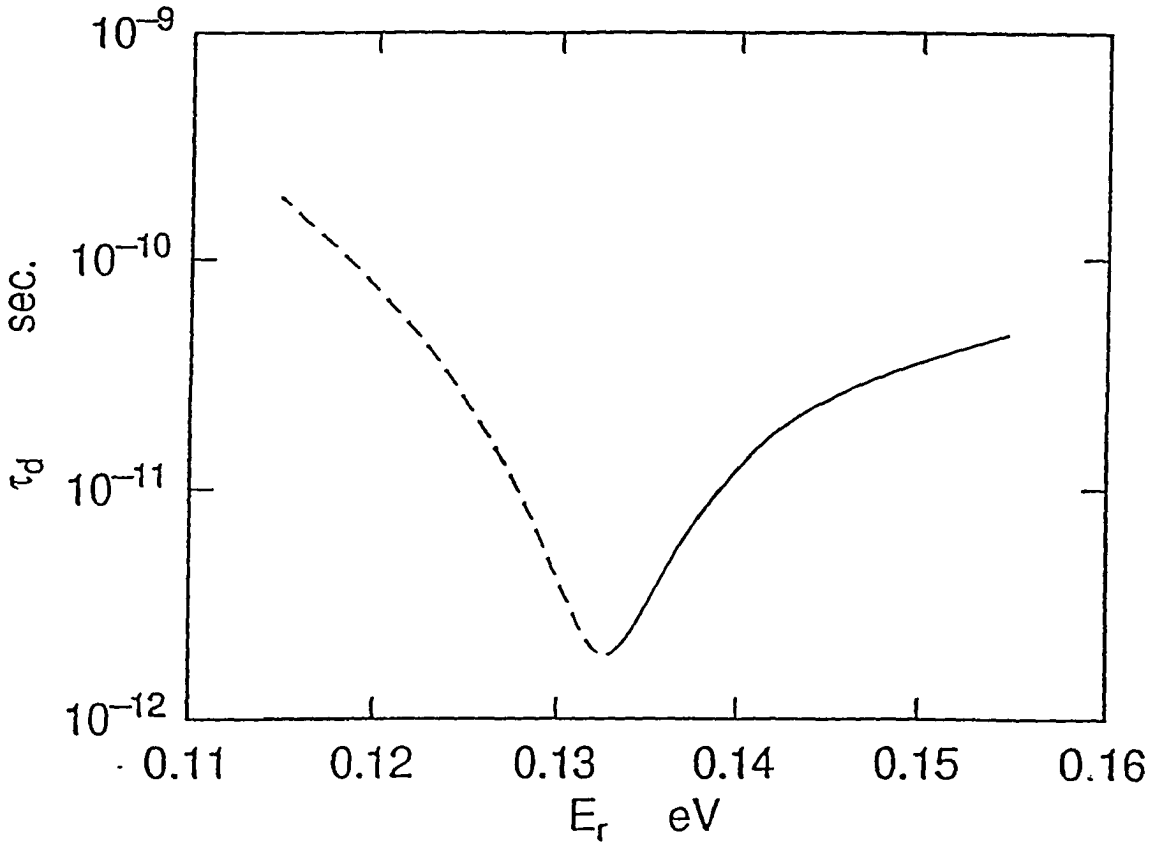

Fig. 2.10

$\tau_d^{\downarrow}$ (solid line) and $\tau_d^{\uparrow}$ (dashed line) vs. E_r for $d_w^r = 100\text{Å}$, $d_b^l = d_b^r = 50\text{Å}$, and $V_0 = 0.3eV$. The minimum point on the dashed curve corresponds to $\Delta x_w = -10\text{Å}$ of Fig. 2.9 and the maximum point corresponds to $\Delta x_w = 10\text{Å}$ of Fig. 2.9. The minimum point on the solid curve corresponds to $\Delta x_w = 10\text{Å}$ of Fig. 2.9 and the maximum point corresponds to $\Delta x_w = -10\text{Å}$ of Fig. 2.9.

Reproduced with permission of the copyright owner. Further reproduction prohibited without permission.

n^l and n^r will be used for the fraction of the norm for a quasi-level at real energy E in the left and right wells, resectvely. The norm in the left well is given by the equation:

$$n^l = \frac{\ell^l_w}{\ell^l_w} \tag{2.30}$$

where ℓ^l_w is given by Eq. (2.10). The fraction of the norm in the right well is $n^r = 1 - n^l$.

The following notation is used: $n^l_{+,w} = n^l(E_{0+}, \Delta x_w, \Delta x_b = 0)$; $n^l_{-,w} = n^l(E_{0-}, \Delta x_w, \Delta x_b = 0)$; $n^l_{+,b} = n^l(E_{0+}, \Delta x_w = 0, \Delta x_b)$; and, $n^l_{-,b} = n^l(E_{0-}, \Delta x_w = 0, \Delta x_b)$.

From Figure 2.11 (on the next page) it is seen that for $\Delta x_w = 0$, $n^l_{+,w} = n^l_{-,w} = 0.5$. ($n^l_{+,w}$ is shown as a solid curve and $n^l_{-,w}$ is shown as a dashed curve.) For $\Delta x_w < 0$, $n^l_{+,w} > n^l_{-,w}$. Again, as Δx_w decreases (the left well width decreases) the higher energy level in the left well moves up in energy pulling up the higher energy level in the right well. Therefore, as Δx_w decreases $\ell^l_w(E_{0+})$ shifts from the right to the left well and $\ell^l_w(E_{0-})$ shifts from the left to the right well. For $\Delta x_w > 0$, $n^l_{-,w} > n^l_{0+,w}$. This is not unexpected since as Δx_w increases, the left well width increases and as explained above the lower energy level in the left well moves down in energy pulling down the lower energy level in the right well. Therefore, for the lower energy quasi-level, as Δx_w increases, $\ell^l(E_{0-})$ shifts from the right to the left wells and $\ell^l(E_{0+})$ shifts

Reproduced with permission of the copyright owner. Further reproduction prohibited without permission.

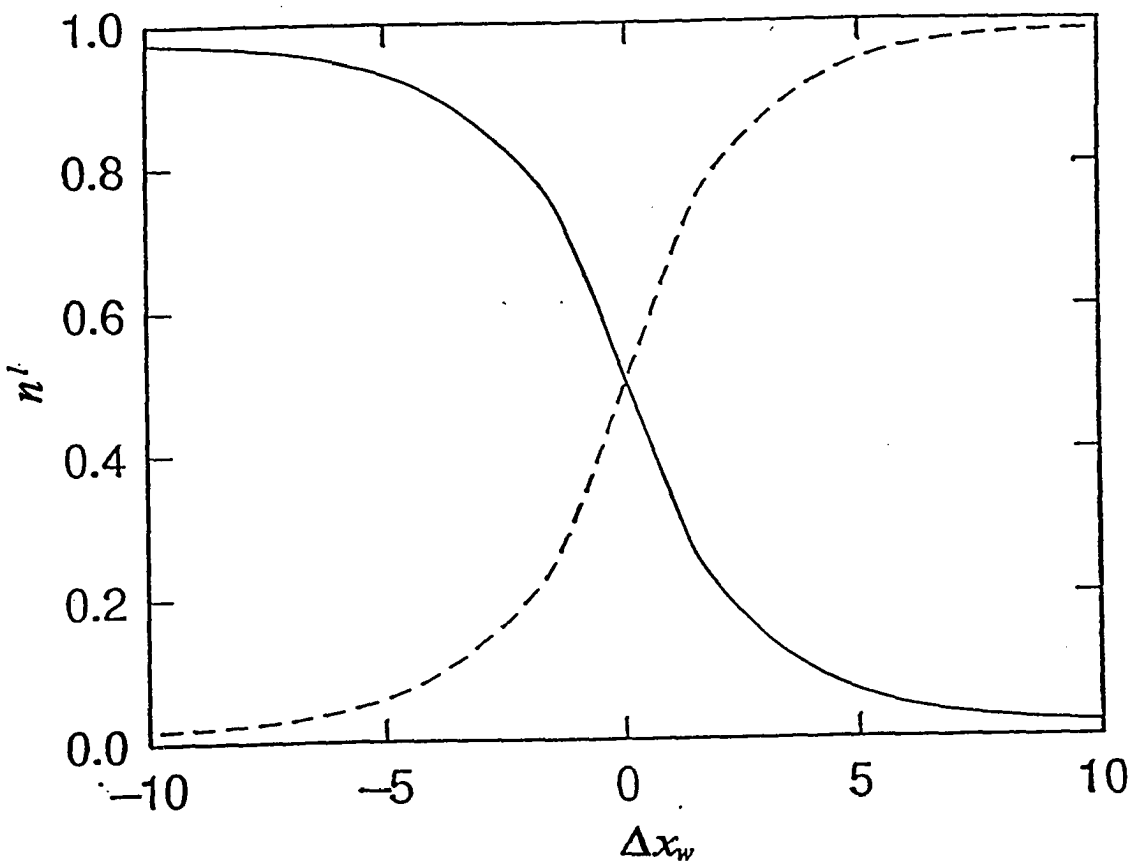

Fig. 2.11

$n^l(E_{0+})$ (solid line) and $n^l(E_{0-})$ (dashed line) vs. Δx_w for $d_w^r = 100\text{Å}$, $d_b^l = d_b^r = 50\text{Å}$, and $V_0 = 0.3eV$.

Reproduced with permission of the copyright owner. Further reproduction prohibited without permission.

from the left to the right wells. Current in a DBRTS with an accumulation layer will result in part from the rate of transition of electrons in the cathode continuum reaching quasi-levels in the accumulation layer. The rate of transition to these quasi-levels will decrease with the energy separation from the cathode level and increase with the magnitude of the norm in the accumulation layer (left well). However, as the norm shifts into the left well the rate of transition to an anode state decreases since the lifetime of the quasi-level increases which tends to decrease the current. Since the increase in the norm in the left well is associated with an increase in the lifetime, these have competing effects on the current. For $\Delta x_w < 0$ the lower energy quasi-level moves further away in energy from the cathode continuum which tends to decrease the transition onto this quasi-level and correspondingly to lower the current and its norm shifts to the left well which tends to increase the rate of transition into this quasi-level. However, since the lifetime increases the current tends to decrease. For $\Delta x_w > 0$ the higher energy quasi-level moves closer in energy to the cathode continuum which tends to increase the current and its norm shifts to the left well which tends to lower the current since the lifetime increases.

Figure 2.11 is a plot of $n^l_{+,w}$ and $n^l_{-,w}$ vs. Δx_w computed from the algebraic model. In the two level model $n^l_{\pm,w} = 1/[1 + E_s^2/(E_{0\pm} - E_r)^2]$. Using the same $\varepsilon = \varepsilon'$ which resulted in a close fit of $E_{0\pm}$ from Eq. (2.18) with $E_{0\pm}$ computed from the algebraic model results in values of $n^l_{\pm,w}$ for the two level model which are in good agreement with those computed from the al-

Reproduced with permission of the copyright owner. Further reproduction prohibited without permission.

gebraic model. It is thus clear that the two level model accurately predicts the properties of $E_{0\pm}$ and the distribution of the peaks of the norm in the left and right wells ($\ell^{l/r}_{w}(E_{0\pm})$) as a function of $\varepsilon = E_l - E_r$ which can therefore be used as a parameter for modeling the current through accumulation layer quasi-levels for the potential of Figure 1.5 as described in Chapter 3.

Figure 2.12 shows the lifetime of the higher energy $\tau^{\ddagger}_{\bar{a}}$ (solid curve) and lower energy $\tau_{\bar{a}}$ (dashed curve) quasi-levels vs. $n^{l}_{+,w}$ and $n^{l}_{-,w}$. Both $\tau^{\ddagger}_{\bar{a}}$ and $\tau_{\bar{decay}}$ increase as $n^{l}_{-,w}$ and $n^{l}_{+,w}$ increase, respectively. This is expected since when more of the wave function is confined in the left well there are two barriers through which the wave function must pass to leak out to Region 6. From Figure 2.12 it is apparent that $\tau^{\ddagger}_{\bar{a}}(n^{l}_{+,w}\approx 0)\approx\tau_{\bar{a}}(n^{l}_{-,w}\approx 0)$. This corresponds to the point in Figure 2.10 for which $E_r\approx 0.1325eV$ and to the points in Figure 2.11 for which $n^{l}_{-,w}(\Delta x_w\approx -10\text{Å})$ and $n^{l}_{+,w}(\Delta x_w\approx 10\text{Å})$, for which it is expected that the lifetimes should be equal. From Figure 2.12 it is apparent that $\tau^{\ddagger}_{\bar{a}}(n^{l}_{+,w}\approx 1) < \tau_{\bar{a}}(n^{l}_{-,w}\approx 1)$. This corresponds to the right most and left most points of Figure 2.10 for which it is expected that $\tau^{\ddagger}_{\bar{a}} < \tau_{\bar{decay}}$. In Figure 2.12 as $n^{l}_{+,w}$ and $n^{l}_{-,w}$ vary from 0 to 1, Δx_w varies from -10Å to 10Å for the lower energy quasi-level and varies from 10Å to -10Å for the higher energy quasi-level.

For $\tau^{\ddagger}_{\bar{a}}(n^{l}_{+,w}\approx 1) < \tau_{\bar{a}}(n^{l}_{-,w}\approx 1)$ which corresponds to the right most and left most points of Figure 6. $\tau^{\ddagger}_{\bar{a}}$ calculated with the algebraic model is reasonably accurately predicted by $\hbar/(2\tau^{\ddagger}_{\bar{a}}) = n^{r}_{\pm,w}\chi^{\ddagger}_{F}T^{\ddagger}_{F}$ where $n^{r}_{\pm,w} = 1 - n^{l}_{\pm,w}$ is the norm fraction in the right well, $\chi^{\ddagger}_{F}$

Reproduced with permission of the copyright owner. Further reproduction prohibited without permission.

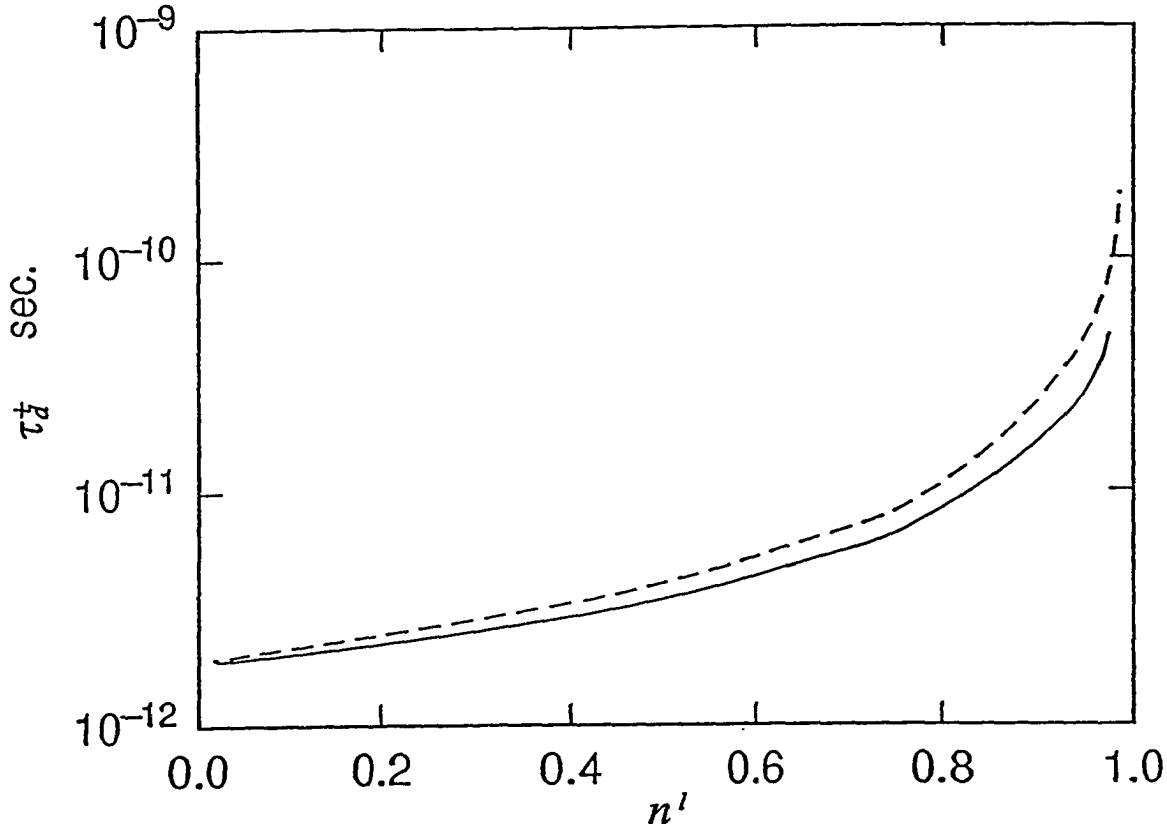

Fig. 2.12

$\tau_d^{\pm}$ (solid line) vs. $n'(E_{0+})$ and $\tau_d^{-}(E_{0-})$ (dashed line) vs. $n'(E_{0-})$ for $d_w' = 100\text{Å}$, $d_b' = d_b' = 50\text{Å}$, and $V_0 = 0.3eV$.

Reproduced with permission of the copyright owner. Further reproduction prohibited without permission.

is the attempt frequency in the right well, and $T_F^{\ddagger}$ is the transition probability through the right barrier. $T_F^{\ddagger} = 1/[1 + 4\sinh^2(d_b'\kappa)/C]$, where $C = 16k^2\kappa^2/(k^2 + \kappa^2)^2$ [17]. k is given by Eq. (2.12) for $V(x) = 0$ and κ is given by the negavive of Eq. (2.12) for $V(x) = 0.3$eV. If $\chi_F^{\ddagger} = L/v(E)$ where $L = 2d_w'$ (which is the distance travelled in the right well between reflections off the left side of the right barrier and the right side of the left barrier.) $v(E)$ is the velocity given by Eq. (2.4). The expression for $\hbar/(2\tau_{\ddagger})$ is an upper bound since the effect of the wave function reaching the left well is not taken into account. The round trip path between reflections from the left side of the right barrier has two components since at the right side of the left barrier, part of the wave is reflected back to the right barrier and part is transmitted through the left barrier to the left side of the left well from which the wave reflects back to the left side of the right barrier. (In this discussion penetration of the wave into the region $x < x_1$ in Figure 1.7 and the reflections from the right side of the left barrier are neglected.) If L is replaced by $L' = 1/[1/2d_w' + 1/[2(d_w' + d_b' + d_w')]]$ in the expression for $\hbar/(2\tau_{\ddagger})$, there is very good agreement with $\tau_{\ddagger}$ calculated with the algebraic model.

2.6 Change in Phase and Number of Electrons Over a Quasi-level

In the potential of Figure 1.7, if the DBRTS structure is located at $x \leq 0$, where $x_5 = 0$, the wave function for $x > 0$ is given by Eq. (2.13) with the coefficients $A_6(E)$ and $B_6(E)$ related by

Reproduced with permission of the copyright owner. Further reproduction prohibited without permission.

$A_6(E) = B_6(E) \exp i\theta$. In the one dimensional case under consideration here, the "dwell time", τ_{dwell}, which is the time spent by an incident particle in a region of space, $x \leq x_5$, is defined by Eq. (2.6) with $\ell(E) = \ell^T(E)$ from Eq. (2.9). For real E a property of the Schrödinger equation is [73]

$$\tau_{dwell} = \hbar \frac{d\theta}{dE} + \frac{\hbar}{2E} \sin\theta \tag{2.31}$$

A derivation of this equation is in the appendix. The first term, $\hbar d\theta/dE$, is the Wigner-Eisenbud delay time or the reflection delay time [74]. It is dominant over the second term at a sharp resonance, being proportional to $1/E_i$.

If $g_0(E)$ is the logarithmic derivative at $x = x_5$ from Eq. (2.29) and if x_5 is set equal to 0 so that the potential of Figure 1.7 is at $x < 0$ after some algebraic manipulation the following equation is obtained from Eq.(2.13) and from the definition of $g(E)$ plus $S = B/A$:

$$S(E) = -\left[\frac{g_0(E) + ik(E)}{g_0(E) - ik(E)} \right] \tag{2.32}$$

The logarithmic derivative can be expanded about E_0 in the series:

$$g_0(E) = g_0(E_0) + \frac{dg_0(E_0)}{dE}(E - E_0) + \ \ldots \tag{2.34}$$

Reproduced with permission of the copyright owner. Further reproduction prohibited without permission.

Then, at a zero of $g_0(E)$, $g_0(E_0) = 0$, and neglecting higher order terms in the series expansion, $S(E)$ at a quasi-level resonance has the form:

$$S(E) = -\frac{E - E_0 - i\Delta E}{E - E_0 + i\Delta E} \tag{2.35}$$

where

$$\Delta E = k(E_0)\left[\frac{dg_0(E_0)}{dE}\right]^{-1} \tag{2.36}$$

As E increases from 0 to V_0, the phase, θ, of $S(E)$ varies rapidly where E passes through a quasi-level. Using Eq. (2.5) we obtain:

$$\frac{d\theta(E)}{dE} = \frac{2}{\Delta E}\Lambda(E) \tag{2.37}$$

where $\Lambda(E)$ is given by Eq. (2.19) and where ΔE is given by Eq.(2.36) from which $\int_{E=-\infty}^{E=+\infty} d\theta(E) = 2\pi$. Therefore, $\theta(E)$ increases by 2π over a resonance. From Eqs. (2.6) and (2.31) neglecting the second term in Eq. (2.31) the following equation is obtained:

$$\frac{d\theta(E)}{dE} = \frac{\ell^T(E)}{\hbar v(E)} \tag{2.38}$$

showing that a plot of $d\theta(E)/dE$ shows the structure of $\ell^T(E)$.

At each of the three pairs of resonances of Figure 2.1 there is a 4π change in the value of θ, a 2π increase over each quasi-level.

Reproduced with permission of the copyright owner. Further reproduction prohibited without permission.

Therefore, the 4π increase indicates a double level. Figure 2.13 shows the change in θ over the pairs of quasi-levels shown in Figures 2.1 and 2.2.

In Eq. (2.32) the preceding negative sign corresponds to scattering from a perfectly reflecting potential at the outer boundary of the scattering potential and from Eq. (2.5) corresponds to $\theta = -\pi$. The part of the equation to the right of the negative sign corresponds to the resonance scattering which adds an additional amount to the value of θ. At a resonance $g_0(E) = 0$ so that using Eq. (2.5) $\theta = n\pi$ for n equal to odd integers (excluding 0) at a resonance and thus θ changes by 2π between resonances. Also, from Eq. (2.29) between resonances $g_0 \to \pm\infty$ so that $\theta = n\pi$ for n equal to even integers including 0 between resonances. This is in agreement with the plot of $\theta(E)$ vs. E shown in Figure 2.13.

As seen in Figure 2.13 between the pairs of resonances θ is approximately constant and thus $d\theta/dE \sim 0$. From Figures 2.1 and 2.2 $\ell'_w(E)$ and $\ell''_w(E)$ smoothly reach a minimum value between the pairs of quasi-levels. On the other hand, between E_{0-} and E_{0+} ℓ''_w and consequently ℓ^T_w will have a sharp minimum. On close examination of the plots in Figure 2.13, it is seen that at each resonance the plot of $\theta(E)$ rapidly changes from approximately horizontal to approximately vertical and then back to approximately horizontal. Between pairs of quasi-levels the transition from a large value of $d\theta/dE$, to a small value and back to a large value is over an extended energy range and therefore, $d\theta/dE$ is

Reproduced with permission of the copyright owner. Further reproduction prohibited without permission.

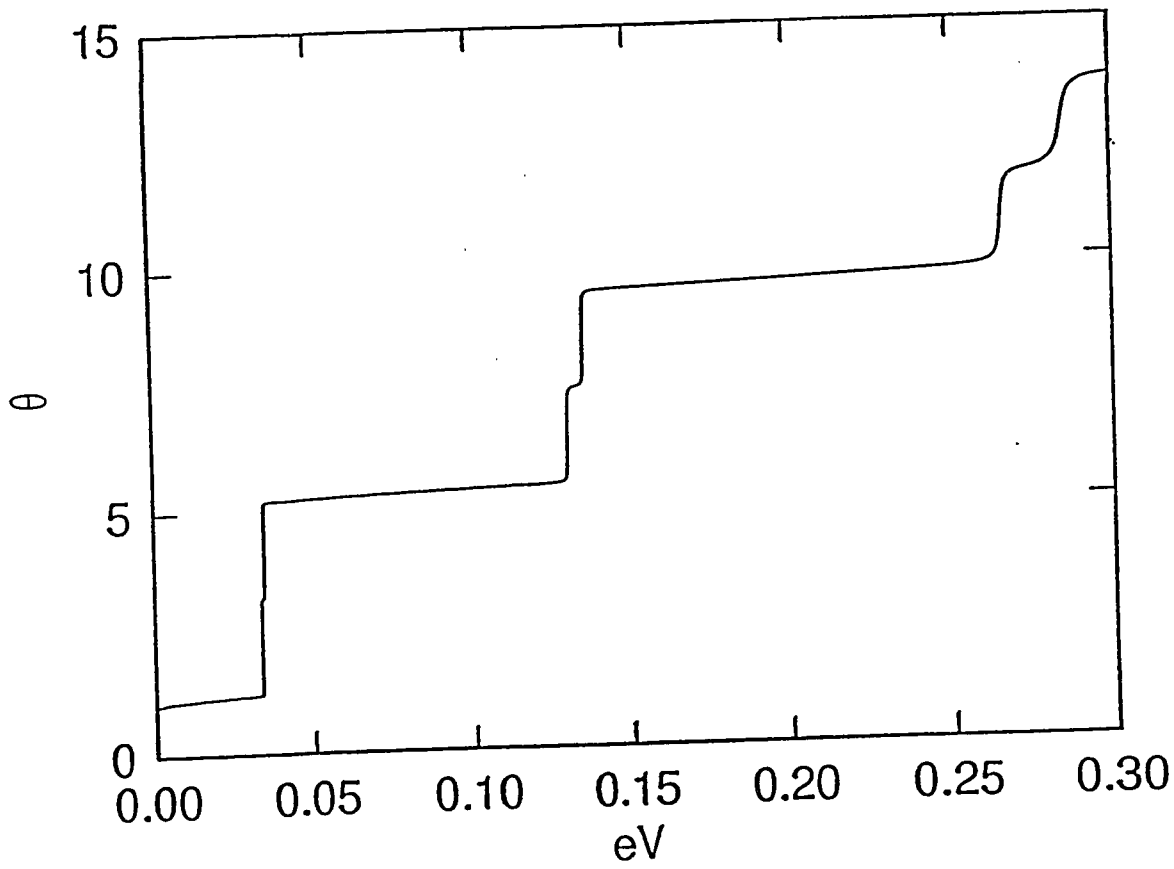

Fig. 2.13

Phase of $S(E)$, θ in units of π for $d_w^l = d_w^r = 100\text{Å}$, $d_b^l = d_b^r = 50\text{Å}$, and $V_0 = 0.3eV$.

Reproduced with permission of the copyright owner. Further reproduction prohibited without permission.

smooth. On the other hand, between quasi-levels of a pair the transition is rapid. If the energy separation of a pair of quasi-levels is very small, the high energy tail of the lower energy quasi-level merges with the low energy tail of the higher energy quasi-level. The transition is sufficiently rapid to form a cusp shown as a sharp minimum in $\ell^T_w(E)$.

Since $|B(E)_6| = 1$ (for $\psi_6(E)$) for $0 < E < V_0$ for a particle incident on the DBRT structure, it is expected that a quasi-level should contain one electron. From Eqs. (2.4) and (2.38) we obtain $d\theta = \ell^T(E)dk$. Therefore, since from Eq. (2.37) $\int_{E=-\infty}^{E=+\infty} d\theta(E) = 2\pi$, over a resonance [75]

$$N(k_0 - \Delta k, k_0 + \Delta k) = \int_{k_0 - \Delta k}^{k_0 + \Delta k} \ell^T(k)\omega(k)dk \qquad (2.39)$$

where $N(k_0 - \Delta k, k_0 + \Delta k)$ is the number of particles contained within the states $k_0 - \Delta k < k < k_0 + \Delta k$ It should equal 1 over a resonance. $\ell^T(k)$ is the norm as a function of k. $\omega(k)$, the density of states, is equal to $1/2\pi$ and k_0 is the value of k corresponding to the peak of $\ell(k)$. It has been found that $N(k(E = 0), k(E = V_0)) = 6$ indicating that each of the six quasi-levels of Figures 2.1 and 2.2 contain one electron where the right boundary x_5 of the potential of Figure 1.7 is set equal to 0 so that the scattering potential is at $x < 0$. The integration can be performed numerically over E giving:

Reproduced with permission of the copyright owner. Further reproduction prohibited without permission.

$$N(0,E') = \int_0^{E'} \ell^T(E) \frac{1}{2\pi} \sqrt{\frac{m^*}{2\hbar^2 E}}\, dE \qquad (2.40)$$

As a check of the numerical routine, N was computed over both E and k and gave the same result to many significant digits.

Figure 2.14 shows $N(E)$ corresponding to the quasi-levels shown in Figures 2.1 and 2.2. At each quasi-level there is a unit change in $N(E)$ indicating that the states associated with each quasi-level contain 1 electron (for each spin state).

2.7 Effect of Narrowing the Outer Barrier

In the potential of an actual DBRTS with an accumulation layer as shown in Figure 1.5, for a quasi-level at an energy E as the applied bias is increased the energy difference between a quasi-level and the top of the right barrier decreases which results in the right barrier being more transparent at that energy. This effect is simulated by decreasing the width of the right barrier. Heuristically it may be expected that the splitting of the degenerate levels of two isolated wells would decrease since as $d_b \to 0$ the right well vanishes. This then raised the physical question of the effect of a broadening of the quasi-levels being comparable to the splitting; what would happen?

Reproduced with permission of the copyright owner. Further reproduction prohibited without permission.

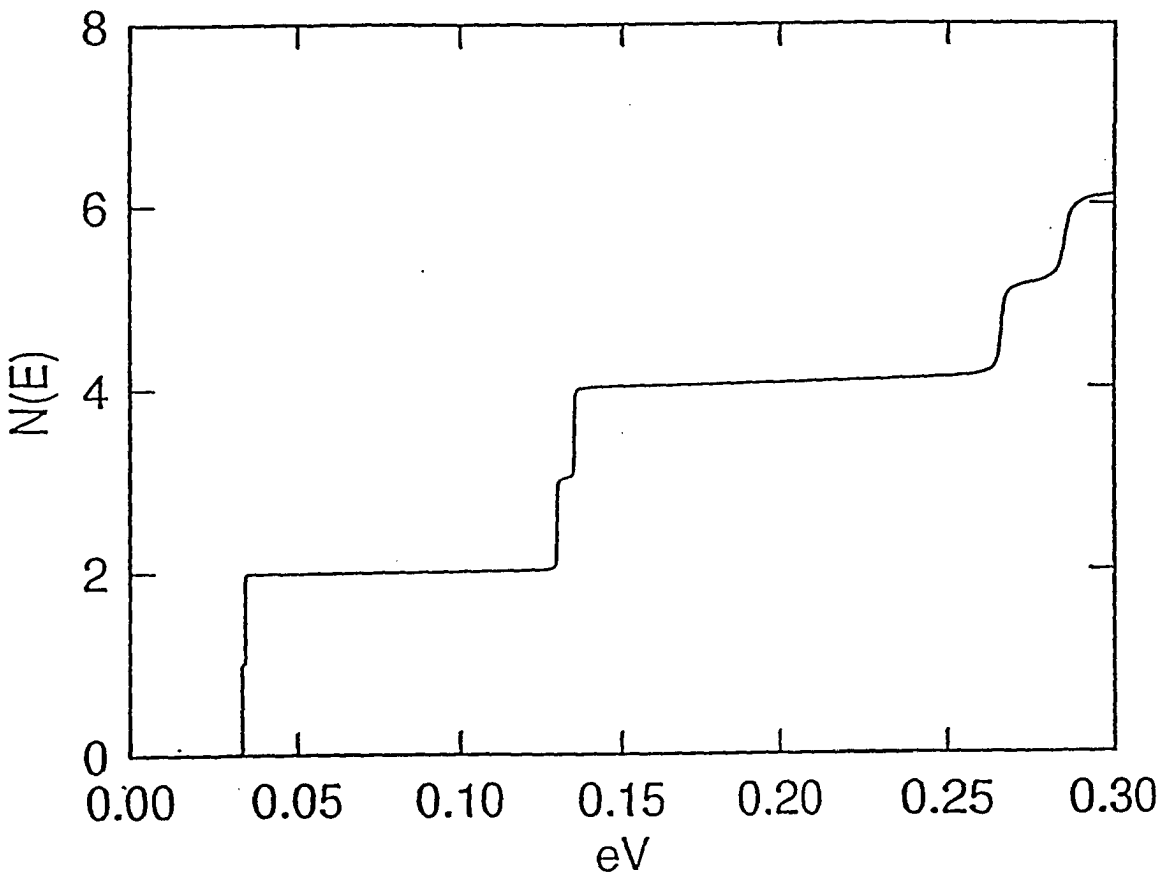

Fig. 2.14

Number of electrons, $N(E)$, vs. energy for $d_w^l = d_w^r = 100\text{Å}$, $d_b^l = d_b^r = 50\text{Å}$, and $V_0 = 0.3eV$.

Reproduced with permission of the copyright owner. Further reproduction prohibited without permission.

When the outer barrier is narrowed there is a change in the shape of $\ell^l_w(E)$ and $\ell^r_w(E)$. As d_b^l is decreased from a value equal to d_b the two peaks in $\ell^l_w(E)$ shown in Figure 2.3 merge into one peak at $d_b^l \simeq 20$Å while the two peaks in $\ell^r_w(E)$ remain separate since the sharp minimum between the two peaks in $\ell^r_w(E)$ as seen in Figure 2.3 remains.

Figure 2.15 shows $\ell^l_w(E)$ (solid curve) and $\ell^r_w(E)$ (dashed curve) for $d_w^l = d_{well}^r = 100$Å and $d_b^l = 30$Å. Comparing Figures 5 and 17 it is apparent that the two peaks of $\ell^l(E)$ are merging and the two peaks of $\ell^r_w(E)$ remain separate.

Figure 2.16 shows $\ell^l_w(E)$ (solid curve) and $\ell^r_w(E)$ (dashed curve) for $d_b^l = 5$Å; $\ell^l_w(E)$ has one peak and $\ell^r_w(E)$ still has two peaks; but barely "peaks"! Notwithstanding that there are two peaks in $\ell^r_w(E)$ the following relationships exist: $\ell^r_w(E_{0-}) > \ell^r_w(E_{0+})$; $\ell^l_w(E_{0+}) > \ell^r_w(E_{0+})$; and $\ell^l_w(E_{0-}) < \ell^r_w(E_{0+})$. Thus the norm of the higher energy peak in the right well is less than the norm in the left well at that energy. Also, the norm of the lower energy peak in the right well is greater than the norm in the left well at that energy. Thus for $d_b^l < 0.5 d_b$ the two peaks of $\ell^T_w(E)$ only appear to merge. For $d_b^l = d_b$ and $d_w^r = d_{well}^l$, $\ell^l_w(E_{0-}) \simeq \ell^r_w(E_{0-})$ and $\ell^l_w(E_{0+}) \simeq \ell^r_w(E_{0+})$. Therefore, under these conditions both higher and lower energy quasi-levels are approximately equally distributed between the left and right wells. However, when the right barrier is thinned, the norms of the higher and lower energy quasi-levels are not equally distributed between the right and left wells.

Reproduced with permission of the copyright owner. Further reproduction prohibited without permission.

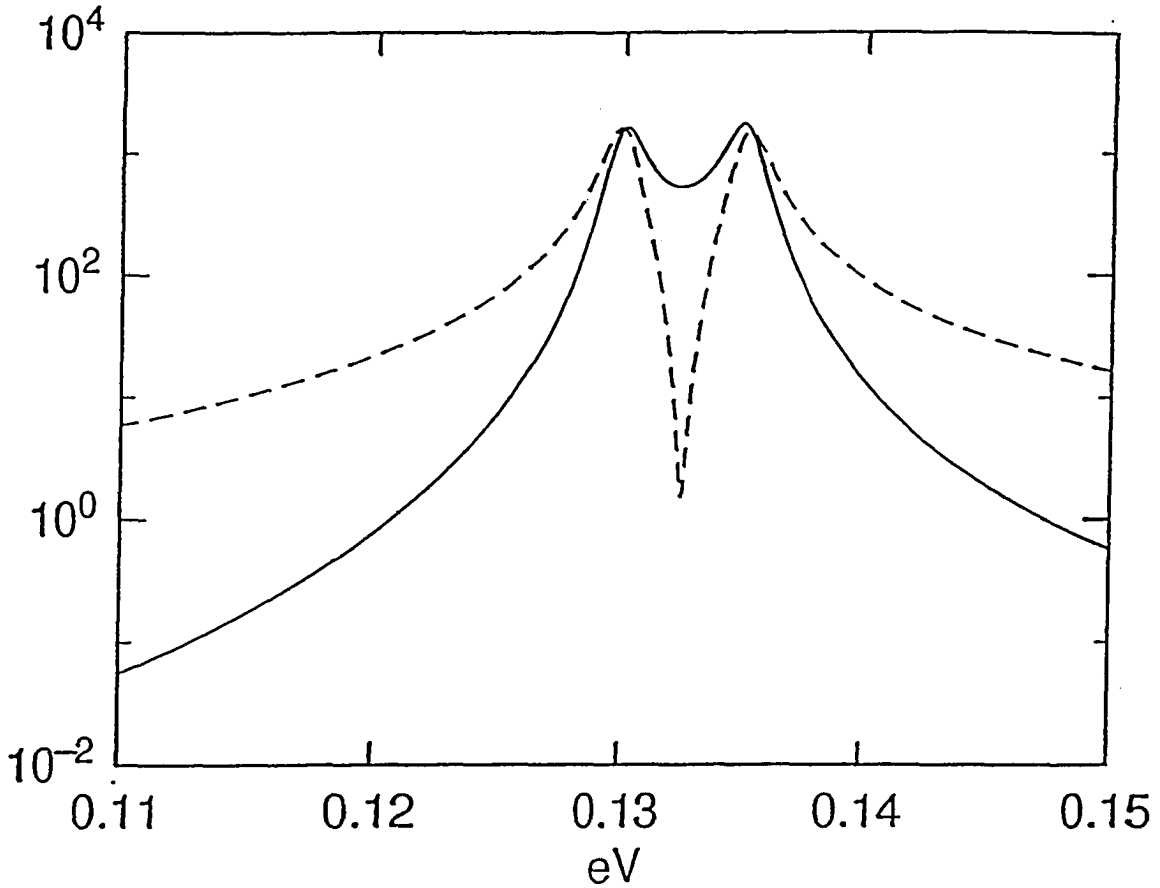

Fig. 2.15

$\ell^l_w(E)$ (solid line) and $\ell^r_w(E)$ (dashed line) vs. energy for $d^l_w = d^r_w = 100\text{Å}$, $d_b = 50\text{Å}$, $d_b = 30\text{Å}$, and $V_0 = 0.3eV$

Reproduced with permission of the copyright owner. Further reproduction prohibited without permission.

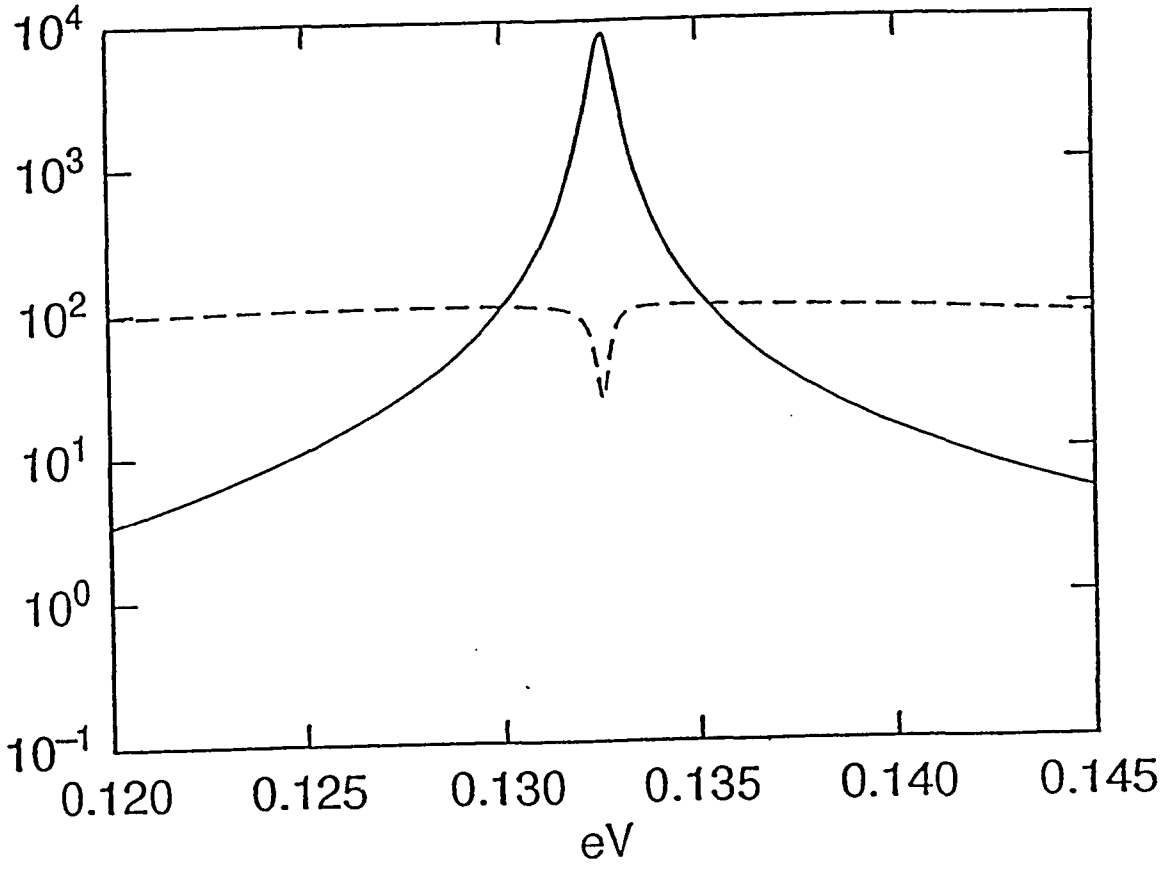

Fig. 2.16

$\ell^l_w(E)$ (solid line) and $\ell^r_w(E)$ (dashed line) vs. energy for $d^l_w = d^r_w = 100\text{Å}$, $d_b = 50\text{Å}$, $d_\delta = 5\text{Å}$, and $V_0 = 0.3eV$.

Reproduced with permission of the copyright owner. Further reproduction prohibited without permission.

Figure 2.17 shows a curve of E_{0-}^{l} and E_{0+}^{l} (which are the real energies corresponding to the lower and higher energy peaks, respectively, of $\ell_w^l(E)$) and E_{0-}^{r} and E_{0+}^{r} (which are the real energies corresponding to the lower and higher energy peaks, respectively, of $\ell_w^r(E)$) versus Δx_b which is defined by Eq. (2.2). From the plot of Figure 2.17 for $\Delta x_b > 30\text{Å}$ it appears that there are three quasi-levels: one from the merged peaks in the left well and two from the two peaks in the right well that remain separate. However, there are only two as determined from the poles of $S(E)$. Also, as will be described below, $\theta(E)$ changes by 4π over these levels. The curves or Figure 2.17 are generated following the procedure described in Section 2.2 which finds the real energy corresponding to a peak. As the width of the right barrier is changed, the energy corresponding to each peak in the left and right wells is determined. When the width of the left and right barriers are equal ($\Delta x_b = 0$), the energy of the higher (lower) energy peak in the left well is equal to the energy of the higher (lower) energy peak in the right well. As the right barrier is made thinner, the peaks in the left well merge, but the peaks in the right well do not merge.

The complex energies at which $S(E)^{-1} = 0$ are determined as described above using as initial starting complex values $E_{0-}^{l} - i\Delta E_{ave-}^{l}$, $E_{0+}^{l} - i\Delta E_{ave+}^{l}$, $E_{0-}^{r} - i\Delta E_{ave-}^{r}$, and $E_{0+}^{r} - i\Delta E_{ave+}^{r}$, where E_{0-}^{l}, E_{0+}^{l}, E_{0-}^{r}, and E_{0+}^{r}, are the real energies corresponding to the peaks of the left and right wells of the lower and higher

Reproduced with permission of the copyright owner. Further reproduction prohibited without permission.

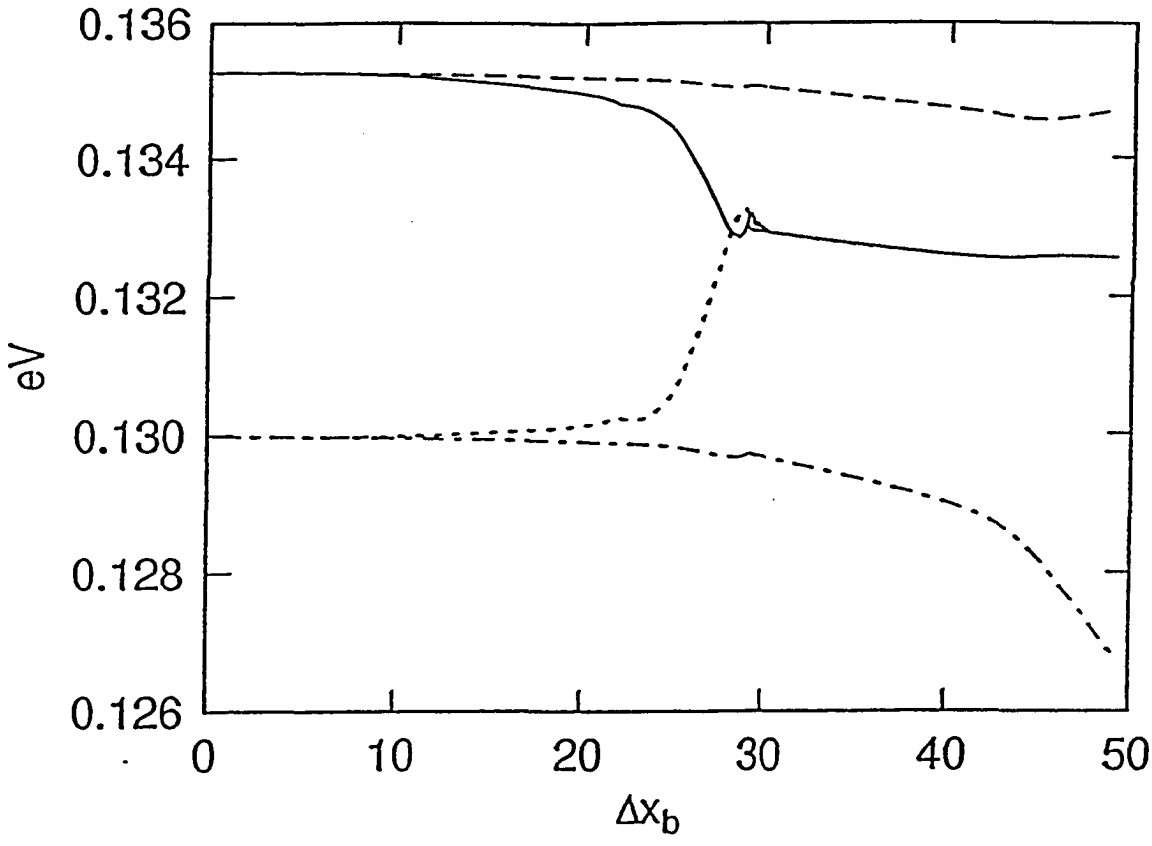

Fig. 2.17

E_{0+}^{l} (solid line), E_{0+}^{r} (dashed line), E_{0-}^{l} (dotted line) and E_{0-}^{r}(dot-dashed line) vs. Δx_b for $d_w^r = d_w^r = 100$Å, $d_b^l = 50$ angstrom, and $V_0 = 0.3$ eV.

Reproduced with permission of the copyright owner. Further reproduction prohibited without permission.

energy peaks, respectively, and where ΔE^{l}_{ave-}, ΔE^{l}_{ave+}, ΔE^{r}_{ave-}, and ΔE^{r}_{ave+}, are the average Lorentzian width determined as described above for the left and right wells and for the lower and higher energy peaks, respectively. When these initial complex energies are used to determine the zeros of $S(E)^{-1}$ there are only two quasi-levels for $1\text{Å} < d^{l}_{b} \leq d^{l}_{b}$.

Figure 2.18 shows a plot of the zeros of $S(E)^{-1}$ in the complex energy plane ($E = E_r + iE_i$) with the imaginary part of the complex energy plotted as $\tau_d = -\hbar/(2E_i)$, from Eq. (2.8). The solid curve is a plot of the path of the higher energy quasi-level and the dashed line is a plot of the path of the lower energy quasi-level in the complex E plane as d^{l}_{b} varies from 50Å to 1Å with $d^{l}_{w} = d^{r}_{well} = 100\text{Å}$. At $d^{l}_{b} = 50\text{Å}$ both the higher and lower quasi-levels have about the same lifetime. Both decrease in value as d^{l}_{b} decreases, as expected. The real part of the complex energy, E_r for both the lower and upper energy quasi-levels remains initially approximately constant and then begins to change rapidly with the E_r decreasing for the upper energy quasi-level and increasing for the lower energy quasi-level with what appears to be a trend towards merging. Before E_r for the lower and higher quasi-levels merge, however, the lifetime of the upper energy quasi-level rapidly increases to a value at $d^{l}_{b} = 1\text{Å}$ approximately equal to the lifetime at $d^{l}_{b} = 50\text{Å}$ with E_r again remaining approximately constant. On the other hand, the lifetime of the lower energy quasi-level continues to decrease at a less rapid rate to a value $\sim 10^{-14}$ seconds at $d^{l}_{b} = 5\text{Å}$ while E_r changes direction and steadily decreases.

Reproduced with permission of the copyright owner. Further reproduction prohibited without permission.

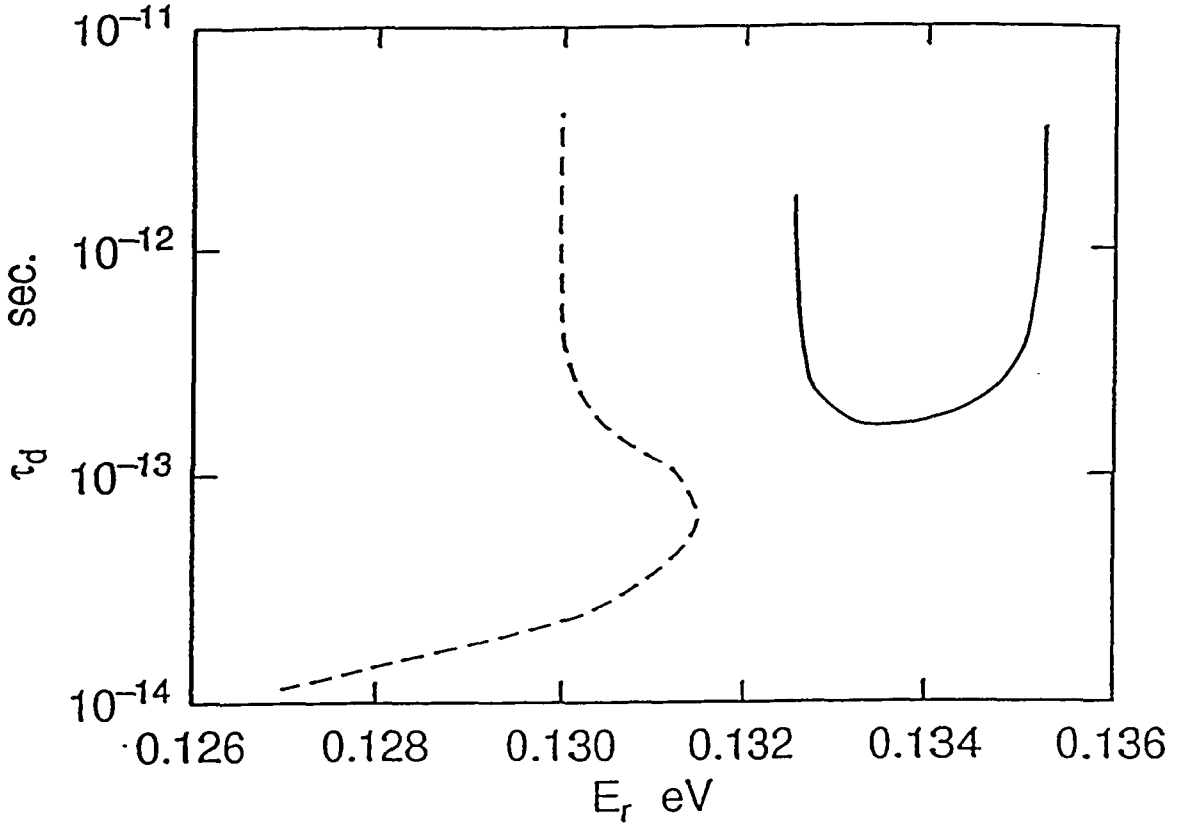

Fig. 2.18

$\tau_{\bar{d}}^{+}$ (solid line) and $\tau_{\bar{d}}^{-}$ (dashed line) corresponding to the imaginary part of the complex energy at which $S(E)$ has a pole vs. the real part of the complex energy at which $S(E)$ has a pole. The maximum point on the dashed curve corresponds to $d_{\bar{b}} = 50\text{Å}$ and the minimum point corresponds to $d_{\bar{b}} = 5\text{Å}$. The right maximum point on the solid curve corresponds to $d_{\bar{b}} = 50\text{Å}$ and the left maximim point corresponds to $d_{br} = 1\text{Å}$.

Reproduced with permission of the copyright owner. Further reproduction prohibited without permission.

Figure 2.19 shows a plot of E_r, the real component of the pole of $S(E)^{-1}$ for the plots in Figure 2.18. vs. Δx_b. Values of E_r for both the higher energy (solid curve) and lower energy (energy) quasi-levels begin merging at about $\Delta x_b = 25\text{Å}$ which corresponds to $d_b'/d_b' = 0.5$ The energy separation of the lower and higher quasi-levels is a minimum at $\Delta x_b \approx 33\text{Å}$ after which E_r for the higher energy quasi-level remains about constant and significantly decreases for the lower energy quasi-level.

Figure 2.20 shows a plot of $\tau_{\bar{d}}^{\ddagger}$ (solid curve) and $\tau_{\bar{d}}$ (dashed curve) vs. Δx_b. For $\Delta x_b = 0$ both lifetimes are approximately equal with $\tau_{\bar{d}}^{\ddagger}$ slightly lower than $\tau_{\bar{d}}$ as described above. As Δx_b increases (d_b' decreases), both $\tau_{\bar{d}}^{\ddagger}$ and $\tau_{\bar{d}}$ decrease and for $d_b' \simeq d_b'/2$, $\tau_{\bar{d}} \simeq \tau_{\bar{d}}^{\ddagger}$. $\tau_{\bar{d}}$ decreases and reaches a minimum at $\Delta x_b \approx 30\text{Å}$ ($d_b' \approx (2/5)d_b'$) after which it increases. $\tau_{\bar{d}}$ steadily decreases as Δx_b increases. The lower and higher energy quasi-levels which have about the same lifetime when $\Delta x_w = \Delta x_b = 0$ differ by more than two orders of magnitude when well and barrier parameters are $\Delta x_w = 0$ and $\Delta x_b = 5\text{Å}$. From Figures 2.16, 2.18, and 2.20 for $d_b' > 1/2d_b'$ the quasi-levels behave in a "regular" manner, that is the norm is distributed between the right and left wells and the lifetimes vary in an expected way with n^l. Thus, for $d_b' > d_b'/2$, the two level model is good representation of the properties of the potential of Figure 1.5. The transmission probability T, for tunneling through the right barrier is given by $T \propto \exp\left[-2d_{rb}\sqrt{(2m^*/\hbar^2)(V_0 - E)} \right]$. Thus $d_b' \rightarrow 1/2d_b'$ is equiv-

Reproduced with permission of the copyright owner. Further reproduction prohibited without permission.

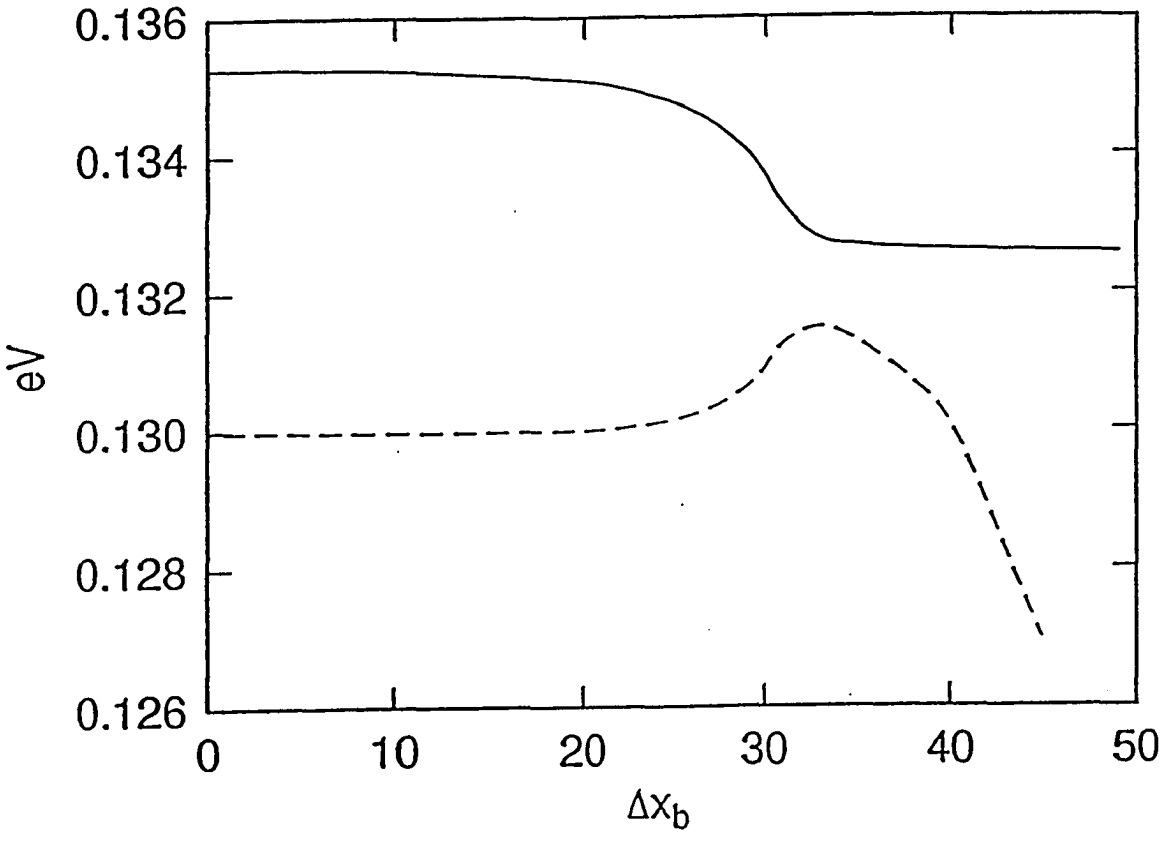

Fig. 2.19

The real part, E_r of the complex energy at which $S(E)$ has a pole vs. Δx_b for E_{0+} (solid line) and E_{0-} (dashed line).

Reproduced with permission of the copyright owner. Further reproduction prohibited without permission.

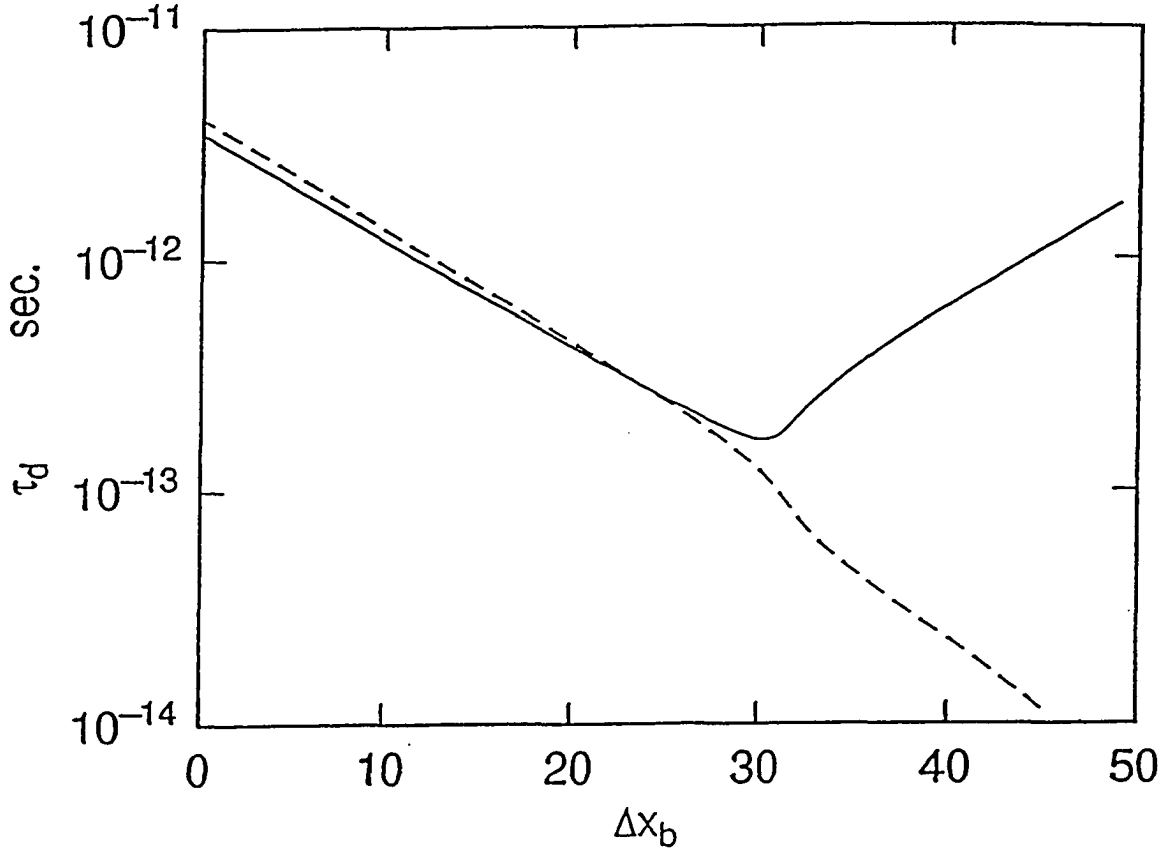

Fig. 2.20

$\tau_{\vec{d}}$ (solid line) and $\tau_{\bar{d}}$ (dashed line) corresponding to the imaginary part of the complex energy at which $S(E)$ has a pole vs. Δx_b for $d_w^l = d_w^r = 100\text{Å}$ $d_b^l = 50\text{Å}$.

Reproduced with permission of the copyright owner. Further reproduction prohibited without permission.

alent to $(V_0 - E) \rightarrow 1/4(V_0 - E)$ to maintain the same transmission probability. Therefore, if E_{0b}^{l} and E_{0b}^{r} are the energies of the top of the left and right barriers, respectively, so long as the condition $E_{0b}^{l} - E_{0\pm} > 1/4(E_{0b}^{l} - E_{0\pm})$ is satisfied, for a quasi-level of the potential of Figure 1.5, the quasi-levels will be in the "regular" domain.

Figure 2.21 shows a plot of the lifetimes $\tau_d^{\ddagger}$ (solid curve) and $\tau_{\bar{d}}$ (dashed curve) vs. $n_{+,b}^{l}$ and $n_{-,b}^{l}$. From Figure 2.21 is seen that, for $\Delta x_b = 0$, $n_{-,b}^{l} \simeq 0.5$ and $n_{+,b}^{l} \simeq 0.5$ for both the lower and higher energy quasi-levels, i.e. each is equally distributed between the left and right wells. From Figure 2.20 as Δx_b increases (d_b^{l} decreases) both $\tau_{\bar{d}}$ and $\tau_d^{\ddagger}$ decrease as Δx_b varies from 0 to $\simeq$25Å. This corresponds to the rapid decrease in $\tau_{\bar{d}}$ and $\tau_d^{\ddagger}$ shown in Figure 2.21 as $n_{-,b}^{l}$ and $n_{+,b}^{l}$ increase slightly from 0.5. From Figure 2.20 as Δx_b changes from 25Å to 30Å both $\tau_{\bar{d}}$ and $\tau_d^{\ddagger}$ continue to decrease and from Figure 2.21 within the corresponding range $n_{-,b}^{l}$ and $n_{+,b}^{l}$ increase significantly. Thus both $\ell_w^{l}(E_{0-})$ and $\ell_w^{l}(E_{0+})$ shift into the left well. Comparing Figures 2.20 and 2.21 the shift into the left well continues between $\Delta x_b = 30$Å and $\Delta x_b = 33$Å. However, thereafter, $\tau_d^{\ddagger}$ begins rapidly increasing and $\ell^{l}(E_{0+})$ continues to almost completely shift into the left well while $\tau_{\bar{d}}$ decreases at a more rapid rate again and $\ell^{l}(E_{0-})$ almost completely shifts into the right well.

Figure 2.22 shows a plot of $n_{+,b}^{l}$ and $n_{-,b}^{l}$ vs. Δx_b which clearly indicates the significant shifting of the norm into the right and

Reproduced with permission of the copyright owner. Further reproduction prohibited without permission.

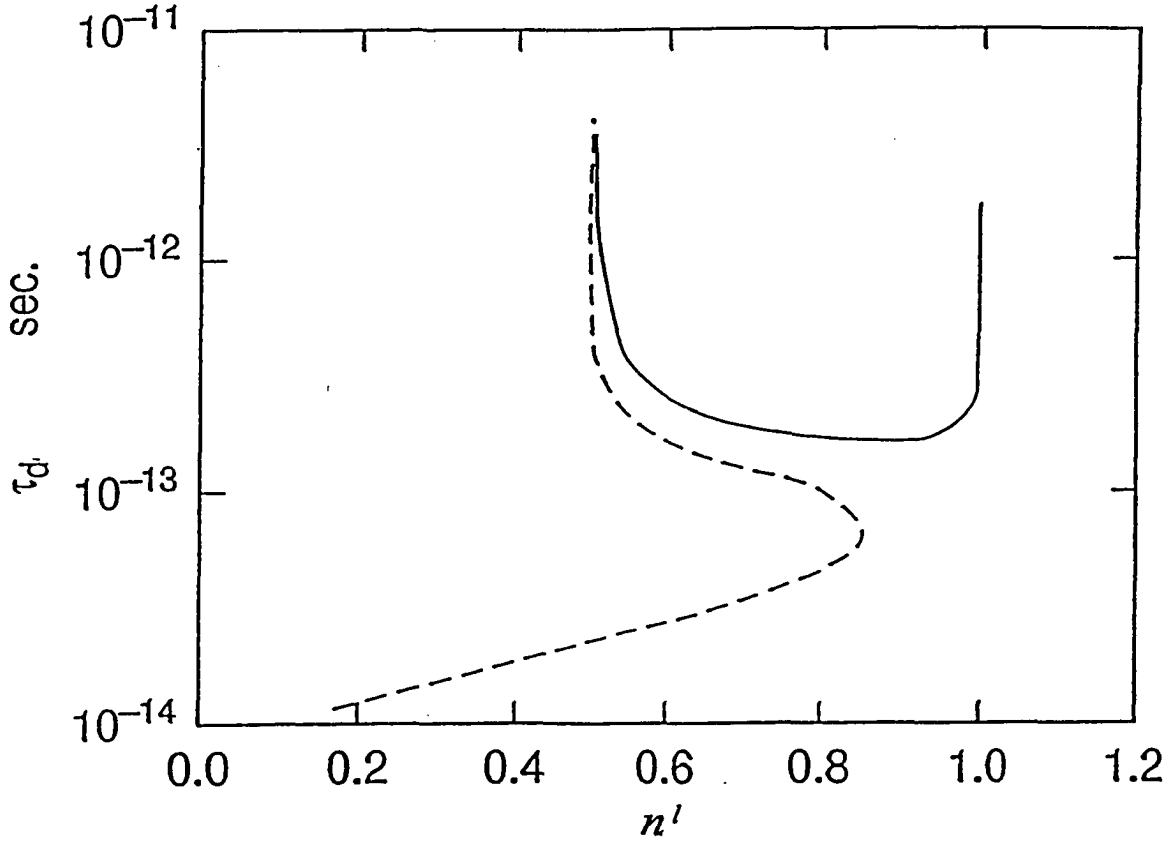

Fig. 2.21

$\tau_d^{\pm}$ vs. $n_{+,b}^{l}$ (solid line) and τ_d^{-} vs. $n_{-,b}^{l}$ (dashed line) for $d_w^l = d_w^r = 100\text{Å}$, $d_b^l = 50\text{Å}$ and $V_0 = 0.3eV$.

Reproduced with permission of the copyright owner. Further reproduction prohibited without permission.

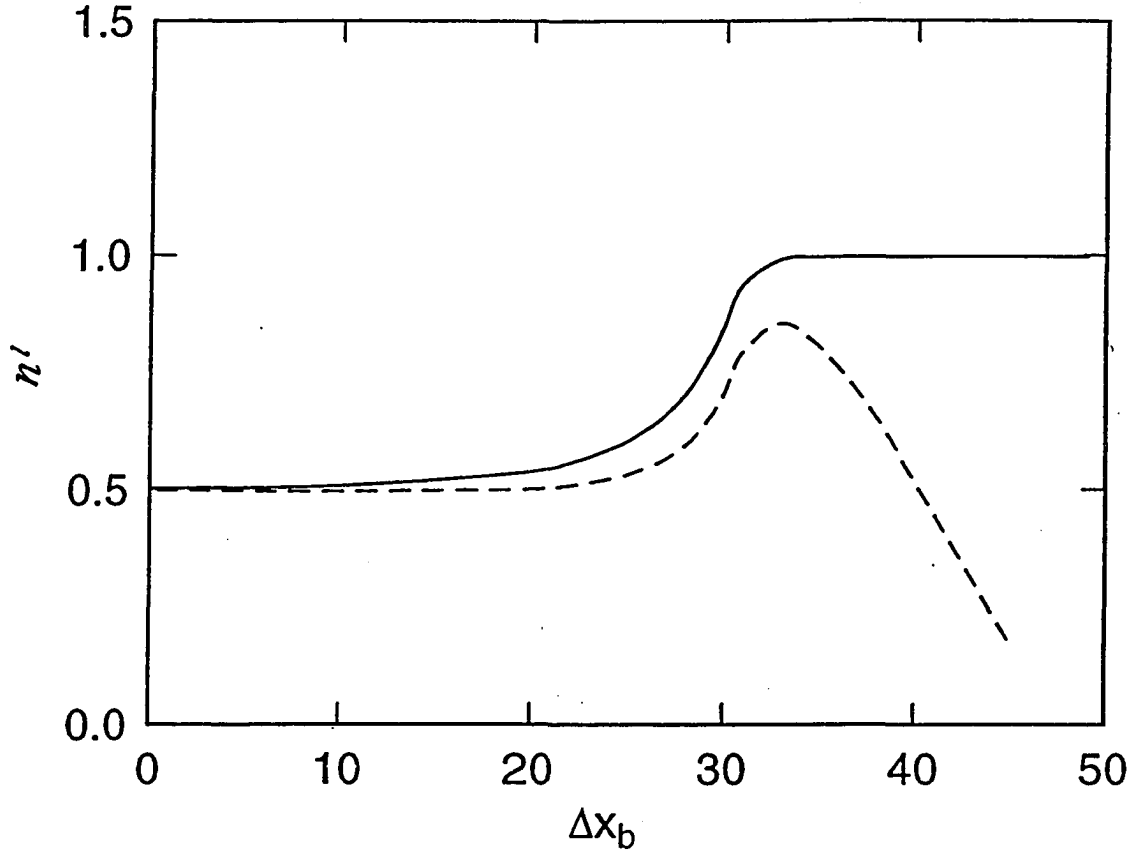

Fig. 2.22

$n^l_{+,b}$ (solid line) and $n^l_{-,b}$ (dashed line) vs. Δx_b for $d^l_w = d^r_w = 100\text{Å}$, $d^l_b = 50\text{Å}$ and $V_0 = 0.3eV$.

Reproduced with permission of the copyright owner. Further reproduction prohibited without permission.

left wells after a critical thinness ($\Delta x_b \simeq 33$Å) of the right barrier is exceeded.

As the right barrier is thinned it is expected that $\tau_{\bar{d}}$ and $\tau^{\ddagger}_{decay}$ will decrease since there is less quantum confinement of the wave functions. After a critical thinness of the right barrier (here about 20 Å) the right barrier reflects the wave resonating in the DBRTS less efficiently and both higher and lower energy quasi-levels begin shifting into the left well where they resonate more efficiently. If both quasi-levels shifted completely into the left well, there would be six particles in a well which has only states sufficient to hold three particles. This tendency to over populate the states in the left well results in the reduction of $n^{l}_{,b}$ so that three particles are in each of the left and right wells. From Figure 2.21 it is seen that the lower energy quasi-level shifts into the right well and the higher energy quasi-level shifts into the left well. Initially it would appear that this is the reverse of what it ought to be. It might be expected that since the lower energy quasi-level is more confined than the higher energy quasi-level, the lower energy quasi-level would shift into the left well for which there is more confinement and the higher energy quasi-level which is less confined would shift into the right well. If this occurred the plots of Figure 2.18 would have an intersection between the trace of the lower energy quasi-level and the higher energy quasi-level in the complex E plane corresponding to the zeros of $S(E)^{-1}$. There would be a two fold degeneracy with each state having the same lifetime. The norm $\ell^{T}(E)$ would have a single peak. Since each well has the same width, each contributes

Reproduced with permission of the copyright owner. Further reproduction prohibited without permission.

a level of the same energy to the pair of quasi-levels. The degenerate levels are split by the interaction of these two degenerate levels through the left barrier. Therefore, the plots of Figure 2.18 cannot intersect and the lower energy level must shift into the right well and the higher quasi-level into the left well.

Figure 2.23 shows the phase, θ, of $S(E)$ for $0 \leq E \leq 0.3$ eV when $d_b = 1$Å. In the energy range of each pair of quasi-levels there is a 2π jump in θ. Between the pairs of quasi-levels there is an approximately linear increase in θ by 2π. The 2π jump in θ corresponds to the higher energy quasi-level whose $\ell^T(E)$ plot is narrow and localized in the left well. The linear increase in θ by 2π corresponds to the lower energy quasi-level whose norm is broad and localized in the right well. The width of the resonance determines how rapidly the phase changes.

Figure 2.24 shows a plot of $N(E)$ for the same conditions as in Figure 2.23. In the energy range of each pair of quasi-levels there is a unit jump in $N(E)$. Between the pairs of quasi-levels there is an approximately linear increase in $N(E)$ by a unit. The unit jump in $N(E)$ corresponds to the higher energy quasi-level whose norm is narrow and localized in the left well. The linear increase in $N(E)$ by 1 corresponds to the lower energy quasi-level whose norm is broad and localized in the right well. The width of the resonance determines how rapidly $N(E)$ changes.

Over the entire energy range $0 < E < 0.3eV$ there is a bit less than the expected 12π change in θ in Figure 2.23 and a bit less than

Reproduced with permission of the copyright owner. Further reproduction prohibited without permission.

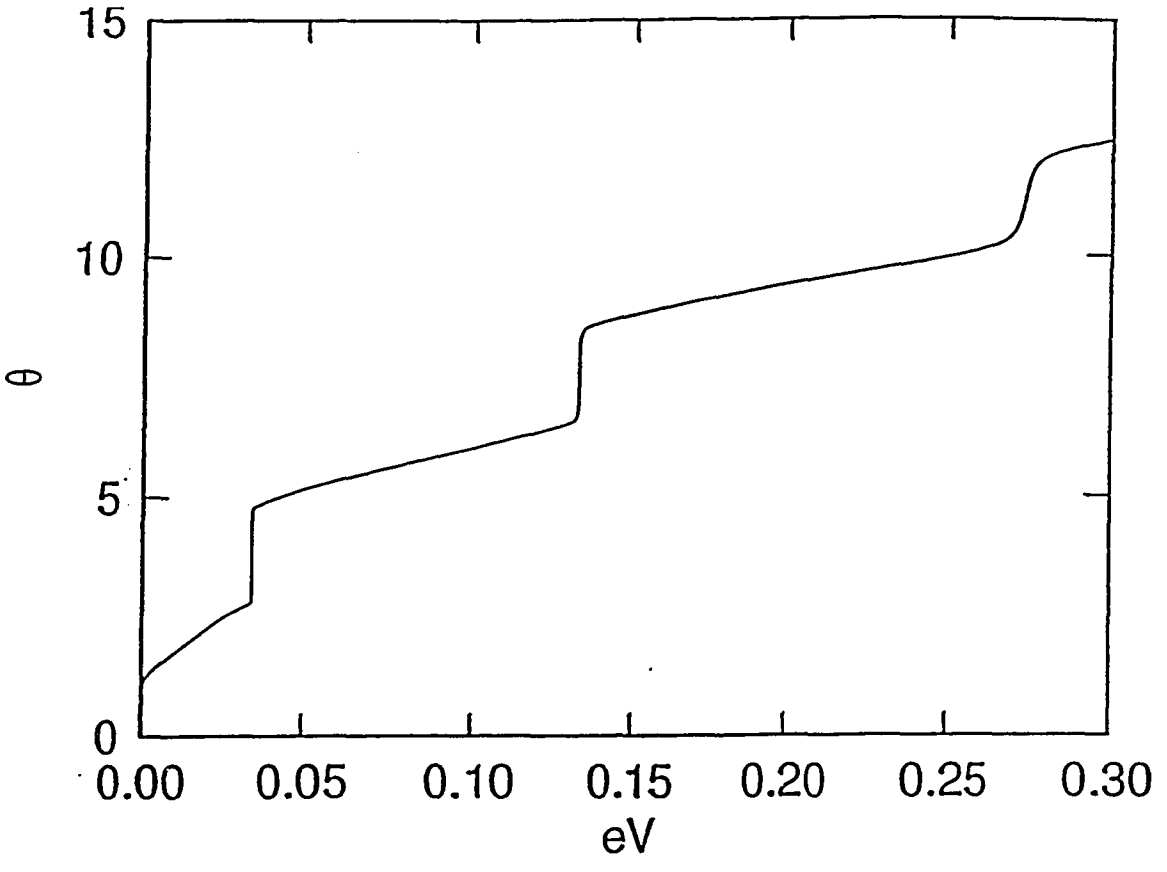

Fig. 2.23

Phase of $S(E)$, θ in units of π for $d_w^l = d_w^r = 100\text{Å}$, $d_b^l = 50\text{Å}$, $d_b^r = 1\text{Å}$ and $V_0 = 0.3eV$.

Reproduced with permission of the copyright owner. Further reproduction prohibited without permission.

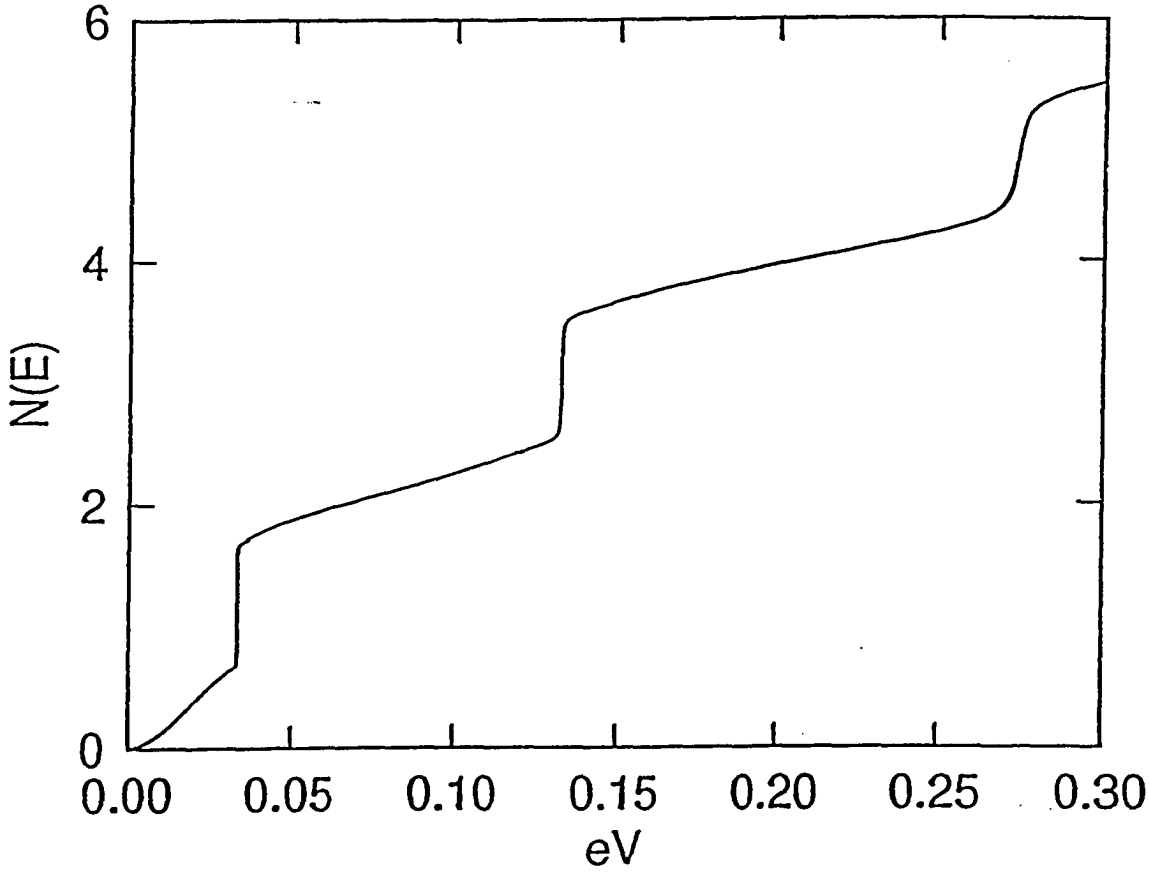

Fig. 2.24

Number of electrons, $N(E)$, vs. Energy for $d_w^l = d_w^r = 100\text{Å}$, $d_b^l = 50\text{Å}$, $d_b^r = 1\text{Å}$, and $V_0 = 0.3eV$.

Reproduced with permission of the copyright owner. Further reproduction prohibited without permission.

the expected change of 6 in $N(E)$ in Figure 2.24. This is attributed to the extremely degenerate situation of having a 1Å right barrier width.

It would appear that in the plots of Figures 2.23 and 2.24 for $\theta(E)$ and $N(E)$ that the second term of Eq. (2.31) should be taken into account.

Figure 2.25 shows $\ell^T(E)$ for $d_w^l = d_w^r = 100\text{Å}$, $d_b^l = 50\text{Å}$, $d_b^r = 1\text{Å}$, and $V_0 = 0.3eV$. There are three single peaks which would appear to be similar to the norm for a single barrier tunneling structure. However, from Figures 2.23 and 2.24 the total change in phase is greater than 6π and the total number of particles is greater than 3 which would be the values for a single barrier resonant tunneling structure. The sharp peaks in Figure 2.25 correspond to the norm in the left well. Comparing Figures 2.1, 2.2 and 2.25 it is seen that the norm between the peaks of Figure 2.25 is greater than the the norm between the pairs of peaks in Figures 2.1 and 2.2. This corresponds to the norm in the right well.

2.8 Conclusions

Resonances of a DBRTS having an accumulation layer have been studied using a rectangular model potential with the accumulation layer and the barrier layer represented by square wells. The effect of applying a potential across the DBRTS is simulated

Reproduced with permission of the copyright owner. Further reproduction prohibited without permission.

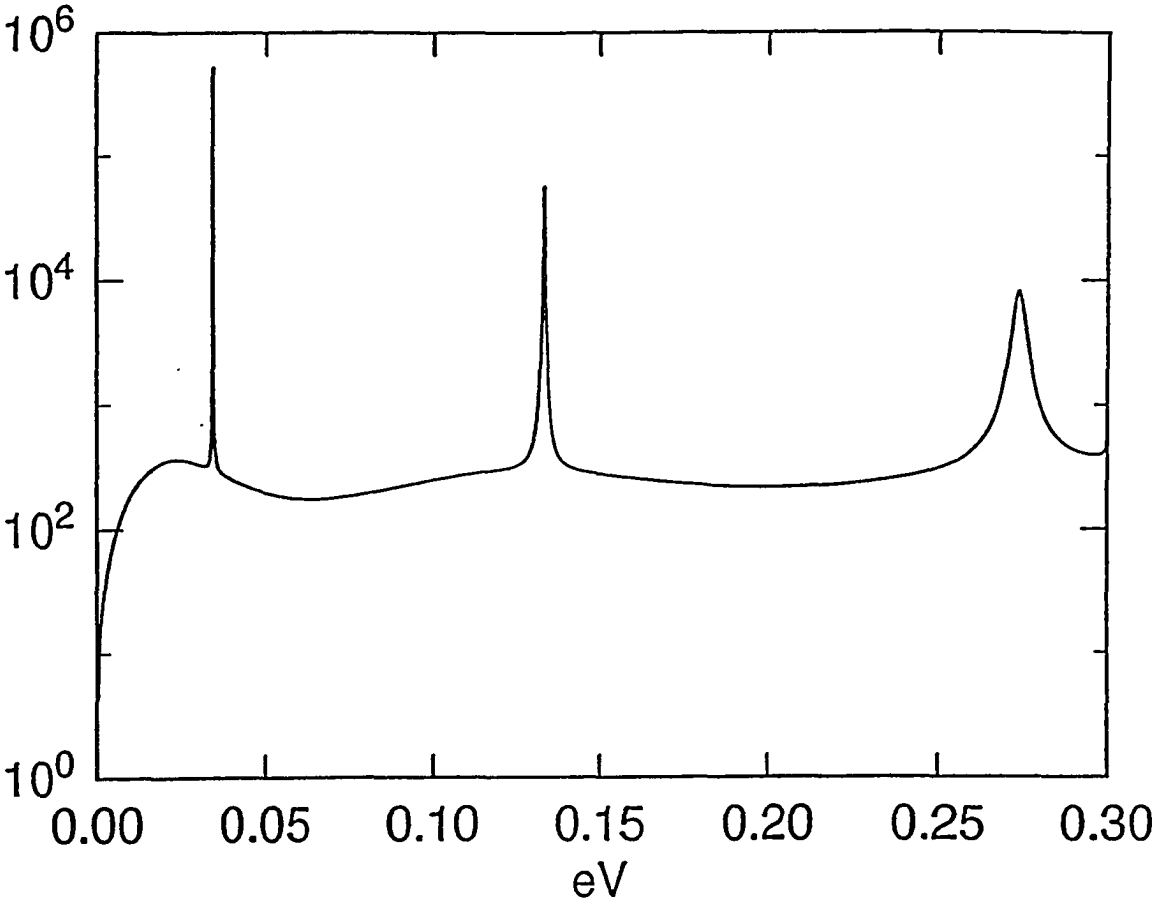

Fig. 2.25

$\ell^T(E)$, vs. energy for $d_w^l = d_w^r = 100\text{Å}$, $d_b^l = 50\text{Å}$, $d_b^r = 1\text{Å}$, and $V_0 = 0.3eV$.

Reproduced with permission of the copyright owner. Further reproduction prohibited without permission.

by varying the width of the left (inner) well and the width of the barrier on the anode side of the DBRTS. These widths are varied separately to understand the effect each has on the properties of the DBRTS. The resonances of the DBRTS are pairs of closely spaced quasi-levels (having a higher and lower energy quasi-level) derived from one level generated by each of the wells.

Each level is represented by a peak in the norm versus energy. The energy width of each of these resonance peaks is related to the lifetime of each level. The distribution of the integrated norm of each quasi-level between the right and left wells is a function of Δx_w and Δx_b where $\Delta x_w = d_w^l - d_w^r$ (with d_w^l, the width of the left well, variable and d_w^r, the width of the right well, held fixed) and d_b^l, the width of the left barrier equal to d_b^r the width of the right barrier) and where $\Delta x_b = d_b^l - d_b^r$ (with $d_w^l = d_w^r$ and d_b^r variable and d_b^l held fixed). When $\Delta x_w = 0$ (equal well widths), the norms of the upper and lower energy quasi-levels are about equally distributed between the right and left wells. When $\Delta x_w < 0$, the norm of the higher energy quasi-level is primarily in the left well and consequently has a increased lifetime and the norm of the lower energy quasi-level is primarily in the right well and has a shorter lifetime. The situation reverses when $\Delta x_w > 0$. The energy separation of the quasi-levels is a minimum at $\Delta x_w = 0$. As Δx_w is varied from 0, the quasi-levels anti-cross as in atomic systems.

Reproduced with permission of the copyright owner. Further reproduction prohibited without permission.

When the outside barrier is narrowed, the lifetime of both quasi-levels initially decrease until the lifetime of the higher energy quasi-level reaches a minimum after which it increases as its norm shifts into the left well while the lifetime of the lower energy quasi-level continues to decrease as its norm shifts into the right well.

In an actual DBRTS with an accumulation layer, these effects which are separately studied here will occur simultaneously as a bias is applied over the DBRTS. The potential of the accumulation layer is not square but approximately triangular. Therefore, the width of the potential well in the accumulation layer increases with energy and consequently for a given potential bias across the diode the effective width of the accumulation layer equals the width of the right well only at one energy, an intermediate energy between the top and bottom of the accumulation layer. For energies greater than the intermediate energy the accumulation layer effective width is greater than the barrier layer (right well) width and for energies less than the intermediate energy the accumulation layer effective width is less than the barrier layer width. Therefore, the energy separation of the two quasi-levels, the distribution of the norm between the accumulation layer and the barrier layer and the lifetimes for groups of quasi-levels of the DBRTS is different depending on whether the energy of the pair of quasi-levels is greater or less than the intermediate energy.

Reproduced with permission of the copyright owner. Further reproduction prohibited without permission.

When a bias is applied, the anode side barrier is lower in energy than the cathode side barrier. Consequently, for a pair of quasi-levels near the top of the accumulation layer the energy difference of the pair of quasi-levels from the top of the cathode side barrier is greater than the energy difference from the top of the anode side barrier which has the equivalent effect of the anode side barrier being thinner than the cathode side barrier. Therefore, the two peaks in the left well should have a tendency to merge as a result of the effective thinning of the anode side barrier. This is opposite to the effect of the widening of the accumulation layer width which tends to separate the two peaks in the left barrier. The widening of the accumulation layer width shifts the norm of the lower energy quasi-level into the left well. Whereas the effective thinning of the anode side barrier after a critical thinning tends to shift the norm of the lower energy quasi-level into the right well. Therefore, it is apparent that the two effects of the variation in the accumulation layer width and in the effective thickness of the anode side barrier are competing effects which will result in a complex variation in the properties of the paired quasi-levels of a DBRTS with an accumulation layer, such as the current voltage characteristics.

As the width of the outer barrier is made thinner than the inner barrier, the properties of the barrier remain "regular" up until the outer barrier is about 1/2 the thickness of the inner barrier, that is, the real energies corresponding to the peaks of the norms and the escape times both decrease at about the same rate and the

Reproduced with permission of the copyright owner. Further reproduction prohibited without permission.

norms are approximately uniformly distributed between the inner and outer wells. When the outer barrier becomes thinner, the higher energy quasi-level almost completely shifts into the inner well having a long lifetime and the lower energy quasi-level almost completely shifts into the outer well having a short life time. The current through a DBRTS with an accumulation layer can be modeled using a two level model as a function of $\varepsilon = E_l - E_r$, the energy difference of the eigenvalues of the isolated wells so long as the quasi-levels are sufficiently far away in energy from the top of the outside barrier to remain in the "regular" domain over the variation in ε over a resonance which is satisfied if the quasi-levels are deep enough in the accumulation layer.

The analysis in this chapter by separating out the effect of the variation of the width of the accumulation layer and the anode side barrier will provide greater understanding for the analysis of Chapter 3 of an actual DBRTS with an accumulation layer where the competing effects discussed here will be occurring at the same time.

Reproduced with permission of the copyright owner. Further reproduction prohibited without permission.

CHAPTER 3

RESONANT TUNNELING THROUGH A DIODE ACCUMULATION LAYER

3.1 Introduction

The phenomenon equivalent to resonant tunneling, in a double-barrier diode with a spacer layer and consequent accumulation layer on the cathode (source) side, is elucidated. The accumulation layer and the inter-barrier well each support an electron quasi-level (or several) which may be expected to combine coherently into a doublet of states that are filled by in-scattering of the source electrons and emptied by tunneling to the "anode" side. The resulting current depends on the distribution of electron density (norm) between these two component orbitals, with a peak (as a function of bias) at the "level crossing" point where the norms are each 1/2. The analysis draws on the computational study in Chapter 2 of Gamow-like tunneling out of a double-well system, as a model of the electron states. The in-scattering rate due to acoustic-mode phonons in particular is calculated. Corresponding diode current characteristics are obtained.

as described in Chapter 1 resonant tunneling in a semiconductor diode has been investigated in double-barrier structures [6] where the current versus bias depends essentially on the dependence of

Reproduced with permission of the copyright owner. Further reproduction prohibited without permission.

transmission probability T on normal-direction energy E for an electron incident on the barrier structure: $T = T_0 \Lambda(E)$ where

$$\Lambda(E) = 1/[1 + ((E - E_0)/\Delta E)^2] \qquad (3.1)$$

This Lorentzian dependence of T on E is characteristic for a continuum of electron states incident on a double-barrier structure [23]. If, however, the cathode doping of the diode is separated from the barriers by an undoped spacer layer, there can be a resulting accumulation layer adjacent to the barrier on the cathode side, and consequently a "local quantization" of electron states (quasi-levels) instead of a continuum in this layer. The resonance-like feature in the diode current versus bias that is still observed [23] may heuristically be attributed [23, 31] to the crossing of this level with the local level belonging to the space between the two barriers, in place of the usual displacement, with bias, of the energy distribution of source electrons relative to E_0. This "level crossing" interpretation is investigated here, in terms of properties of the electron states of this diode system that have been elucidated by the computational study of Chapter 2.

Figure 1.5 shows a stylized picture of the situation. The cathode continuum of incident states may be assumed to have only a small probability of direct transmission through the two barriers B_l (left barrier) and B_r (right barrier), while the resonant path goes through the L_l, L_r levels (levels in the left and right wells, respectively) -- by either elastic or inelastic scattering processes, with the accompanying transitions between the two-dimensional lateral wave vectors K of these states taken into account. (Two-dimensional vectors parallel to the interface planes of the diode

Reproduced with permission of the copyright owner. Further reproduction prohibited without permission.

structure are represented by capitals **K, R, Q** and the components normal to the planes by k, z, q .) The formulation that is elucidated here considers the quantum combination of L_l and L_r to be a single state (i.e., one of the doublet of states resulting from the interaction through the separating barrier B_l) with a definite lifetime for "decay" into the anode continuum on the right of B_r in Figure 1.5. We expect (see below) the overall transition rate to be proportional to $1/(\tau_l + \tau_r)$ where $1/\tau_l$ is the scattering rate from the C continuum into this compound state and $1/\tau_r$ is the rate of tunneling out of this state.($\tau_r \equiv \tau_d$) The observed resonance feature can then be interpreted in terms of the "crossing" phenomenon for coupled levels, as follows: When L_l and L_r are far apart in energy, the two electron states of the resulting doublet have their norms (fractions of the integrated electron density) mainly in the left well and mainly in the right well, respectively. For the former case, $\tau_l << \tau_r$ and the current channel is suppressed by filling up the level, while for the latter $\tau_r << \tau_l$ and the tunneling out is abated because the level is nearly empty. When the L_l and L_r levels cross, with increasing bias, then there is a range where $\tau_l \approx \tau_r$ and hence a peak in the current.

The quantum system has been investigated computationally in Chapter 2 in terms of Figure 1.7, where there are two "square wells" (with the L_l, L_r difference conveniently obtained by making their widths d_w^l, d_w^r different). As described in Chapter 2 the quantum states for real energy E are then given by trigonometric formulas, supplying the phase angle for reflection of an electron incident from the right, and the relative norms n^l, n^r

Reproduced with permission of the copyright owner. Further reproduction prohibited without permission.

(with $n^l + n^r = 1$) in the two wells. The decay lifetimes are obtained by a special algorithm as described in Chapter 2 that quantifies the Gamow treatment of the tunneling decay. [76., 69.] It computes the ratio of incident amplitude to reflected amplitude for a *complex* E and searches for the (small) imaginary part of E at which that ratio is zero. This imaginary-part energy is then interpreted as $\hbar/2\tau_r$.

The transition rate through a compound L_l, L_r state (contribution to diode current from a given value of lateral wave-vector, **K**) has some analogy to the laser generation process. The scattering rate into a level with occupation number f is $(1/\tau_l)(1-f)$ and the tunneling rate out of the level is $(1/\tau_r)f$. Equating these two, we find $f = \tau_r/(\tau_l + \tau_r)$ and for the rate $R = 1/(\tau_l + \tau_r)$ as noted above. We shall assume that scattering between these compound (L_l, L_r) states (between the lateral wave-vectors), after scattering in from the cathode states and before tunneling out to the anode side, may be disregarded.

To a good approximation, a wave function of an electron incident from the source continuum (and mostly reflected back), and a wave function of the L_l, L_r double-well state, will overlap only on the L_l (cathode) side, and hence $1/\tau_l$ is proportional to the norm n^l. On the other hand, one expects $1/\tau_r$ to be proportional to the complementary norm $n^r = 1 - n^l$, and this is confirmed by the computational investigation of Chapter 2 for the Figure 1.7 system. Thus the variation of R with bias (with L_l, L_r splitting) is given by

Reproduced with permission of the copyright owner. Further reproduction prohibited without permission.

$$R_{\pm} = \frac{1}{(t_l/n^l) + (t_r/n^r)} \tag{3.2}$$

with coefficients t_l, t_r. The $\pm$ subscript represents the fact that there is a current contribution from each state (+ and −) of the doublet of states that results from the interaction through the left-hand barrier, B_l. It can be verified that the n^l value for one state of this doublet (say, +) is equal to the n^r value for the other state (−); i.e. norm and complementary norm interchange. The t_l and t_r constants will be the same for each state of the doublet (the splitting being small), and consequently we find after some algebra, for the sum of the two contributions,

$$R \equiv R_+ + R_- = \frac{(t_l + t_r)\,\Omega}{t_l\,t_r + (t_l - t_r)^2\,\Omega} \tag{3.3}$$

where

$$\Omega \equiv n^l\,n^r \tag{3.4}$$

($\Omega_+ = \Omega_- \equiv \Omega$, the same for either state of the doublet.)

3.2 Model System

We may model the bias dependence of Ω by treating the L_l, L_r combination states of Figure 1.5 or of Figure 1.7 as belonging, for this purpose, to a closed system (as though the right-hand barrier B_r were infinitely thick). Then the doublet system may be represented -- whether or not symmetrical -- by a "two-by-

Reproduced with permission of the copyright owner. Further reproduction prohibited without permission.

two" Hamiltonian with two real diagonal elements E_l, E_r (being the uncoupled L_l, L_r levels) and (two equal, real) off-diagonal elements E_{l2} representing the coupling via B_t. The doublet splitting of the energy eigenvalues is then

$$E_+ - E_- = [(E_l - E_r)^2 + 4\,E_{l\,r}{}^2\,]^{1/2} \tag{3.5}$$

The n^l and n^r norms are given by the squares of the eigenvectors of this Hamiltonian, the result for the product $n^l n^r$ being

$$\Omega = 1/[4 + ((E_l - E_r)/E_{l\,r})^2] \tag{3.6}$$

Thus, Ω is a Lorentzian function of $E_l - E_r$, with maximum value 1/4. On substituting eq(3.6) in eq(3.3), we obtain

$$R = \frac{1/(t_l + t_r)}{1 + \dfrac{t_l\,t_r}{(t_l + t_r)^2}\left(\dfrac{E_l - E_r}{E_{l\,r}}\right)^2} \tag{3.7}$$

Then the strength of the current peak, where the L_l and L_r levels cross ($E_l = E_r$), is given by $R_0 = 1/(t_l + t_r)$, summed over the K contributions, while the width of the peak depends on t_l/t_r as well as on E_{l2}. With the normal-direction quantum states independent of K, we expect from (3.7) that the R_0 peak of R will occur at the same bias, where $E_l = E_r$, for all these contributions to the current. But t_l varies with K, and hence the form of the current contributions will vary accordingly.

Reproduced with permission of the copyright owner. Further reproduction prohibited without permission.

3.3 Scattering Rate

It remains to calculate the scattering rate, $1/t_l$, for incident source electrons, from the occupied wave vectors $(\mathbf{K}, k)$, into a given accumulation-layer quasi-level state (the rate with $n' = 1$). That is, into a single final state with lateral wave vector $\mathbf{K}_l$ from initial states with occupation function $f(\mathbf{K}, k)$, which will be assumed to be degenerate: $f = 1$, for $0 < E < E_F$. We consider the specific process of deformation (non-polar) scattering by acoustic mode phonons. This should be favored over other processes because the scattering change of lateral wave-vector $\mathbf{K} \rightarrow \mathbf{K}_l$ will be large,

$$\Delta(K^2) \simeq (2\, m^*/\hbar^2)\, E_0 \tag{3.8}$$

where E_0 is the energy drop from incident band edge to the quasi-level. (We assume, throughout, the "parabolic" electron energy function.) Because of this large wave-vector change, it appears justified also to disregard screening of the electron scattering force. The acoustic-mode phonon energy may be estimated from (3.8) to be $\hbar\omega \simeq (2E_s\, E_0)^{1/2}$ where $E_s = m^* s^2$ and s is velocity of sound. For n-GaAs, in thermal units $E_s = 0.11$ kelvin. Then for example if $E_0 = 0.3$ eV (3500 kelvin), the phonon energy is 28 kelvin. This is small compared with E_0 and also compared with 300 kelvin (thermal energy, $k_B T$), so we shall make the "equipartition" approximation $N, N+1 \rightarrow k_B\, T/\hbar\omega$ for the phonon occupation numbers.

Reproduced with permission of the copyright owner. Further reproduction prohibited without permission.

The selection rules for an absorption or emission of a phonon of wave vector $(\mathbf{Q}, q)$, to a given "final" quasi-level having lateral wave vector $\mathbf{K}_l$, are

$$\mathbf{K}_l = \mathbf{K} \pm \mathbf{Q} \tag{3.9}$$

with energy change

$$\Delta E = (\hbar^2/2\,m^*)\,(K_l^{\,2} - K^2 - k^2) - E_0 \quad \pm \hbar\,\omega(\mathbf{Q}, q) \tag{3.10}$$

where we are going to neglect the final term $\pm \hbar\,\omega$. The "energy conservation" delta function $\delta(\Delta E)$ in the applicable Golden Rule formula then results in the factor

$$\int d^2\,\mathbf{K}\;\delta(\Delta E) = 2\pi\,m^*/\hbar^2 \tag{3.11}$$

from summation over *initial* states $(\mathbf{K}, k)$. If $\phi(z)$ is the incident and reflected (normal component of) electron wave function, normalized in unit length, and $\phi_l(z)$ the "final" quasi-level wave function (normal component) of the accumulation layer, with $\int |\,\phi_l\,|^2\,dz = 1$, then the transition matrix element is proportional to a form factor (with $\phi(z)$ real)

$$I(q) = \int \phi(z)\,\phi_l(z)\;\exp i\,qz\,dz \tag{3.12}$$

(As with electron-phonon scattering in other parallel-plane structures, there is no selection rule like eq. (3.9) for the normal-direction component of phonon wave-vector. All q values are allowed, with non-zero scattering matrix elements.)

Reproduced with permission of the copyright owner. Further reproduction prohibited without permission.

Collecting factors, the rate is the sum of absorption and emission terms $1/t_+$ and $1/t_-$ given by

$$\frac{1}{t_\pm} = \frac{2\pi}{\hbar} \frac{1}{(2\pi)^4} \frac{2\pi m^*}{\hbar^2} \int dk \int dq\, C_\pm \mid I(q) \mid^2 \qquad (3.13)$$

where (for deformation-coupled acoustic modes, with $\hbar\omega << k_B T$)

$$C_+ = C_- = k_B T (D^2/2\rho s^2) \qquad (3.14)$$

where D is the deformation potential and ρ is the mass density of the semiconductor (taken as homogeneous and isotropic).

To evaluate (3.13) we make use of Parseval's Theorem (taking the limits of the q integral to be effectively $\pm\infty$):

$$\int \mid I \mid^2 dq = 2\pi \int \mid \phi \mid^2 \mid \phi_l \mid^2 dz \qquad (3.15)$$

and combine the absorption and emission rates, $1/t_l = 1/t_+ + 1/t_-$:

$$\frac{1}{t_l} = v_0 \int dk \int \mid \phi \mid^2 \mid \phi_l \mid^2 dz \qquad (3.16)$$

where

$$v_0 = \frac{m^*}{2\pi\hbar^3} \frac{k_B T D^2}{\rho s^2} \qquad (3.17)$$

Reproduced with permission of the copyright owner. Further reproduction prohibited without permission.

For GaAs at 300 kelvin, taking $D = 12$ eV, [77] and $\rho s^2 = 1.4 \times 10^{12}$ cgs, the value of value of υ_0 is 9.07×10^4 cm/sec.

To complete this estimating calculation, we require (1) a model for $\phi(z)$ and (2) the applicable limits for the k integral in (3.16). For the incident (and reflected) wave function we adopt the WKB approximation

$$\phi(z) = (2k/g)^{1/2} \sin(\int^z g(z')\, dz') \tag{3.18}$$

where $g(z)$ is the "local" value of incident wave vector within the accumulation layer ($g(z) \to k$ when $z \to -\infty$) [78]. Also in the second integral of (3.16) we replace $\sin^2 \int^z g(z')\, dz'$ by 1/2 . Then

$$\int |\phi|^2 \, |\phi_l|^2 \, dz \simeq k \, < \frac{1}{g} > \tag{3.19}$$

where $< \ldots >$ means average over the quasi-level electron density $\phi_l(z)^2$ in the accumulation layer. $\phi_l(z)$ can be approximated by a Fang-Howard type wave function [80]. If $E_F << E_0$, then this average does not vary much over the allowed range of k in (3.16); so we remove it from the k integral, which becomes proportional to the range of k^2 , over the initial states, for which the incident energy relative to band edge is between 0 and E_F .

Conservation of energy (here neglecting phonon energies $\hbar\omega$), and confinement of incident energy to the range (0, E_F) , requires

$$0 \le K_l^2 - K_0^2 \le k_F^2 \tag{3.20}$$

Reproduced with permission of the copyright owner. Further reproduction prohibited without permission.

and

$$0 \leq k^2 \leq K_l^2 - K_0^2 \tag{3.21}$$

where

$$K_0^2 \equiv (2\,m^*/\hbar^2)\,E_0 \tag{3.22}$$

Eqs. (3.20-3.22) specify the range of states that contribute to the current (with $\mathbf{K}_r = \mathbf{K}_l$ for the tunneling-out process), and show that the factor $\int k\,dk$ from (3.13) and (3.19) should be set equal to $X\,k_F^2/2$ where

$$X = (K_l^2 - K_0^2)/k_F^2 \tag{3.23}$$

with X in (0,1) Finally, we have

$$\frac{1}{t_l} = \frac{1}{2}\,v_0\,k_F^2 \left\langle \frac{1}{g} \right\rangle \quad X \equiv \frac{X}{t_{l\,\min}} \tag{3.24}$$

If we calculate a peak current from this t_l value alone -- i.e. as an upper limit, disregarding t_r -- the current per unit area (counting both spin states) will be

$$J = 2\,e\left[\frac{1}{2}\,v_0\,k_F^2 \left\langle \frac{1}{g} \right\rangle\right] \frac{1}{2}\,\frac{\pi k_F^2}{(2\,\pi)^2} = \frac{e}{t_{l\,\min}}\,\frac{k_F^2}{4\pi} \tag{3.25}$$

where the factor after the [...] includes an average value 1/2 for X.

With the above value of v_0, and assuming $k_F = 3 \times 10^6\,\mathrm{cm}^{-1}$, then $1/t_{l\,\min}$ would be $(k_F \langle 1/g \rangle)$ times $1.36\times\ 10^{11}$/sec. (For

Reproduced with permission of the copyright owner. Further reproduction prohibited without permission.

$1/t_{l\,\min} = 3 \times 10^{10}$/sec , the current density according to eq. (3.25) is then 3.44×10^3 amp./cm^2.) The tunneling-out rate, $1/t_r$, can be taken as equal to $\nu\, T$, where T is the probability of tunneling transmission through the B_r barrier by an electron incident at the energy, E, of the quasi-level, and ν is the "attempt frequency" in the W2 well at this energy. If the well is of width W then, to sufficient approximation, $\nu\, W^2 = \pi\hbar/2\, m^*$, which for n-GaAs is equal to 27.2 cm^2/sec. For a single barrier, T can be taken to be equal to $M \exp - 2\lambda$ where $M \sim 1$ takes account of wave-function matching at the barrier interfaces and λ is the usual integral $\int \kappa\, dz$ of the "imaginary wave vector" κ over the barrier width. The exponential factor makes possible a wide range of numerical values for the tunneling rate.

3.4 Diode Characteristic

In eq(3.25), the effect of tunneling out was neglected (by setting $t_r = 0$). To include it, in this result for the peak current, we set $t_l = t_{l\,\min}/X$ and replace the factor 1/2 (the average value of X) in (25) by the factor

$$F = \int_0^1 \frac{dX}{\frac{1}{X} + \frac{t_r}{t_{l\,\min}}} = \frac{1}{c} - \left(\frac{1}{c}\right)^2 \ln(1 + c) \qquad (3.26)$$

where

$$c \equiv t_r/t_{l\,\min} \qquad (3.27)$$

Reproduced with permission of the copyright owner. Further reproduction prohibited without permission.

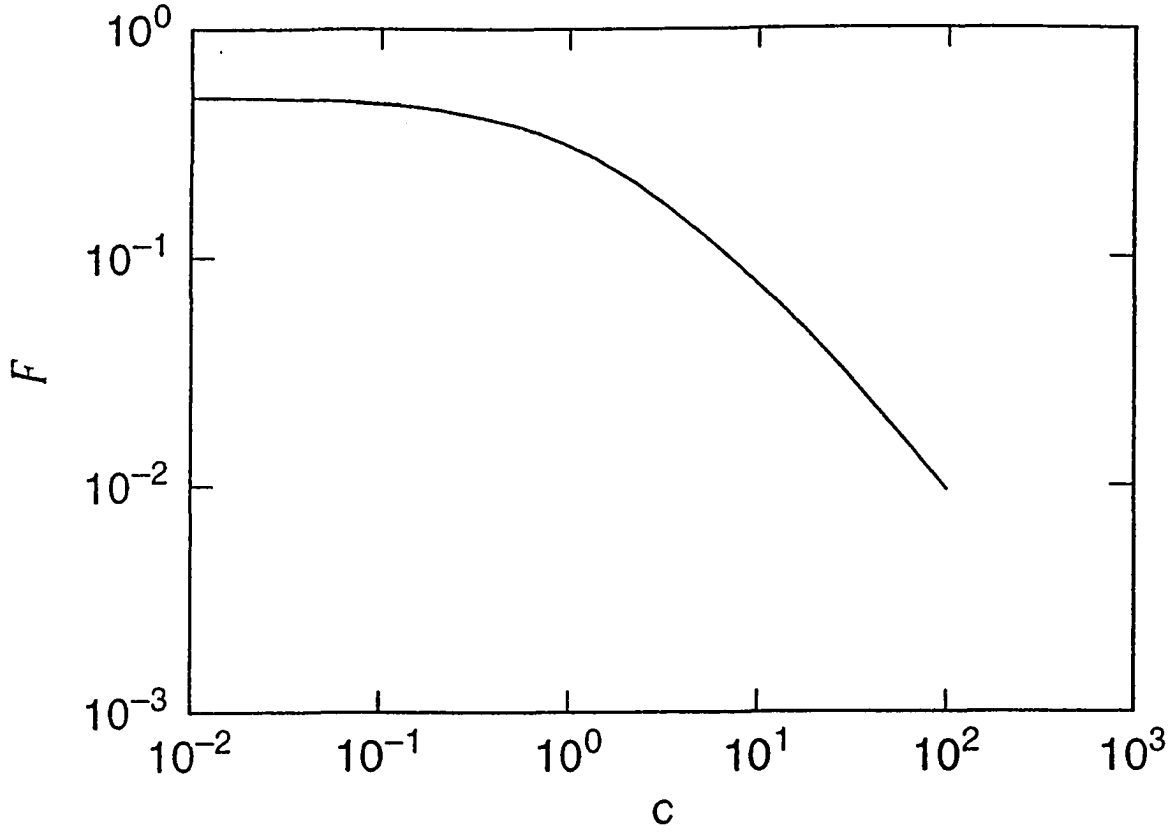

Fig. 3.1

F versus c $(G = 0)$.

Reproduced with permission of the copyright owner. Further reproduction prohibited without permission.

Figure 3.1 shows this F versus c in a log-log plot, illustrating its fall off from $F = 0.5$ at $c = 0$ and asymptotic approach to $1/c$ for large c values. Thus, a prediction of our model is that peak current increases with increasing $1/c$. That is, it increases with tunneling-out rate.

Away from the peak, where $E_l \neq E_r$, this factor (3.26) generalizes to

$$F(c, G) \equiv t_{l\,\min} \int_0^1 R\, dX = \int_0^1 \frac{dX}{\frac{1}{X} + c + G/(X + \frac{1}{c})} \tag{3.28}$$

in terms of (3.7), where

$$G \equiv \left(\frac{E_l - E_r}{E_{l\,r}} \right)^2 \tag{3.29}$$

That is,

$$\begin{aligned} c^2 F(c, G) &= \int_0^c \frac{u(1+u)}{(1+u)^2 + uG}\, du \\ &= c - \frac{1}{2}(1+G) \ln [(1+c)^2 + cG] \\ &+ \frac{1}{2} G(3+G) \frac{\alpha}{1-\alpha^2} \ln \left(\frac{1 + c/\alpha}{1 + c\alpha} \right) \end{aligned} \tag{3.30}$$

where α and $1/\alpha$ are the roots of

$$\alpha + 1/\alpha = 2 + G \tag{3.31}$$

Reproduced with permission of the copyright owner. Further reproduction prohibited without permission.

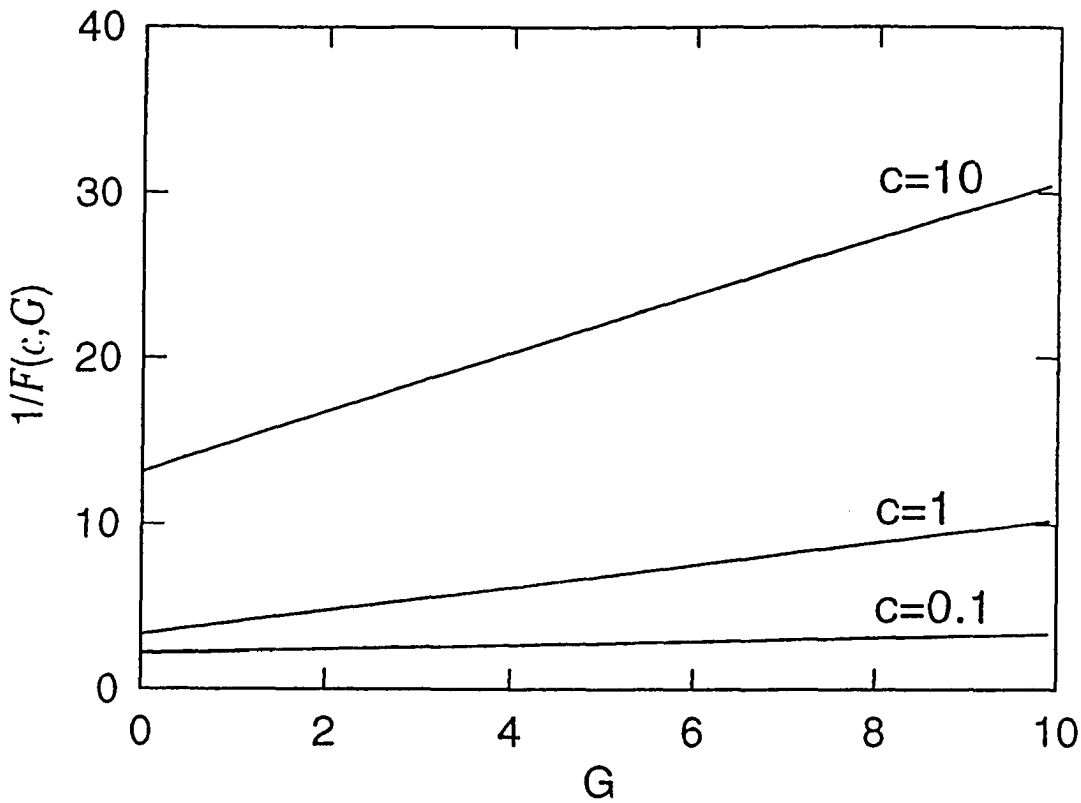

Fig. 3.2

$1/F(c, G)$ versus G for indicated c values.

Reproduced with permission of the copyright owner. Further reproduction prohibited without permission.

Figure 3.2 plots $1/F(c, G)$ versus G for representative c values. The approximate straight lines correspond to a Lorentzian dependence of this F on $G^{1/2}$. Expressed as $F = A/(B + G)$, the quantity $B(c)$ is found to increase with increasing c, and hence a prediction of the model is that the width of the current peak *decreases* when the tunneling-out rate increases relative to scattering-in rate [79].

The result (3.30) may be expressed more simply in terms of the separate contributions from the two quasi-levels in the doublet, as in (3.2), rather than first combining them as in (3.3) and (3.7):

$$\int_0^1 R_{\pm}\, dX =$$

$$\int_0^1 \frac{dX}{\frac{1}{X}\frac{t_{l\,\min}}{n^l} + \frac{t_r}{n^r}} = \frac{n^r}{t_r} - \frac{c}{t_r}\frac{(n^r)^2}{n^l}\ln\left(1 + c\,\frac{n^l}{n^r}\right) \quad (3.32)$$

The G dependence in (3.32) comes from the variation of n^r and $n^l = 1 - n^r$ given by eq (3.6): $n^l n^r = 1/(4 + G)$. The R_+ and R_- contributions have separate maximums, as functions of G, which merge into the single peak given by (3.30),(3.31).

Reproduced with permission of the copyright owner. Further reproduction prohibited without permission.

CHAPTER 4

SUMMARY AND CONCLUSIONS

In this thesis we have developed a procedure to numerically analyze the current in a double barrier resonant tunneling structure having an accumulation layer. This structure is a reflecting double barrier structure. A model potential is initially analyzed to understand the properties of such a double barrier resonant tunneling structure and this understanding is applied to derive an equation for the current through quantized states in the accumulation layer.

The model potential is a rectangular potential, having two wells and two barriers, which is open on one side and closed on the other side. Since solutions to Schrödinger's equation for the model potential can be represented by algebraic expressions, the effect of varying the widths of the wells and the thicknesses of the barriers have been investigated providing a detailed characterization of a reflecting double barrier structure which appears not to have been done previously. This characterization, which is described in Chapter 2, provided and understanding of the properties of a double barrier resonant tunneling structure with an accumulation layer which permitted the derivation for the expression for the current through the quasi levels in the accumulation layer reported in Chapter 3.

Reproduced with permission of the copyright owner. Further reproduction prohibited without permission.

The peaked current seen in a double-barrier resonant tunneling diode having a quantizing accumulation layer on the source (cathode) side is considered in this thesis as due to electron scattering from incident source states to hybrid "final" states that combine an accumulation-layer level with a "well" level and in which the resulting doublet is coupled, through the second barrier, to the anode continuum. The resonance appears as an "anti-crossing" of the pair of levels derived from the pair before coupling, as the latter shift with increasing bias. The coupling with the anode continuum gives level broadening effects. The current will depend on the accumulation-layer fraction of the "norm" (space integral of the square of the wave function, appropriately normalized). The lifetime for emission from the coupled levels into the anode continuum may be obtained from the complex energy at which the reflection "S function" has a pole, with the usual relation of the negative imaginary energy to the lifetime and to the broadening.

To study these properties in detail, in Chapter 2 the potential profile was replaced by a model "square" one in which the fields in the accumulation layer and in the two barriers and the well between them are zero. The above properties are then computed in detail. The norm and its two complementary fractions are found to exhibit the level broadening as a function of energy. The predominant norm fraction shifts between the "well" and "accumulation" sides of the structure over the anti-crossing process. The reflection phase is also computed as a function of energy, and its relationship to the total charge (fraction of one

Reproduced with permission of the copyright owner. Further reproduction prohibited without permission.

electron) within the diode structure, when all of the system states are occupied, is elucidated. Of special interest is the consequences of having a thinner anode-side barrier (representing the actual lowering of this barrier, with increasing bias, in the diode).

As the width of the anode-side barrier is decreased with the accumulation layer well width equal to the anode-side well width, the lifetime of both quasi-levels decreases until the anode-side barrier is about one half the width of the cathode-side barrier after which the lifetime of the higher energy quasi-level increases and its norm shifts into the accumulation layer and the lifetime of the lower energy quasi-level continues to decrease and its norm shifts into the right well.

The phase of the "S function" increases by 2π over each quasi-level and thus by 4π over a pair of quasi-levels and the integral of the norm weighted by the density of states is equal to one over each quasi-level thus indicating that each quasi-level is occupied by one electron even when the anode-side barrier is much thinner than the cathode-side barrier.

It has been shown in Chapter 2 that the properties of the distribution of the norm between the accumulation layer well and the anode side well is accurately represented using a two level model. It is also shown in Chapter 2 that the two level model accurately represents the anticrossing properties of the eignevalues of the interacting accumulation layer well level and the anode side well level. This model is used in Chapter 3 to

Reproduced with permission of the copyright owner. Further reproduction prohibited without permission.

derive an expression for the current in a DBRTS with an accumulation layer.

It has been shown in Chapter 3 that the model, in which diode current is due to electron scattering from the cathode side into the states formed by coherently combined accumulation-layer and inter-barrier quasi-levels, followed by Gamow tunneling out to the anode side, mimics conventional resonant tunneling by a current peak at the "level crossing" point. A quantitative calculation has been made for this system, subject to a number of simplifying approximations. The expression derived for the current has Lorentzian form having a peak when the energy level of the accumulation layer is equal to the energy level of the well between the two barriers where these energy levels are the energy levels of the non-interacting accumulation layer and the well between the two barriers. The energy levels of the interacting accumulation layer an the well between the two barriers anti-cross.

There appears to be insufficient experimental data available for a detailed comparison with the quantitative calculation.

Reproduced with permission of the copyright owner. Further reproduction prohibited without permission.

APPENDIX

Derivation of Eq. (2.31)

The following is an unpublished derivation of Peter J. Price. Schrödinger's equation for wave function ψ_i of energy E_i is

$$E_i\psi_i(x) = -\frac{\hbar^2}{2m^*}\frac{d^2}{dx^2}\psi_i(x) + V(x)\psi_i(x) \qquad (A.1)$$

For a stationary state the energy E_i is real. Take the complex conjugate of Eq. (A.1) for $i = 2$ and multiply by ψ_1 and subtract from this equation ψ_2^* times Eq. (A.1) with $i = 1$ to get

$$(E_2 - E_1)\psi_2^*\psi_1 = -\frac{\hbar^2}{2m^*}\frac{d}{dx}\left[\psi_1\frac{d}{dx}\psi_2^* - \psi_2^*\frac{d}{dx}\psi_1\right] \qquad (A.2)$$

Let $V(x) = 0$ for $x > 0$ and let $V(x)$ be a reflecting potential for $x < 0$. Thus $\lim_{x\to-\infty}\psi_i \to 0$ for $i = 1, 2$. Intergating Eq. (A.2) from $-\infty$ to 0 results in

$$(E_2 - E_1)\int_{-\infty}^{0}\psi_2^*\psi_1 dx = -\frac{\hbar^2}{2m^*}\left[\psi_1\frac{d}{dx}\psi_2^* - \psi_2^*\frac{d}{dx}\psi_1\right]_{x=0} \qquad (A.3)$$

where the integral is finite if $\lim_{x\to-\infty}\psi_2^*\psi_1 \to 0$. For $x > 0$ the wave functions ψ_1 and ψ_2 have form

$$\psi_i = e^{-ik_ix} + S_ie^{ik_ix} \qquad (A.4)$$

from which it follows

Reproduced with permission of the copyright owner. Further reproduction prohibited without permission.

$$\frac{d\psi_i}{dx} = ik_i\left[-e^{-ik_ix} + S_ie^{ik_ix}\right] \qquad (A.5)$$

where $S_i = S(E_i)$. From Eqs. (A.4) and (A.5) Eq. (A.3) and since $S(E) = \exp[i\theta(E)]$, $S_i^* = 1/S_i$, Eq. (A.3) can be rewritten as

$$\frac{2m*}{\hbar^2}(E_2 - E_1)\int_{-\infty}^{0} \psi_2^*\psi_1 dx =$$

$$i(k_2 + k_1)\left(\frac{S_1 - S_2}{S_2}\right) + i(k_2 - k_1)\left(\frac{1}{S_2} - S_1\right) \qquad (A.6)$$

Let $E_2 \to E_1$ so that $E_2 - E_1 \to dE$, $S_2 - S_1 \to dS$, and $k_2 - k_1 \to dk$ so that Eq. (A.6) can be written as

$$\frac{2m*}{\hbar^2}\int_{-\infty}^{0} |\psi|^2 dx = i\left(-\frac{2k}{S}\frac{dS}{dE}\right) + i\frac{dk}{dE}\left(\frac{1}{S} - S\right) \qquad (A.7)$$

Using

$$\frac{dS}{dE} = i\frac{d\theta}{dE}e^{i\theta} = iS\frac{d\theta}{dE} \qquad (A.8)$$

and $1/S - S = -2i\sin\theta$ Eq. (A.7) can be rewritten as

$$\frac{2m*}{\hbar^2}\int_{-\infty}^{0} |\psi|^2 dx = \frac{2k}{S}\frac{dS}{dE} + 2\sin\theta\frac{dk}{dE} \qquad (A.9)$$

Using $v = (\hbar k)/m^*$, $E = (\hbar k)^2/(2m^*)$, $dk/dE = [m^*/(2\hbar^2 E)]^{1/2}$ and $\ell = \int_{-\infty}^{0} |\psi|^2 dx$ Eq. (A.9) can be rewritten as

Reproduced with permission of the copyright owner. Further reproduction prohibited without permission.

$$t_{dwell} = \frac{1}{v}\ell = \hbar\frac{d\theta}{dE} + \frac{\hbar}{2E}\sin\theta \qquad (A.10)$$

which is Eq. (2.31).

Reproduced with permission of the copyright owner. Further reproduction prohibited without permission.

REFERENCES

1. R.H. Fowler and L. W. Nordheim Proc. Roy. Soc. A **119**, 173, (1928).
2. J.R.Oppenheimer, Phys.Rev. **31**, 914 (1928).
3. C. Zener, Proc. Roy. Soc. A **145**, 523 (1934).
4. L.Esaki, Phys. Rev. **109**, 603 (1958).
5. R. Tsu and L. Esaki, Appl. Phys. Lett. **22** (1973) 562.
6. L. L. Chang, L. Esaki, and R. Tsu Appl. Phys. Lett. **24** (12) 593 (1974).
7. E. R. Brown ,T. C. L. G. Sollner, W. D. Goodhue, and C. D. Parker, Appl. Phys. Lett. **50**, 83 (1987).
8. N.Yokohama, K. Imamura, S. Muto, S. Hiyamizu, and H. Nishi, Jpn. J. Appl. Phys. **24**, L853 (1985).
9. R. C. Potter, A. A. Lakhani, and H. Hier, J. Appl. Phys **64**, 3735 (1988).
10. M. Tsuchiya, T. Matsusue, and H. Sakaki, Phys. Rev. Lett **59**, 2356 (1987).
11. C. Weisbuch and B. Vinter, Quantum Semiconductor Structures: Fundamentals and Applications, Academic Press, New York 1991.
12. D. Bohm, "Quantum Theory" Prentice Hall, p. 283, (1951).
13. C. B. Duke, "Tunneling in Solids: Solid State Physics Supplement 10" (1969).

Reproduced with permission of the copyright owner. Further reproduction prohibited without permission.

14. G. Bastard, "Wave Mechanics Applied To Semiconductor Heterostructures", Halstead Press, (1988).

15. S. Datta, "Electronic Transport in Mesoscopic Systems", Cambridge University Press, (1988).

16. H. Mizuta and T.Tonoue, "The Physics And Applications of Resonant Tunnelling Diodes", Cambridge University Press (1995.)

17. P. J. Price, "Electron Tunneling in Semiconductors" in "Basic Properties of Semiconductors", Volume 1, P. T. Landsberg editor, North Holland, (1992).

18. D. J. BenDaniel and C. B. Duke, Phys. Rev. **152** (2), 683 (1966).

Akara et al., Phys. Rev. B "40" (1989) 11609, 11619.

19. Reference 13 at page 83.

20. M. Büttiker, IBM J. Res Develop. **32** (3), 63 (1988).

E.Gerjuoy and D.D.Coon, Supperlat. Microstruct.**5** 305(1989).

21. N. G. Einspruch and W. R. Frensley, Heterostructures and Quantum Devices, Vol. 24 in VLSI Electronics: Microstructure Science (Academic Press, New York, 1994).

22. Reference 21. at page 358.

23. J. S. Wu, C. Y. Chang, C. P. Lee, K. H. Chang, D. G. Liu and D. C. Liou, Appl. Phys. Lett. **57**, 2311 (1990).

24. K. S. Wu, C. Y. Chang, C. P. Lee, K. H. Chang, and D. G. Liu, Solid State Electronics **34** (4), 403 (1991).

Reproduced with permission of the copyright owner. Further reproduction prohibited without permission.

25. A. S. Ignat'ev, V. E. Kaminskii, V. B. Koylov, V. G. Mokerov, G. Z. Nemtsev, S. S. Shmelev and V. S. Shubin, Sov. Phys. Semicon, **26** (10), 1005 (1992).

26. J. S. Wu, K. H. Chang, C. P. Lee, C. Y. Chang, D. G. Liu, and D. C. Liou, Appl. Phys. Lett. **59**, 87 (1991).

27. P. Mouniax, O. Vanbesian, and D. Lippens, Appl. Phys. **57** (15), 1517 (1990).

28. E. T. Koenig, B. Togai, M. J. Paulis, C. I. Huang, and C. A. Bozada, J. Appl. Phys. **68** (7) 3425 (1990).

29. M. J. Paulis, E. T. Koenig, B. Togai, C. A. Bozada, C. I. Huang, C. E. Stutz, and K. R. Evans, Superlattices and Microstructures **7** (2), 135 (1990).

30. P. H. Rivera, and P. A. Schultz, Appl. Phys. Lett. "67"(18), 2675 (1995).

31. P. J. Price, Phys. Rev. **45** (16), 9042 (1992).

32. T. Nagakawa, H. Imannota, T. Kojima, and K. Otha, Appl. Phys. Lett. **49**, 73 (1986);

T. Nagakawa, T. Fujita, Y. Matsumota, T. Kojima and K. Otha, Jpn. J. Appl. Phys. 26, L980 (1987).

33. D. A. Collins, D. H. Chow, D. Z. Y. Ting, E. T. Yu, J. R. Soderstrom, and T. C. McGill, Solid-State Electron. **32**, 1095 (1991). D. X. Xu, G. D. Shen, M. Wildander, F. Schaffler, and J. F. Luy; Solid-State Electron. **35**, 611 (1992).

34. D. X. Xu, G. D. Shen, M. Wilander, and G. V. Hanson, J. Appl. Phys. **71**, 3859 (1992).

35. J. Leo, G. A. Toombs, Phys. Rev. B, **43** (12), 9944 (1991).

Reproduced with permission of the copyright owner. Further reproduction prohibited without permission.

36. E. E. Mendez, L, Esaki, and W. I. Wang, Phys. Rev. **B 33**, 2893 (1986).

37. H. Yamamoto, Y. Kanie, M. Arakawa, and K. Taniguchi, Appl. Phys. A **50**, 577 (1990).

38. H. Yamamoto, K. Tsuji, and K. Taniguchi, Phys. Stat. Sol. (B) **188**, 679 (1995).

39. H. Yamamoto, A. Kurita and K. K. Taniguchi, Jpn. J. Appl. Phys. **34**, 4529 (1995).

40. H. Yamamoto, K. Tsuji, Y. Ikeda, and K.Taniguchi, Materials Sci. and Engineering, **B35**, 421 (1995).

41. H. Yamamoto, K. Tsuji, Y. Ikeda, and K.Taniguchi, Superlattices and Microscructures "17"(1), 35 (1995).

42. P. J. Price, Rhys. Rev. B 36, 1314 (1987).

43. J. S. Wu, C. D. Lee, C. Y. Chang, J. H. Chang, D. G. Liu, J. Appl. Phys. **69** (2), 1122, (1991).

44. T. Strutz and Y. Shiraki, Semidond. Sci. Technology **11**, 103 (1996).

45. H. Zheung, F. Uang, Int. Semicond. Conf. World Scientific 1317 (1990).

46. H. M. Yoo, S. M. Goodnick, and J. R. Arthur, Appl. Phys. Lett. **56** (1), 84 (1990).

47. F. W. Sheard and G. A Toombs, Semicond. Sci. Technology, **7**, B460 (1992).

48. J. S. Wu, K. H. Chang, C. P. Lee, C. Y. Chang, D. G. Liu, and D. C. Liou, Appl. Phys. Lett. **59**, 87 (1991).

49. J. A. Wheeler, Phys. Rev. **52**, 1107 (1937).

Reproduced with permission of the copyright owner. Further reproduction prohibited without permission.

W. Heisenberg, Z. Naturforsch, **1**, 608 (1946).

R. G. Newton, "Scatering Theory of Waves and Particles" (McGraw-Hill 1966).

G. F. Chew, "The Analytic S Matrix" (W. A. Benjamin, New York 1967).

M. Büttiker, IBM J. Res Develop. **32** (3), 317 (1988).

50. Quantum Mechanics, A. S. Davydov, Pergamon Press, Second Edition, p414 (1976).

51. D. L. Landau, E. M. Lifshitz, Quantum Mechanics (Non-Relativistic Theory) p. 265 (1958).

52. H. Yamamoto, Y. Kanie, and K. Tamguchi, Phys. Status Solidi B 167, 571 (1991).

53. R. Romo, G. Garcia-Calréron, Phys. Rev. B. **49**, 14016, (1994).

54. G. Garcia-Caldéron, R. Romo, A. Rubio, Phys. Rev. B **47**, 9572 (1993).

55. G. Gildenblat, B. Gelmont, S. Vatannia, J. Appl. Phys. **77** (12), 6327 (1995).

56. H. Yamaoto, K. Tsuji, and K. Tamiguchi, Phys. Stat. Solidi B **188**, 679 (1995).

57. G. A. Toombs and F. W. Sheard, in Electronic Properties of Multilayer and Low-Dimensional Structures, edited by J. M. Chamberline, L. Eaves and J.C. Portal (Plenum, New York 1990) p257.

58. E. E. Mendez, Physics of Resonant Tunneling in Semiconductors in Physics and Applications of Quantum Wells and

Reproduced with permission of the copyright owner. Further reproduction prohibited without permission.

Superlattices, NATO ASI Series, Series B: Physics Vol. 170, p 159 (1987).

59. J. A. Porto, J.Sanchez-Dehesa, L. A. Cury, A. Nogaret and J. C. Portal, J. Phys. Conds. Matter **6**, 887 (1994).

60. Blatt and V.F. Weisskopf, Theoretical Nuclear Physics, John Wiley & Sons, Inc., Chapter 8, (1951).

61. H. Feshbach, D. C. Peaslee, and V. F. Weisskopf, Phys. Rev. **71** (3), 145 (1947).

62. A. P Thorne, Spectrophysics, John Wiley & Sons p. 59 (1974).

63. U. Fano, Phys. Rev. **124** (6), 1866 (1961).

64. E. Tekman and P. F. Bagwell, Phys. Rev. B **48**(4), 2553 (1993).

65. K. U. Nöckel and A. D. Stone, Phys. Rev. B **50** (23), 17415 (1994).

66. L. I. Schiff, Quantum Mechanics, Third Edition, p. 39, McGraw-Hill Book Company.

67. Quantum Mechanics, C. Cohen-Tannoudji, B. Diu and F. Laloë, John Wiley & Sons, 461 (1977).

68. See page 41 of reference 32.

69. M. Wigner and H. Mizuta Phys. Rev. B **48**(19), 14393 (1993).

70. M. Wigner and H. Mizuta Jpn. J. Appl. Phys. **32** L520 (1993).

71. See page 420 of ref. 67.

72. See page 399 of ref. 45.

73. P. J. Price, Superlattices and Microstructures, **20** (3), 253 (1996).

Reproduced with permission of the copyright owner. Further reproduction prohibited without permission.

74. E. P. Wigner and L. Eisenbud, Phys. Rev. **72** (1), 29 (1947).

75. See a similar relationship shown by N. Levinson, Kgl. Danske Videnskab. Selskab, Mat.-Fys. **25**,(9) (1949).

L. I. Schiff, Quantum Mechanics, Third Edition, p. 353, McGraw-Hill Book Company.

76. G.Gamow, Zeits. f. Physik. **53**, 601 (1929),

77. There is not a general agreement on this particular value, but the old figure 7 eV is evidently too small. See, for example, E.E.Mendez, P.J.Price and M.Heiblum, Appl. Phys. Lett. **45**, 294 (1984), W.Walukiewicz, Phys. Rev. **B37**, (1988) 8530, and references therein.

78. We are disregarding the effects of a "hump" in the potential profile on the cathode side, which would to some extent modify these initial-state wave functions.

79. A more complete analysis is needed to take account of effects of scattering between double-well states. These processes will modify the result expressed by eq.(3.2), especially by tending to equalize the occupation probabilities of the doublet of states with given lateral wave-vector but complementary norm fractions, and thus affect the wings of the current peak.

80. F. F. Fang and W. E. Howard, Phys. Rev. Lett. **16**, 797 (1966).

Reproduced with permission of the copyright owner. Further reproduction prohibited without permission.